University of Alberta

Petrophysical Properties of Bitumen from the Upper Devonian Grosmont Reservoir, Alberta, Canada

by

Yi Zhao

A thesis submitted to the Faculty of Graduate Studies and Research
in partial fulfillment of the requirements for the degree of

Master of Science

Department of Earth & Atmospheric Sciences

Fall 2009
Edmonton, Alberta

Examining Committee

Hans G. Machel, Department of Earth & Atmospheric Sciences

George Pemberton, Department of Earth & Atmospheric Sciences

Julia Foght, Department of Biological Sciences

This thesis is dedicated to

my parents

for all their

love

谨以此文献给我的父母

ABSTRACT

The Upper Devonian Grosmont reservoir in Alberta, Canada, is the single largest carbonate bitumen reservoir in the world, with an estimated 400 billion barrels of bitumen in place. The Grosmont bitumen formed from light crude oil via extensive biodegradation, which produced extremely high *in-situ* viscosities of >1 million cP. Forty nine samples from fifteen wells were selected for rheological behavior, viscosity, and biodegradation pattern analysis. In addition, various methods of viscosity determination were compared.

Results indicate that the Grosmont bitumen is essentially a non-Newtonian fluid at *in-situ* conditions, exhibiting a distinctive shear-thinning behavior at T < 40°C. Neglecting this character will cause inaccurate viscosity measurements. The viscosity variations in the Grosmont reservoir are cyclic with depth and are stratigraphically controlled. The bitumen exhibits 3 levels of biodegradation. Biodegradation parameters from hopanes and tricyclic terpanes may potentially be used for bitumen quality prediction.

ACKNOWLEDGEMENTS

This thesis was financially supported by a grant from Shell Exploration & Production Company, Houston, TX, to Professor Hans G. Machel at the University of Alberta. Further financial support was provided by a Natural Science and Engineering Research Council (NSERC) operating grant to Hans G. Machel. The author further acknowledges the financial assistance from the American Association of Petroleum Geologists (AAPG) through their Grant-in-Aid Foundation. I also would like to acknowledge the Graduate Students` Association (GSA) and the Faculty of Graduate Studies and Research (FGSR) at the University of Alberta for providing travel assistance to present parts of this thesis at conferences.

“Thank you” to Hans G. Machel for your supervision and editorial work during this project. Dr. Bob McNeil (Shell, Houston) provided highly valuable guidance and encouragement throughout the course of this study, and also editorial comments on an earlier draft. Professors Jacob H. Masliyah and Zhenghe Xu generously provided laboratory and equipments for the extractions and viscosity measurements in this study. Special thanks go to Harold Vinegar (Shell, Houston) for the inspiration to and generous financial support of the entire project.

Last not least, I owe my warmest thanks to my parents for their moral as well as monetary support. Many thanks to Jin for her love and to all my dear friends for their constant support.

TABLE OF CONTENTS

LIST OF TABLES

LIST OF FIGURES

CHAPTER 1

INTRODUCTION

Natural bitumen is generally defined as a hydrocarbon with viscosity greater than 10,000 centipoises (cP) measured at reservoir conditions (Etherington and McDonald, 2004). On a global scale, the estimated volume of technically recoverable natural bitumen is 651 billion barrels, about 81% of which is found in Alberta, Canada (Meyer and Attanasi, 2003). Beneath the giant Cretaceous oil sand deposits in Alberta, the Devonian Nisku, Upper Ireton and the Grosmont formations (collectively referred as the Grosmont reservoir) together host nearly 400 billion barrels of original oil in place (OOIP) (Hein, 2006), which is the single largest bitumen carbonate reservoir in the world. Currently, the Grosmont reservoir is not under production. However, this giant deposit has drawn much attention in recent years, and some new exploitations are underway (e.g., Piron, 2008; Hopkins and Barrett, 2008).

A complex diagenetic history, especially dolomitization at various stages and late karstification, make the Grosmont a very heterogeneous reservoir (Dembicki and Machel, 1996). In addition, the bitumen in the Grosmont is characterized by extremely high viscosities (more than a million cP on average) and very low American Petroleum Institute (API)

gravity (5° to 9°) (Martinez et al., 2006). The variations of the petrophysical properties in the Grosmont bitumen have never been examined. However, in order to develop suitable thermal recovery technology for the Grosmont reservoir, such variations must be understood.

1.1 Objectives

Exploitation of the Grosmont reservoir is a great challenge to both geologists and engineers. This is not only because of the heterogeneous nature of the reservoir itself, but also because of the possible spatial variation of bitumen properties in the reservoir. Traditionally, reservoir characterization deals with porosity, permeability, and fluid saturations, which is applicable and sufficient for describing conventional reservoirs. In unconventional reservoirs, especially in heavy oil and bitumen reservoirs characterized by high viscosity and low API gravity, the fluid properties must also be taken into serious consideration. Indeed, viscosity is as important as permeability in terms of the fluid flow rate expressed in Darcy's Law (Figure 1.1), and viscosity becomes a dominant factor when characterizing heavy oil and bitumen reservoirs, such as the Grosmont reservoir. Therefore, the aim of this study is to generate useful petrophysical data for the estimation of bitumen viscosity in the Grosmont reservoir to assist in future exploitation. The specific objectives can be summarized as follows:

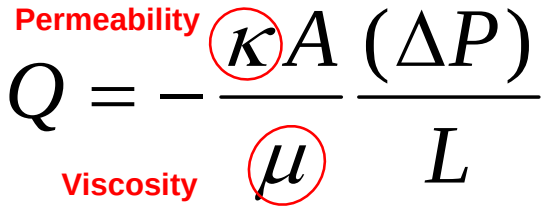

Figure 1.1 Darcy's Law shows that viscosity is as important as permeability in terms of flow rate. Q = discharge rate (volume/time); A = cross-sectional area; ΔP = pressure drop over length L.

1) Evaluate the technique of viscosity measurement; establish intra-laboratory and inter-laboratory comparisons. Previous studies showed that viscosity measurements are problematic (e.g., Miller et al., 2006; Adams et al., 2008). In order to ensure the quality of the viscosity data used in this study, an in-depth evaluation of this parameter and its measurement is felt to be a prerequisite step. In addition, the Intra- and inter-laboratory comparisons can be used for identifying the effects of different factors on viscosity measurements, such as the extraction method, the solvent used, and laboratory procedure

2) Characterize bitumen fluid properties, especially viscosity. It has been suggested that the high viscosities of the bitumen are mainly a result of water washing and biodegradation (Connan, 1984; Head et al., 2003). However, multiple factors, such as oil charge mixing, reservoir temperature-dependent biodegradation rate, and supply of water and nutrients to the biodegrading organisms, may also constrain the final distribution of viscosity (Larter et al., 2006). In addition, after bitumen has been brought to the surface in a core barrel, it undergoes modifications

from exposure to light, air, water, and fluctuations in temperature, a process called “aging”. Adams et al. (2008) showed that aging had a great influence on bitumen viscosity. In the present study area, most of the available cores are so called “legacy” cores, i.e., from wells that are 20 to 30 years old, and only a few “fresh” cores have been released from wells drilled in the last 1 to 2 years. Therefore, in order to map out the viscosity distribution, legacy samples had to be used. This study attempts to a) clarify whether there is any aging effect in the Grosmont reservoir bitumen, and if so, b) establish the extent of aging on selected bitumen properties, and c) introduce a correlation to correct fluid properties of legacy samples to fresh ones or to in-situ conditions. These tasks were accomplished by comparing bitumen properties from selected legacy and fresh wells that are adjacent to each other.

3) Investigate the biomarker characteristics of the Grosmont reservoir and correlate viscosities with the biodegradation levels if possible. The biomarker information stored in bitumen has been proved to be a reliable indicator of the biodegradation level (Peters et al., 2005). A study by Brooks et al. (1989) contributed insight into biomarker characteristics in Nisku, Upper Ireton, and the Grosmont formations. The aim in the present study is to provide a more detailed account of the biomarker distribution in the study area, and of the biodegradation level. The relationship between the level of biodegradation and bitumen viscosity in the Grosmont reservoir has never been examined. Yet, such a correlation may exist (e.g.,

McCaffrey et al., 1995). Therefore, it was expected that biomarker parameters could be identified and used as additional indicators to correlate biodegradation with viscosities of bitumen in this study.

1.2 Study Area

The Grosmont Platform is part of a northwest-southeast trending Upper Devonian shallow marine carbonate platform complex in north-central Alberta. The platform is approximately 150 km wide and at least 600 km in length (Harrison, 1982). The study area encompasses Townships 85 to 95 and Range 19W4 to W5 (Figure 1.2), which is around 4,600 km^2 large and is suspected to be one of the areas with the highest bitumen reserves (Dembicki, 1994). In this area, the Grosmont reservoir is made up of the following stratigraphic units in ascending order (oldest to youngest): LGM, UGM1, UGM2, LGM3, Upper Ireton, and Nisku (will be discussed in Chapter 2).

1.3 Sample Control and Methodology

Over 400 samples (Figure 1.3) from 50 wells in the study area were collected from the Energy Resources Conservation Board (ERCB) Core Research Center in Calgary (Appendix 1). Among them, 49 samples from 15 wells along a NW-SE strike cross section (AA` in Figure 1.4) were

selected for bitumen properties analysis, including viscosity measurement, gas chromatography-mass spectrometry (GC-MS) analysis, elemental analysis (EA), and Thermal Gravimetric Analysis (TGA). These samples covered Nisku, Upper Ireton, and the Grosmont

Figure 1.2: Locations of the Grosmont Platform, Cretaceous oil sands deposits, and the study area.

Formations, in an attempt to reveal both lateral and vertical variations of bitumen properties.

As shown in Table 1.1, these 49 samples were grouped into 4 batches based on testing times, different testing venues, and analysis procedures. The first batch of samples (Batch 1) is concentrated in the region where the highest bitumen concentration has been observed (Dembicki, 1994).

The second batch (Batch 2) was selected and tested from March to May 2008. This batch was chosen from 3 wells that lie along the northwest to southeast transect, in the hope of revealing variations along strike in addition to vertical variations, i.e., across the stratigraphic levels of interests. Few wells cored more than 2 or 3 stratigraphic units, however. Only well 10-29-89-23W4 covers all formations of interest.

In the middle of 2008, several new cores were released to the public domain. Therefore, a third batch consisting of 12 legacy samples and 6 fresh samples (Batch 3) was picked for viscosity and GCMS analyses. The legacy samples were selected to cover all three of the targeted formations in the northern, central, and southern regions of the study area, which partially overlaps with the area covered in Batch 2 samples. Multiple wells that are adjacent to each other have to be used to cover all the formations in northern and southern regions. Also, 6 samples from 3 new wells were picked close to the early legacy wells for examination of the aging effect.

The fourth and last batch of samples (Batch 4) included 12 fresh samples from 8-33-90-23W4 and 2 legacy samples from 10-29-89-23W4.

These two wells were the closest pair of fresh and legacy wells with high bitumen saturation in the Nisku, Upper Ireton and Grosmont Formations.

These 4 batches of samples were tested in 3 different laboratories (Table 1.1). Batch 1 was sent to a commercial laboratory (Lab A) for viscosity tests. Batches 2 and 4 were examined at the University of Alberta for bitumen viscosity measurements, elemental analysis and TGA tests (Lab C). The only difference between Batches 2 and 4 was extraction by toluene and dichloromethane, respectively. Batch 3 was run in another commercial laboratory (Lab B) for viscosity measurements and GC-MS analysis. In addition, the viscosities of 16 duplicates from the first three batches were measured at the university laboratory for the purpose of intra- and inter-laboratory comparison. Among them, 4 pairs were extracted by two solvents, i.e., toluene and dichloromethane, in order to evaluate the potential effects of solvent extraction on bitumen viscosity.

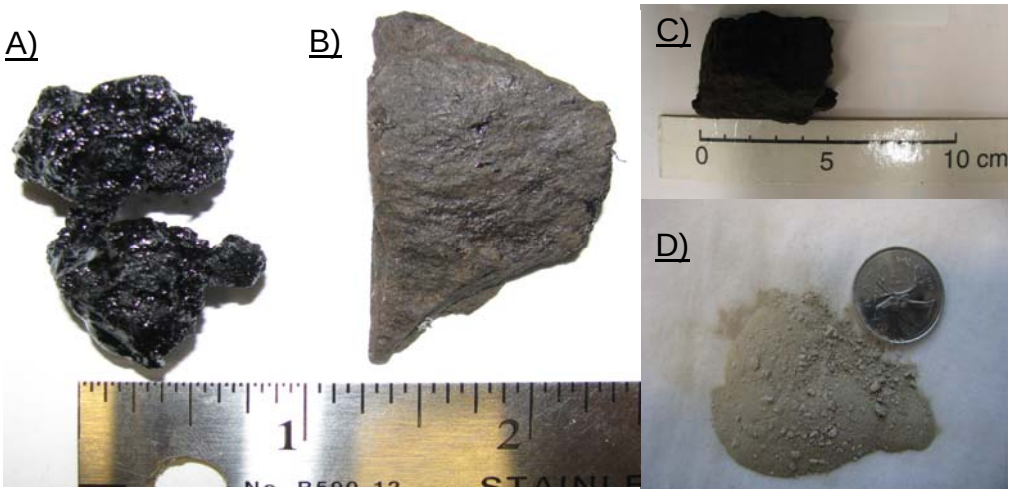

Figure 1.3 Three distinctive host rocks in the Grosmont reservoir. Fracture & Vug host (A), tight matrix host (B), and marl host before (C) and after extraction (D).

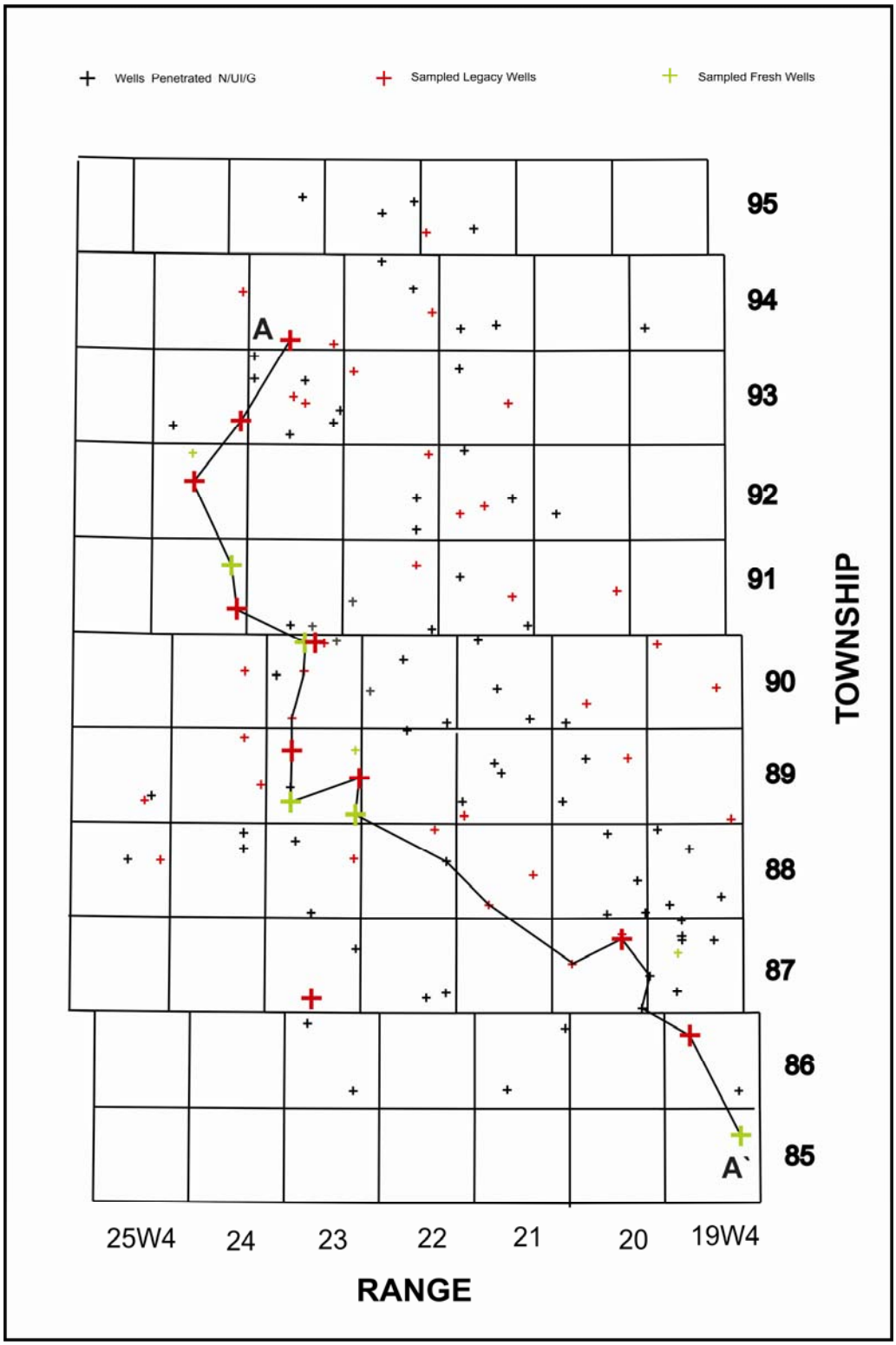

Figure 1.4 Well control map of the study area. Sampled legacy wells and fresh wells are shown in red and green crosses. Large crosses are wells with bitumen properties analyses.

Table 1.1 Sample summary

Source	Well ID	Sample ID	Depth (m)	Formation	Labs A&B Visc[c]	Lab C Visc[c]		GCMS	EA	TGA
						T[d]	DCM[e]			
Batch 1/Lab A										
Legacy	16-13-89-23W4	N-1	289.3	Nisku	√		√			
		N-5	298.8	Nisku	√					
		G3-3	343.1	UGM3[a]	√					
		G3-4	344.0	UGM3	√		√			
	7-34-90-23W4	N-15	278.3	Nisku	√					
		N-18	281.6	Nisku	√					
Fresh	08-01-89-23W4	GRM 124	298.4	Nisku	√					
		GRM 125	290.4	Nisku	√					
		GRM 126	336.1	UGM3	√					
		GRM 127	325.8	UIreton	√		√			
		GRM 128	294.0	Nisku	√					
		GRM 129	343.65	UGM3	√		√			
		GRM 130	331.5	UIreton	√					
Batch 2/ Lab C										
Legacy	10-04-94-23W4	G3-130	518.1	UGM2		√				
		G3-140	565.5-566.8	UGM1		√				
	10-29-89-23W4	N-52	264.75	Nisku		√	√		√	√
		N-57	295.45	Nisku		√				
		UI-81	315.45	UIreton[b]		√			√	√
		G3-35	349.65	UGM3		√			√	√
	10-29-86-19W4	G3-63	309	UGM3		√				
Batch 3/ Lab B										
Legacy	11-12-91-24W4	N1	282.5-285.7	Nisku	√			√		
	10-21-92-24W4	UI1	363-366	UIreton	√			√		
		UI2	377-379	UIreton	√			√		
	10-12-93-24W4	G1	444-446.7	UGM3	√			√		

Continued on next page

Source	Well ID	Sample ID	Depth (m)	Formation	Labs A&B Visc[c]	Lab C Visc[c]		GCMS	EA	TGA
						T[d]	DCM[e]			
Legacy	10-29-89-23W4	N2	265-267	Nisku	√	√	√	√		
		N3	305.3-307.4	Nisku	√	√		√		
		UI3	327.4-328.1	UIreton	√	√		√		
		G2	346-349	UGM3	√	√	√	√		
	6-10-87-23W4	N4	349.4-358.2	Nisku	√			√		
	11-26-87-20W4	UI4	263.4-267	UIreton	√			√		
	10-29-86-19W4	G3	283-283.3	UGM3	√			√		
		G4	303-303.6	UGM3	√			√		
Fresh	11-26-91-24W4	UI5	316.8-319	UIreton	√			√		
		G5	335.25-336.4	UGM3	√			√		
	06-08-89-23W4	N5	270.6-280.6	Nisku	√	√	√	√		
		G6	322.8-324.2	UIreton	√	√	√	√	√	√
	07-26-85-19W4	UI6	325-326.2	UIreton	√			√		
		G7	350.2-350.8	UGM3	√		√	√		
Batch 4/ Lab C										
Legacy	10-29-89-23W4	UI-90	334.2	UIreton			√			
		G3-33	344	UGM3			√			
Fresh	8-33-90-23W4	N-77	274.55	Nisku			√			
		N-79	277.25	Nisku			√		√	
		UI-122	285.25	UIreton			√			
		UI-125	295.13	UIreton			√			
		UI-129	305.55	UIreton			√		√	
		G3-240	316.05	UGM3			√			
		G3-243	321.4	UGM3			√			
		G3-245	339.6	UGM3			√		√	
		G3-246	343.84	UGM3			√			
Total	**15**	**49**			**31**	**13**	**21**	**18**	**8**	**4**

a. UGM3: Upper Grosmont 3. b. UIreton: Upper Ireton. c. Visc: Viscosity. d. T: Toluene. e. DCM: dichloromethane.

CHAPTER 2

REGIONAL GEOLOGY AND PREVIOUS WORK

The strata of interest in this thesis are from the Upper Devonian Woodbend and Winterburn Groups (Figure 2.1). In the study area, the sub-Cretaceous unconformity truncates the Devonian strata, which range from the Nisku Formation in the west to the Grosmont Formation in the east due to a gentle structural dip (Figure 2.2). Only the Woodbend Group will be described in detail here. Other Groups/Formations are used in the construction of maps or cross sections.

2.1 Woodbend Group

The Upper Devonian Woodbend Group can be interpreted as a series of rapid upbuilding of shelf and reefal sediments, followed by a phase dominated by the progressive infilling of basinal areas by shales and marlstones (Switzer et al., 1994). Five stages have been established across the Western Canada Sedimentary Basin. In north-eastern Alberta, the Woodbend Group consists of 4 formations. In

a time ascending order, they are: Cooking Lake Formation (marine shelf & ramp carbonates), Ireton Formation (basin-filling shales), Leduc Formation (reefal buildups), and Grosmont Formation (marine platform carbonates).

2.1.1 Cooking Lake Formation

The Cooking Lake Formation is dominated by extensive sheet-like shelf carbonates (Switzer et al., 1994). With only local exceptions, it is conformable with the underlying Beaverhill Lake Group. The Cooking Lake carbonates consist of peloidal and skeletal limestone (brachiopods, crinoids, stromatoporoids, and bryozoans). Thick, extensively dolomitized Cooking Lake strata are found beneath the Rimbey-Meadowbrook Leduc reef trend and its southerly extension into the Caroline-Cheddarville region (Switzer et al., 1994). The Cooking Lake Formation extends in a north to northeast direction and subcrops in the study area (e.g., Township 92). However, no core penetrating this formation has been found in the study area.

2.1.2 Leduc Formation

The Leduc Formation built up reefs on the Cooking Lake Formation, and is famous for its huge conventional oil and gas reserves. Basin-wide, the Leduc Formation can be divided into three distinct reef

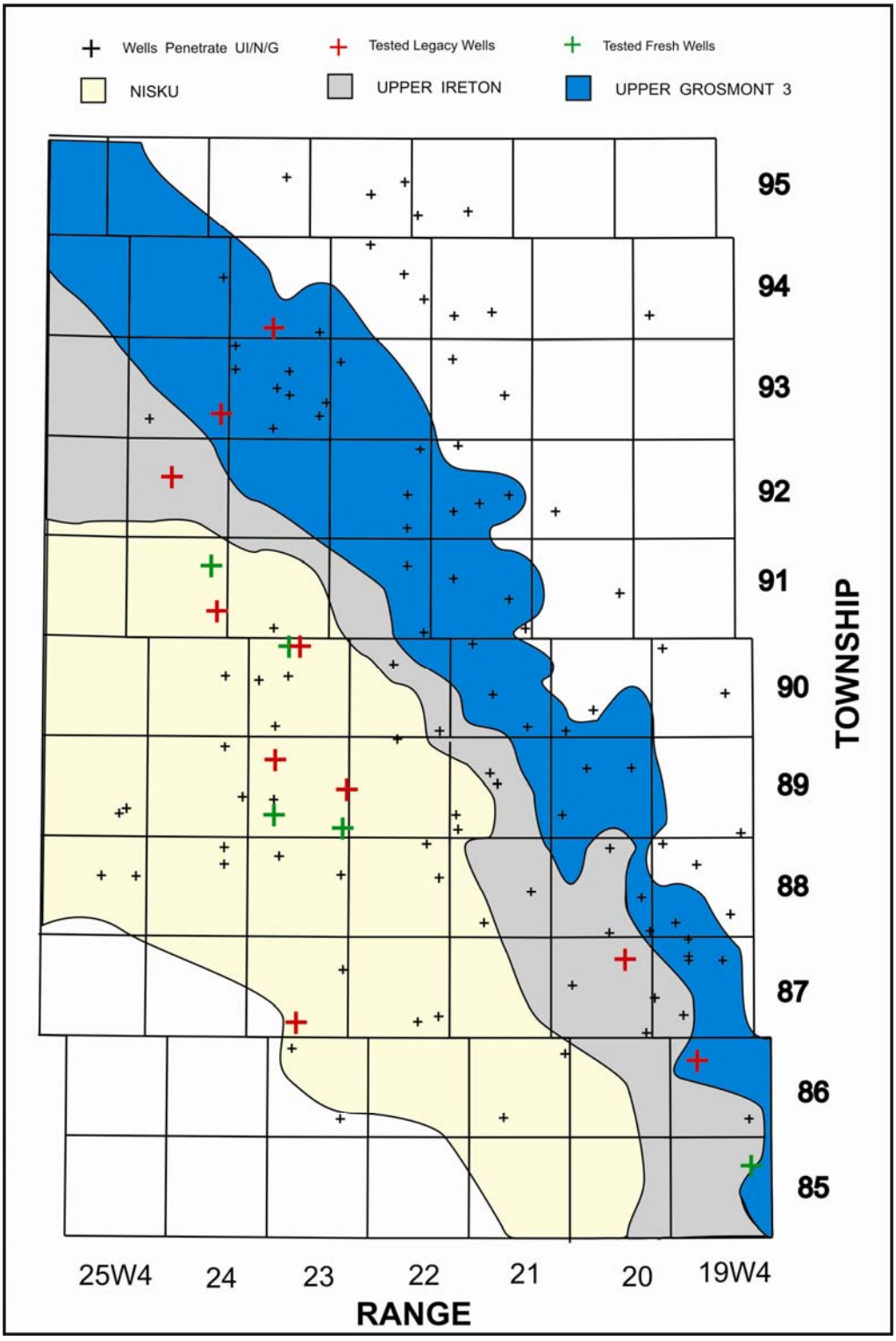

Figure 2.1 Subcrops of Nisku, Upper Ireton, and Upper Grosmont 3 in the study area. Data are from Dembicki (1994).

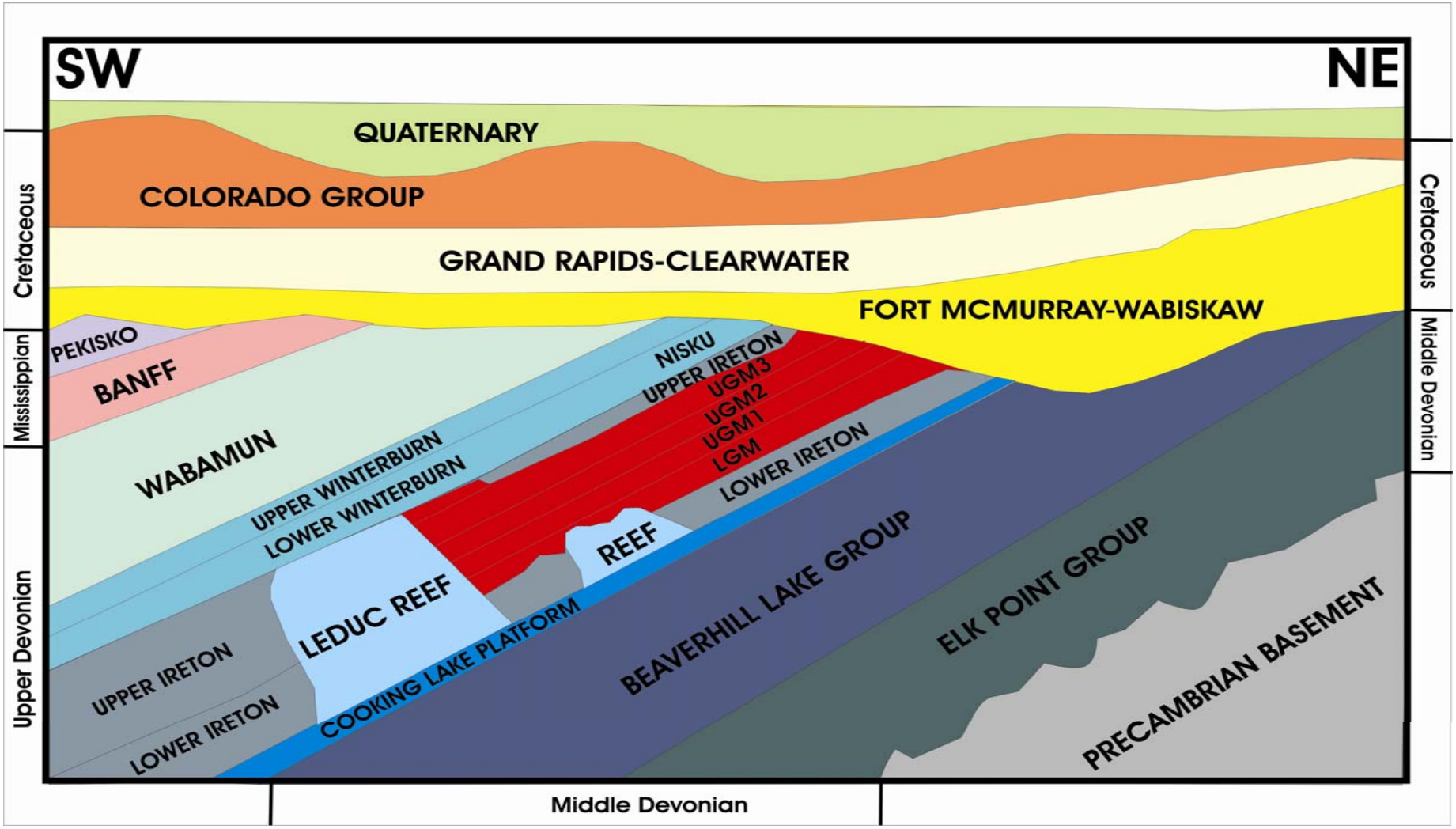

Figure 2.2 Stratigraphic nomenclature in northern Alberta. Modified from Buschkuehle et al. (2007).

stages (i.e. the Lower, Middle and Upper Leduc.), corresponding to the Majeau Lake, Duvernay, and Lower Ireton basin-filling depositional intervals (Switzer et al., 1994). However, the reef growth pattern varies across Alberta. In the study area, the Leduc Formation buildups represent the northern extension of the Rimbey-Meadowbrook reef trend, and are conformably overlain by Grosmont Formation Platform carbonates or by the Ireton Formation calcareous shales and carbonates.

2.1.3 Ireton Formation

The Ireton Formation generally consists of basin-filling calcareous shales and can be divided into Lower and Upper Ireton by the so-called "Z" marker (Stoakes and Wendte, 1987). The Lower Ireton encloses the Leduc reefs or conformably overlies the Cooking Lake Formation (Figure 2.2). The Upper Ireton is the last depositional sequence of the Woodbend Group and represents the most voluminous influx of fine-grained siliciclastics during the Paleozoic (Switzer, 1994). In the study area, where it is not eroded, the Upper Ireton conformably overlies the Grosmont Formation. A large portion of the Upper Ireton Formation is saturated with bitumen.

2.1.4 Grosmont Formation

The Grosmont Formation makes up the a northwest-southeast trending Upper Devonian shallow marine carbonate platform complex in north-central Alberta, which is approximately 150 km wide and at least 600 km in length, covering an area of approximately 100,000 km^2 in the subsurface of Alberta (i.e., Townships 60 to 108 and Ranges 1W4 to 15W5) (Harrison, 1982). The western and southern limits of the Grosmont complex are defined by the depositional changes from platform carbonates into basinal marls of the Ireton Formation. To the east, the platform is bordered by the sub-Cretaceous unconformity, and it crops out along the Peace River in the Vermilion Chutes area and along Harper Creek (Buschkuehle et al., 2007). To date, the northern limit is poorly known due to a lack of well control.

Chronostratigraphically, the Grosmont Formation is equivalent to the Middle and Upper Leduc in other areas of the Alberta Basin. Based on three marl layers called “shale breaks”, the Grosmont can be subdivided into four units, i.e., the Upper Grosmont 1, 2, and 3 (UGM 3, UGM 2, UGM 1), and the Lower Grosmont (LGM), each corresponding to a shallowing-upward cycle (Harrison & McIntyre, 1981; Harrison, 1982, 1984). The Grosmont Formation is generally overlain by calcareous shales of the Upper Ireton Formation, but locally rests directly upon a Leduc reef buildup (e.g., Theriault, 1988).

2.2 Winterburn Group

The Winterburn Group represents continued basin-filling in the late Frasnian. In the study area, the Nisku Formation conformably overlies the Upper Ireton Formation of the Woodbend Group, which in turn is conformably overlain by the Calmar Formation of the Winterburn Group, or truncated by the Cretaceous Unconformity (Figure 2.2). The Nisku Formation has a lithology similar to the Upper Grosmont, which is mainly composed of vuggy dolostone. Its thickness is more than 100 m in the southwest of the study area, where it is not eroded.

2.3 Previous Work

The Grosmont Formation was first described by Belyea (1952) as a "*widespread biostromal coquinoid limestone and dolomitized limestones and associated reefs" with "coarse vuggy porosity.*" In 1963, Norris examined the Grosmont outcrop along the northwest bank of the Peace River within the Vermillion Rapids, and described it as "*a pale brownish grey, pale bluish grey to dark grey, fine grained, granular, coarsely vuggy, massive dolomite of probable reef origin. The vugs vary in size up to about an inch in diameter and in places contain black bitumen of tar-like consistency.*" (Norris, 1963).

Union Oil Company of Canada Ltd. has been active in the evaluation of Grosmont since the late 1960s and began field testing in 1975. Vandermeer and Presber (1980) released the results of an initial investigation carried from the Baffalo Creek 14-05-88-19W4M pilot site and divided the Grosmont into the 4 stratigraphic units: Upper Grosmont 1,2,3 and Lower Grosmont. The field test at this site showed a maximum production of 80 m^3 (500 bbl) of clean bitumen daily by "soak and drive" method. The API gravity of the bitumen was reported to be 7°. A following reservoir simulation study of the pilot (Cordell, 1982) documented the viscosity at reservoir conditions was about 1.6 million cP.

Further geological investigation results around the pilot site were summarized by Harrison and McIntyre (1981) and Harrison (1982, 1984). They accepted the stratigraphy developed by Union and concluded that the Grosmont is a regional carbonate platform that comprises a succession of shallowing upward depositional cycles of varying magnitude. Detailed study within the pilot project area showed that the upper portion of the Grosmont is characterized by high porosities, averaging between 19 and 25 percent, permeabilities of several darcies, and bitumen saturation in excess of 70 percent.

Based on an intensive study of stratigraphy and sedimentology in the southern part of the Grosmont Formation (Townships 55-75,

Ranges 12W4M-8W5M), Cutler (1983) proposed an idealized lithofacies sequence for the Grosmont platform, in ascending order: 1) green calcareous shales, 2) nodular argillaceous wackestones, 3) coral-stromatoporoid floatstones, 4) *Amphipora* wackestones, 5) peloid packstones, and 6) laminated mudstones.

In 1986, the Alberta Research Council (ARC) released two Open File Reports (i.e., Walker, 1986 and Yoon, 1986) that include a series of structure contour, isopach, erosional edge maps in an area of Townships 66–100 and Ranges 13W4M–9W5M, and hydrocarbon pore volume (HPV) maps on a smaller area (Townships 88–98 and Ranges 19W4M–26W4M).

The initial diagenesis studies were conducted by Theriault and Hutcheon (1987) and Theriault (1988) in an area of Township 86–98 and Range 16W4M–25W4M. They discussed the diagenetic history and its effect on the Grosmont reservoir properties, especially with relation to porosity and bitumen saturation. The most comprehensive reservoir studies to date were carried out by a group from the University of Alberta, namely Dembicki (1994), Dembicki et al. (1994), Luo et al. (1994), Luo and Machel (1995), Huebscher and Machel (1995a, b; 1997 a, b), and Dembicki and Machel (1996). These studies show that the reservoir rocks in the Grosmont Formation are heterogeneous karstified dolostones. High porosities (up to 40%) and permeabilities (up to 30,000

mD) were found to be related to dolomitization and later karstification, which are the two most important diagenetic events that control the extremely heterogeneous nature of the Grosmont Reservoir. Karstified intervals were found to be restricted to the Grosmont subcrop edge beneath the sub-Cretaceous unconformity. They are recognized as the prime hydrocarbon reservoirs due to their greatly increased porosity and permeability.

In recent years, led by ERCB, Alberta Research Council, and several companies that are working in this area (e.g., Shell Canada, Husky Energy, and Laricina), a new wave of research and development on the Grosmont reservoir is underway, represented so far by Buschkuehle et al. (2007), Alvarez et al. (2008), Hopkins and Barrett (2008), and Piron (2008). However, these studies are either merely literature reviews or studies on a very local scale (1 to 2 Townships), and they obtained quite similar results to those of the 1990s.

In terms of bitumen properties studies in the region, the majority of the published papers are focused on the Cretaceous oil sands (e.g. Larter et al., 2006). There are very few published bitumen viscosity data from the Grosmont reservoir (e.g., Cordell, 1982; Asgar-Deen, 2008). The only in-depth investigations on Grosmont bitumen are two organic geochemistry studies in the later 1980s. (i.e., Hoffmann and Strausz, 1987; Brooks et al., 1989), which will be discussed in a later chapter.

CHAPTER 3

BITUMEN RHEOLOGY

3.1 Introduction

Rheology is the study of the flow and deformation of matter. As a branch of physics, it reveals information about the flow behavior of liquids and the deformation behavior of solids (Metger, 2006). An important parameter in fluid rheology is viscosity. Viscosity is a measure of the resistance of a material to deform under either shear stress or extensional stress. In other words, viscosity describes a fluid's internal resistance to flow. Viscosity can be expressed as the following shear deformation model（Figure 3.1）:

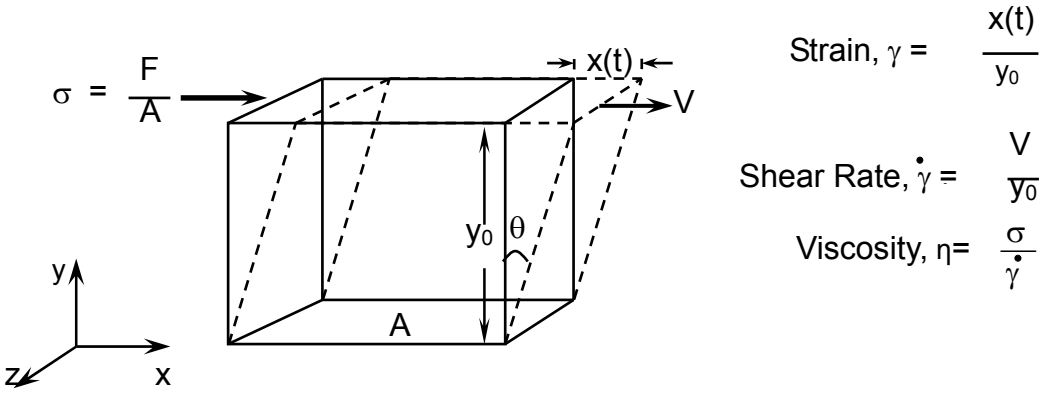

Figure 3.1 Definition diagram for shear deformation.

where:

σ (stress) = force per unit area, expressed as Pa (SI) or dyn/cm² (cgs)

γ (shear strain) = relative deformation in shear (no units)

$\dot{\gamma}$ (shear rate) = change of shear strain per unit time, expressed as s^{-1}

As shown in Figure 3.1, viscosity is mathematically expressed as the ratio between the shear stress applied and the corresponding shear rate generated. Using this expression, liquids are classified into Newtonian fluids and non-Newtonian fluids. In a simplified definition, a Newtonian fluid is an idealized fluid whose viscosity is constant; i.e., the shear rate is proportional to the shear stress that generates it. In general, liquids that display “Newtonian behavior” under a wide range of shear rates are said to be “Newtonian fluids”. Water, for example, is a Newtonian fluid. Many liquids, however, exhibit Newtonian behavior over only a very limited range of shear rate and these are known as “non-Newtonian fluids” (Figure 3.2). They can be further subcategorized into:

1. Non-Newtonian time dependent liquids: The viscosity of a fluid is dependent on shear rate and the time during which shear rate is applied. It includes: a) thixotropy, a decrease in viscosity with time under constant shear rate or shear stress followed by a gradual recovery when the stress or shear rate is removed; and b) rheopexy, an increase in viscosity with time under constant shear rate or shear stress followed by

a gradual recovery when the stress or shear rate is removed.

2. Non-Newtonian time independent liquids: The viscosity of a fluid is dependent on shear rate but independent of the time of shearing. It includes: a) shear thinning, a decrease in viscosity with increasing shear rate, also referred to as pseudoplasticity; and b) shear thickening, an increase in viscosity with increasing shear rate, also referred to as dilatancy.

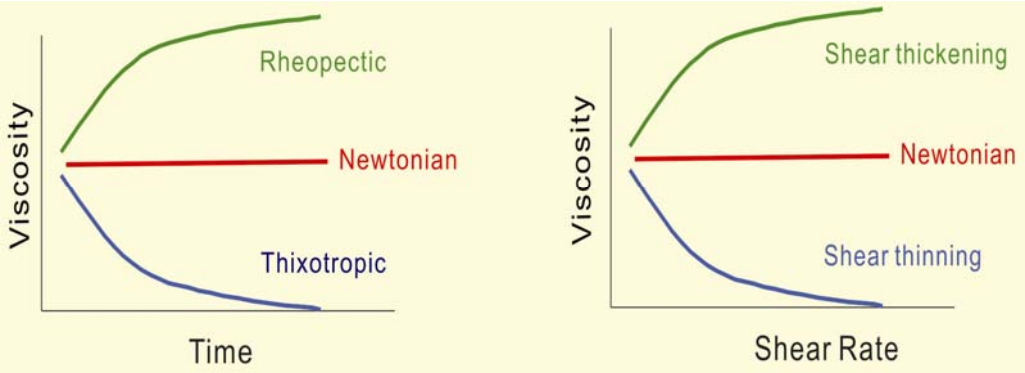

Figure 3.2 Schematic curves of different flow types.

Since the viscosity of a non-Newtonian fluid is not a constant value, the viscosity that presents at a specific shear rate is referred to as the "apparent viscosity" (η_a). Viscosities at very low and very high shear rates are called zero-shear viscosity (η_0) and infinite-shear viscosity (η_∞), respectively. Therefore, it is necessary to include shear rates in the context whenever discussing viscosities of non-Newtonian fluids.

In the literature, little attention has been paid to the flow behavior of natural bitumen. This is because: a) as a type of unconventional resource, bitumen has become a popular exploration target only relatively recently; b) many current bitumen exploitation activities are focused on shallow oil sands deposits using surface mining technology in Alberta. In this technique, the bitumen viscosity is more important at the hot water separation temperature of about 80°C where the bitumen is essentially a Newtonian fluid. Although bitumen properties have been found to vary significantly from site to site, the majority of samples are reported to show Newtonian behavior or only mild non-Newtonian behavior at or above room temperature (25–30°C), therefore, for practical purpose it appeared to be meaningless to further investigate flow behavior of these samples. Meanwhile, few studies paid attention to the flow behavior of Cretaceous oil sands at reservoir temperatures where the fluid potentially tends to become more non-Newtonian.

One objective of this study is to characterize the bitumen viscosity variations in the Grosmont reservoir at *in-situ* conditions, which means examining bitumen fluid properties on the most degraded oil known in Alberta at current formation temperatures (~11°C). As it turns out, the bitumen samples from the Nisku, Upper Ireton, and the Grosmont Formations exhibit different extents of non-Newtonian behavior, especially under low temperatures (<40°C). As a result, viscosity

determinations for bitumens under such conditions are not as straightforward as for Newtonian fluids, such as the many viscosities reported from oil sands bitumens at high temperatures. Therefore, in order to ensure that the viscosities obtained truly represents the *in-situ* conditions, the viscosity measurement method and the results of investigation of its rheological properties are documented in this chapter.

3.2 Previous Studies

The pioneer work on the rheology/viscosity of Alberta bitumen was conducted by Ward and Clark (1950). They obtained Athabasca bitumen samples from various sites and prepared them with their standardized method. Using a pressure driven capillary viscometer, they found that the bitumen from Athabasca oil sands is a Newtonian fluid at 84.4°F (29.1°C). Dealy (1979) studied bitumen extracted from Athabasca, Cold Lake, and Lloydminster and concluded that the bitumen samples studied were mildly non-Newtonian at 27.5°C, with a well established shear-thinning behavior observed from shear rates 0.1 to 1 s^{-1}. The total reduction of viscosity in this shear rate range was about 10%. Dealy (1979) also attempted to explain bitumen rheology with the theory used for asphalt viscosity; that is, viscosity variations

were considered to be the result of molecular aggregation. Schramm and Kwak (1988) investigated the rheological properties of Athabasca bitumen, bituminous froth, and mixtures of these with naphtha, and concluded that bitumen can, for practical purposes, be considered Newtonian in character at the hot water process temperature (80°C). The rheological properties of bitumen at lower temperatures were not investigated in their research. A recent description of bitumen rheology is provided by Ukwuoma and Ademodi (1999). Using Nigerian oil sands bitumen extracted by toluene, they examined the effects of temperature and shear rate on bitumen viscosity. The results showed that the bitumen was a non-Newtonian fluid with a shear thickening behavior, especially at low temperature (<30°C). Also, the bitumen became more Newtonian in the higher temperature region.

Although few studies focus specifically on bitumen rheology, a large number of rheology studies on similar hydrocarbon types, i.e., heavy oil and asphalt, can be found in the literature. Since their composition is quite similar, some important conclusions from these two fields are presented here for further comparison and future reference.

Most heavy oils are Newtonian fluids at ambient temperature; consequently, heavy oil rheology studies are generally investigations of the effects of different factors such as solvent concentration, maltene, and asphaltene content on heavy oil viscosity (e.g., Henaut et al., 2001;

Luo and Gu, 2006). For example, Henaut et al. (2001) examined the effect of asphaltene content on rheological properties of heavy crude oils and concluded that the heavy oils studied were Newtonian fluids under various temperatures. Nevertheless, while Newtonian behavior is obvious at higher temperatures (40°C to 80°C), only limited shear rate data (from 0.01 s^{-1} to 0.1 s^{-1}) were presented for 3°C and 20°C; these data were not sufficient to prove that the samples studied were Newtonian liquids under those temperatures. Similarly, although it is convincing to see that viscosity increased with an increasing percentage of asphaltene content from 0% to 18%, only the Newtonian part of the viscosity–shear rate data was plotted. It seems that at certain temperatures, with increasing asphaltene content, the shearing effects on viscosity increased, that is, the heavy oil became more non-Newtonian. Pierre et al. (2004) were the first (that the author is aware of) to show the shear-thinning behavior of heavy oil at low temperatures (below 10°C) and the influence of asphaltenes on shear-thinning behavior (at 0°C).

Asphalt rheology is more advanced as compared to heavy oil and bitumen rheology, simply because the rheological behaviors of asphalt under various conditions (temperature, time, degree of loading, etc.) are crucial for the characterization of this paving material. Some important conclusions are summarized below.

a) Asphalts often exhibit Newtonian behavior at or near the conventional mix temperature of 60°C. However, when tested at lower temperatures and low shear stress levels, they generally exhibit shear-thinning flow behavior (Tia and Ruth, 1987).

b) Because of the viscoelastic nature of asphalts at intermediate and low temperatures, viscosity is not an absolute value. Recognition of the complexity of asphalt rheological properties and drawbacks of single-point measurements has led many researchers to propose various temperature susceptibility parameters and shear susceptibility parameters to describe the behavior of asphalts (e.g., Bahia and Anderson, 1995).

c) The rheological properties of asphalts are governed by the interaction of individual constituents, so that asphalts can be treated and explained as a colloidal system (Loeber et al., 1998). However, there is limited agreement about which part of any asphalt plays the most important role in its overall rheological behavior (Michalica et al., 2008, and references therein).

3.3 Measurement of Rheological Properties

In this study the rheological behavior of bitumens was determined using AR-G2 Rheometer. The AR-G2 Rheometer is a combined motor

and transducer (CMT) rheometer designed by TA Instruments (Figure 3.3). The body of the rheometer is a single piece aluminum casting consisting of a base and a column. The head of the rheometer, which contains a drag cup motor, magnetic and air bearings, and an optical encoder, is attached on a ball slide that is mounted within the instrument. A draw rod connected to the motor goes through the head from top to bottom, forming the rotating spindle of the rheometer. Various units can be attached to the threaded bottom end of the draw rod. A standard temperature control system, called “Peltier plate”, is mounted on the base of the casing. Using the Peltier thermoelectric effect, the Peltier plate can control the temperature accurately, with rapid heating and cooling. Since the temperature applied in this investigation is from 11°C to 80°C, water is used as a coolant (constantly pumped through the plate from an external tank). A normal force transducer is mounted on the lower stage to determine the normal stress produced from shearing the sample.

Torque is generated when the cup is dragged round by the magnetic rotating field, which is formed by continuously varying the current supplied to stationary pole pieces surrounding the cup. The angular velocity exerted on the rotating spindle as a result of the fluid deformation is detected by an optical encoder and is then transmitted to the motor for torque adjustment until the torque produces the required

angular velocity. Magnetic and air bearings are used to keep the rotation virtually friction-free. This instrument allows for the determination of shear stress up to 95490 Pa and shear rates up to 8556 s^{-1}. The precision of the system can be taken to be at least ±5%, and is routinely calibrated using standard mineral oil provided by Cannon Instruments.

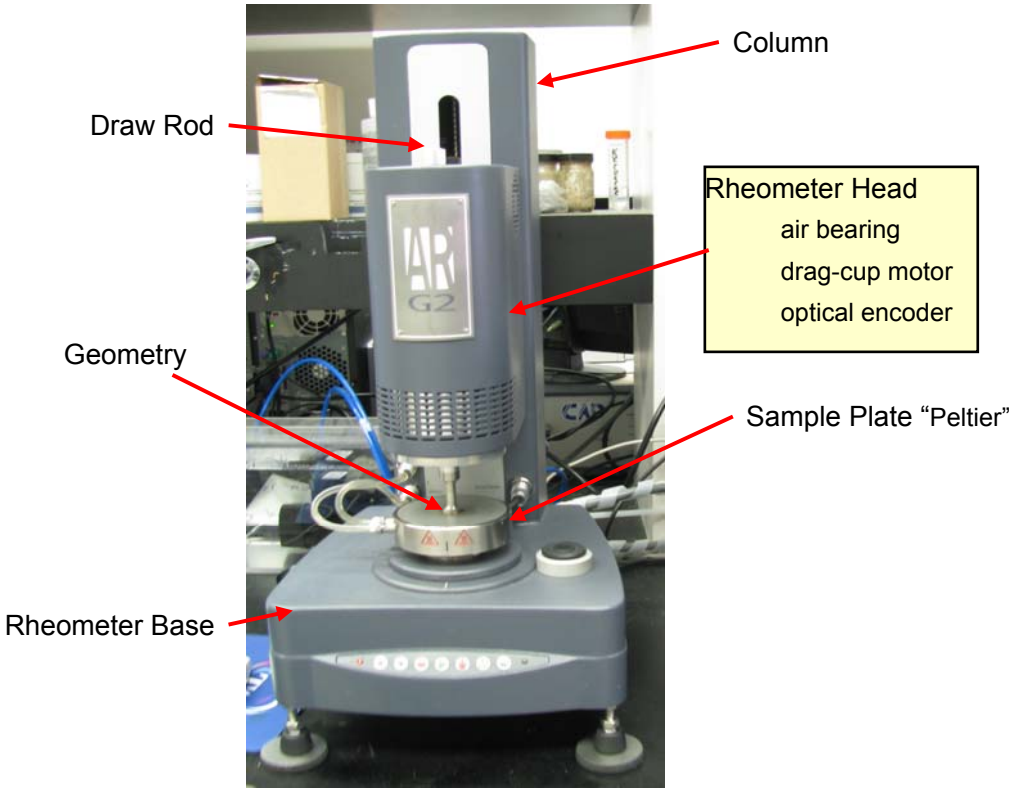

Figure 3.3 AR G2 Rheometer

All the bitumen samples used in this study were extracted by the Dean-Stark extraction (Speight, 2007) using toluene and/or dichloromethane. The extracted bitumens were placed in wide-mouth glass under a fume hood at room temperature for 3 to 7 days to

evaporate the solvent. Occasional stirring was needed to remove all the solvent, as bitumen can trap solvent once it becomes thick. A cone and plate geometry (2 cm in diameter, 2° cone angle) was used as the geometry for all the tests. This is the most suitable geometry for measuring highly viscous fluids like bitumens (Mezger, 2006) as it can generate high and homogenous shear rates in the entire conical gap. A major benefit was that only 0.2 ml bitumen was needed to fill the gap in each test.

Sample loading is critical for obtaining accurate measurements. Both overfilling and underfilling will result in the non-representative values and accurate filling can be difficult to achieve in practice. As a result, the following steps were used for sample loading: 1) Because of the high viscosity of bitumen at room temperature, sample bottles were preheated to 40°C to 60°C in hot water to enable loading on the Peltier plate. 2) The samples were overloaded slightly on the center of the Peltier plate, and then the cone was imposed on top of the load with a preset gap. 3) The extra sample flush with the rim of the cone was trimmed to obtain the correct filling at 80°C with the geometry rotating at a velocity of 2 rad/s.

In this investigation, a wide range of shear rates (0 s^{-1} to 1000 s^{-1}) was applied on bitumen by the “steady state shear procedure”. That is, at a certain temperature, the bitumen was deformed at a series of shear

rates under the selected shear rate range, and the viscosities were recorded. The rheological behavior of bitumen was routinely monitored at 20°C, 40°C, 60°C, and 80°C. Lower temperature could not be investigated, as many carbonate bitumens (bitumens from the Grosmont reservoir) became too sticky to be sheared below 20°C. A second run at 40°C on the same load of sample was conducted immediately after the completion of the previous 4 temperature tests, in order to check the accuracy and consistency of the data, and to avoid errors caused by evaporation, aging, and thermal gradients in the samples. Finally, data for shear stress, shear rate, viscosity, equilibrium time, temperature, normal stress, and torque were collected.

3.4 Rheological Properties of Carbonate Bitumen

It is well known that solvent concentration, temperature, and compositions such as asphaltene content have a great impact on bitumen viscosity (e.g., Ward and Clark, 1950; Dealy, 1979; Adams et al., 2008). However, some of the data obtained from carbonate bitumen samples appeared to be quite different from the results described in clastic deposits (e.g., Dealy, 1979; Ukwuoma and Ademodi, 1999). These differences could be caused by different bitumen origins, different sample preparation methods, and differences in or limits of the

equipment used. For example, under the same conditions, the Athabasca oil sand bitumens exhibit much more Newtonian character than the bitumens from the Grosmont reservoir (Figure 3.4).

It is worthwhile to define the overall rheological properties of the bitumen samples studied before presenting their viscosities in relation to other factors. As shown in this chapter, the shear rate–viscosity relation varies significantly with experimental conditions, as do the shear rate ranges that yield zero-shear viscosity. As a result, measuring viscosity under a single shear rate is insufficient to establish the “innate” viscosity. Indeed, until now, many commercial labs and published papers fail to report the shear rate–viscosity relations, and/or do not report the shear rate under which the measurements were taken. This is insufficient to describe the viscosity of the bitumen, especially at low temperatures (below 40°C). This is one of the reasons why viscosities reported from different laboratories and different studies on the same material yield incompatible results (e.g., Miller et al., 2006; Adams et al., 2008).

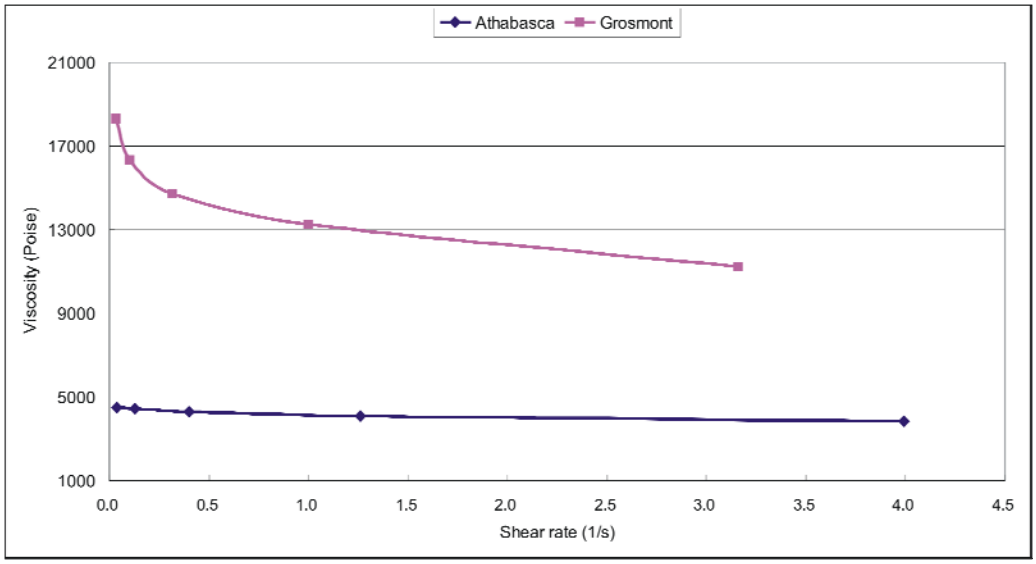

Figure 3.4 Comparison of the rheological behavior of oil sands bitumen from Athabasca and carbonate bitumen from Grosmont at 20°C. Within the same shear rate range, the viscosity of the Grosmont bitumen drops significantly, indicating a non-Newtonian behavior under such conditions. The oil sands bitumen behaves like a Newtonian fluid, as its viscosity remains constant.

3.4.1 Shear susceptibility of carbonate bitumen

A typical time–viscosity plot and a shear rate–viscosity plot of a bitumen extracted from the Grosmont reservoir at 40°C are shown in Figure 3.5 and Figure 3.6. From a rheological point of view, this bitumen could be described as a non-Newtonian time independent liquid with a shear-thinning behavior at 40°C. In general, under the same temperature, the rheological behaviours of the other carbonate bitumen samples were quite similar to this sample and could be divided into 4

“stages”:

1. Anomaly stage (Stage 1). The viscosities measured at very low shear rates (expressed as $\eta_{-\infty}$, generally less than 10^{-3} s^{-1}), are commonly unstable. This is suspected to be caused by the limits of the equipment and the heterogeneity of the bitumen, which is very difficult to equilibrate under very low shear rates.
2. Zero-shear viscosity stage (Stage 2). At a low to moderate shear rate range (0.002–0.8 s^{-1} in this case), the bitumen reaches a high plateau. It is the first Newtonian region where viscosity is comparatively even; this is commonly referred as zero-shear viscosity (η_0).
3. Apparent viscosity stage (Stage 3). At a point, the viscosity falls off rapidly in a very wide range of shear rates, usually beyond the setup limits (500–1000 s^{-1}), showing a distinct shear-thinning behaviour. The viscosity in this shear rate range is highly shear rate-dependent and is called apparent viscosity (η_a).
4. Infinite-shear viscosity stage (Stage 4). After decreasing, viscosity reaches a low plateau at a very high shear rate, called infinite-shear viscosity (η_∞). However, in most of the samples studied it is not possible to obtain the whole curve by cone and plate geometry, as the bitumen would spill out of the cone due to the strong centrifugal force applied at such a high shear rate (> 500 s^{-1}).

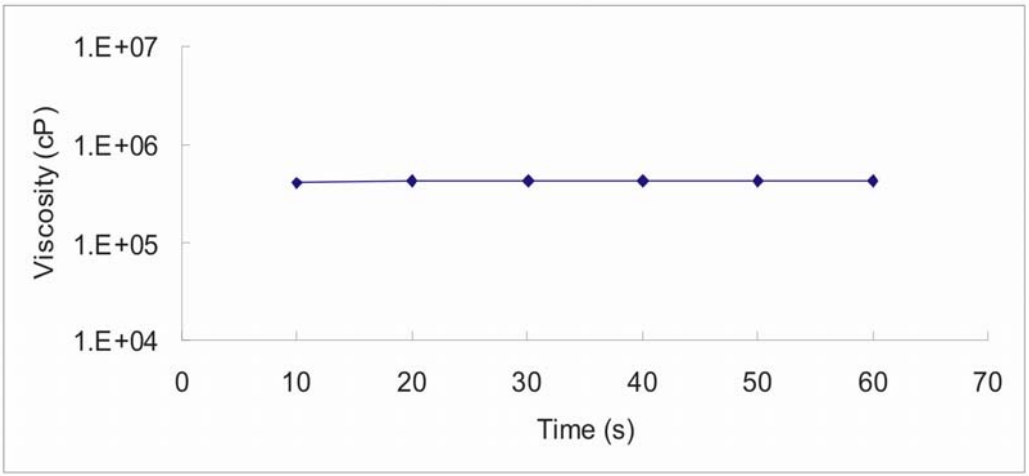

Figure 3.5 The time–viscosity plot indicates that the carbonate bitumens were time-independent. The data shown was taken on sample G3-35 at 40°C with a shear rate held at 0.1 s^{-1}.

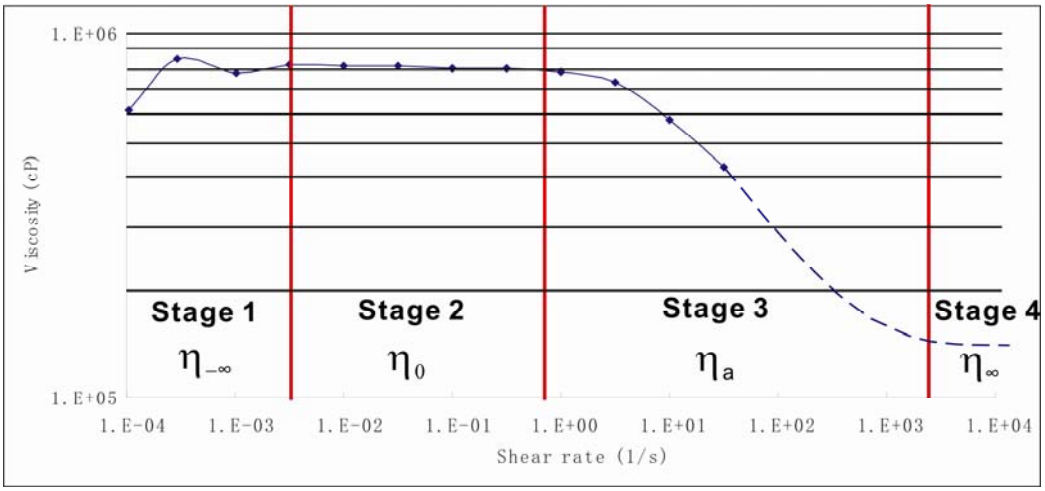

Figure 3.6 A typical base 10 logarithmic plot of the shear rate–viscosity relation for carbonate bitumen at 40°C. It shows four stages of increasing shear rate. Data are based on the results from sample G3-63.

The shear-thinning behaviour observed here is very different from Dealy`s data (1976). Instead of a narrow shear-thinning region (0.1 to 1 s^{-1}) and a total reduction of viscosity about 10% recorded in the Athabasca bitumen at 27.5°C, the shear-thinning region of carbonate bitumen ranges from a shear rate of 1 s^{-1} to more than 1000 s^{-1} at 40°C, and the viscosity reduction is more than two orders of magnitude. This clear difference is most probably caused by the limits of the equipment used 30 years ago: while the viscosity-shear rate relation could be examined in only a very narrow shear rate range (0.05 to 10 s^{-1}) in the 1980s, it has a much wider applicable shear rate range nowadays (0 to +1000 s^{-1}).

The shear-thinning behaviour of bitumen can be best explained by using the entanglement model developed in polymer rheology (Mezger, 2006) and by regarding asphalt as a colloidal system (Loeber et al., 1998). Without an external load, macromolecules like asphaltene in bitumen are entangled with neighbouring molecules, and different components in the bitumen exist in the form of aggregates that exhibit complex structures. During the shearing, a certain number of such macromolecules become oriented in the shear direction, resulting in disentanglement, while others are recoiling and re-entangling. Meanwhile, the aggregates start to disaggregate as well (Stage 1, anomaly stage). The macromolecules and aggregates become stable

again under the shearing, and the flow resistance variation is very slight and the viscosity is almost constant (Stage 2, zero-shear viscosity stage). As the shear rate increases, the number of disentanglements and disaggregations becomes greater than the extent of re-entanglement, causing shear-thinning behaviour, which is the observed apparent viscosity stage (Stage 3). At a high enough shear rate range, most macromolecules, like asphaltenes, are oriented and disentangled, and all the aggregates are completely disintegrated. Therefore, flow resistance is reduced to a minimum value in accord with the infinite-shear viscosity stage (Stage 4).

In this study, zero-shear viscosity (η_0) derived from the zero-shear viscosity stage (Stage 2) is used uniformly as representative of the carbonate bitumen viscosity because it represents the maximum shear stress needed to initially force the fluid to flow. The zero-shear viscosity stage is defined by the following criteria: 1) it is composed of successive viscosity measurements that gently decrease with increasing shear rate; 2) the viscosity changes between two adjacent measurements are less than 5%; 3) the difference between the maximum and minimum viscosity measurements in this stage is less than 10%. The average viscosity of all the measurements in this defined stage is thus reported as the viscosity of the bitumen. As an example, the data source of Figure 3.6 is given in Table 3.1 and the zero-viscosity stage (the

highlighted rows) is selected based on the defined criteria. In Table 3.1, viscosity at 1.02E-03 s^{-1} is not selected because it does not meet criteria 1. Viscosity at 3.162 s^{-1} is not selected as the viscosity decreased more than 5% from 1 s^{-1} (criteria 2). The averaged viscosity, i.e. “803883” in the last row of Table 3.1, is used as the viscosity for this sample.

Table 3.1 Viscosity changes with progressively increasing shear rates in sample G3-63 at 40°C. The zero-shear viscosity range is highlighted; notice the anomaly viscosity data and the apparent viscosity data above and below. Data source of Figure 3.6.

shear stress (Pa)	shear rate （1/s）	viscosity（cP）	equilibrium time (s)*
0.06369	1.04E-04	610700	60.84
0.2489	2.94E-04	847800	115.9
0.7954	1.02E-03	779000	170.9
2.584	3.17E-03	816400	215.8
8.109	9.98E-03	812200	261
25.6	0.03164	809300	305.7
80.31	0.09999	803200	350.8
252.6	0.3162	798700	395.7
783.4	1	783500	440.8
2318	3.162	732900	485.9
5757	10	575700	550.9
13550	31.62	428600	615.6
Average		803883	

* This is the time needed for the rheometer reaching a steady reading. It is a cumulative value.

3.4.2 Temperature susceptibility of bitumen

Apart from the well recorded shear-thinning behaviour in all samples studied, it was noticed that there is a temperature-effect. Specifically,

with increasing temperature the shear rate range that yields zero-shear viscosity moves toward higher shear rates in a base 10 logarithmic plot; and is considerately widened if viewed on the numerical scale (Figure 3.7). For example, the viscosity of sample G3-63 with 0% solvent was measured under 20°C, 40°C, 60°C, and 80°C. The corresponding shear rate ranges that yield zero-shear viscosity increase approximately 10-fold for each 20°C increase. As a result, the shear rate range of zero-shear viscosity changes from 3.12E-04 s^{-1}—0.03 s^{-1} at 20°C to 1 s^{-1}—316 s^{-1} at 80°C. This is a 100-fold increase over a 60°C temperature rise. It is thus clearly shown that the bitumen transforms from a Newtonian fluid at 80°C to a non-Newtonian fluid at 20°C. It appears that higher temperatures lead to molecular relaxation and disaggregation, which allows more ease of movement among molecules in the bitumen. On the other hand, the greater Brownian motion at higher temperatures makes it harder to reach equilibrium under low shear rates. This can explain why the lower limits of zero-shear viscosity shift toward higher shear rates. These changes ease the internal friction and are together responsible for the observed high sensitivity of bitumen viscosity to temperature. As a result, the zero-shear viscosity of sample G3-63 decreased from 12,075,000 cP at 20°C to 5,907 cP at 80°C, a 2,000-fold decrease over this temperature range (Figure 3.8).

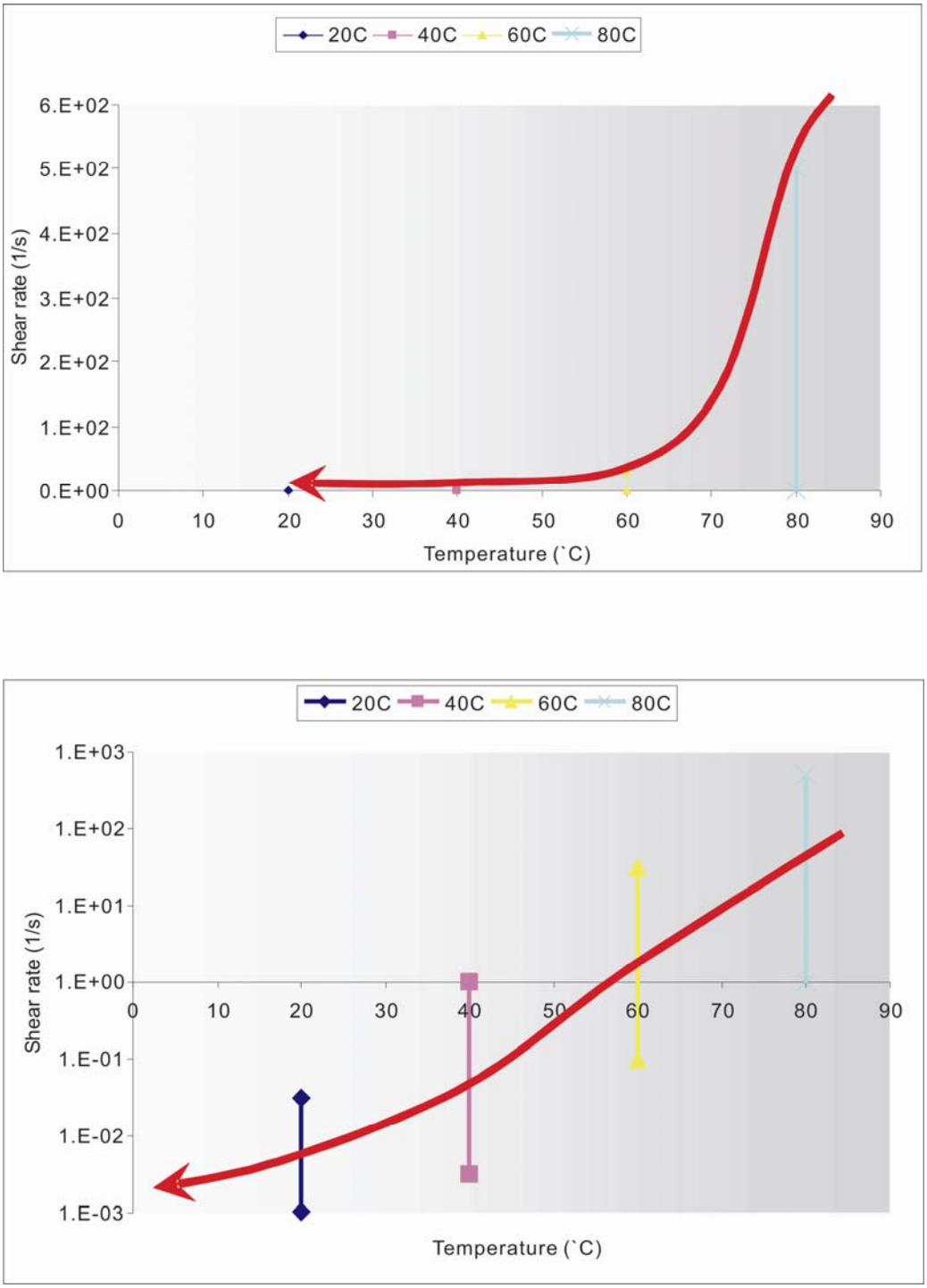

Figure 3.7 Temperature vs. zero-shear viscosity rates under numerical and semi-log plots showing a significant shrink of zero-shear viscosity range with deceasing temperature. It indicates that the bitumen tends to be more non-Newtonian at lower temperature. The results were reproducible in the repeated test at 40°C.

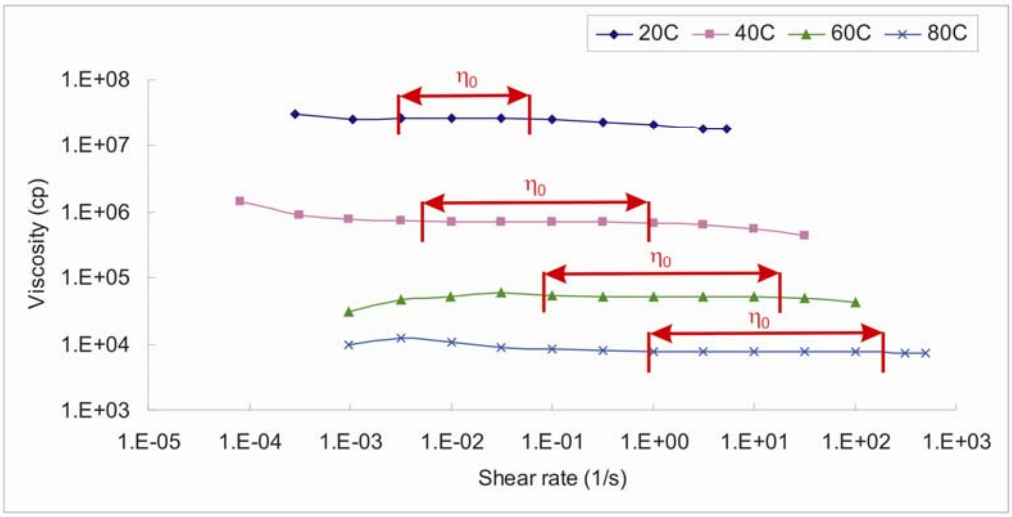

Figure 3.8 Log plots of shear rate vs. viscosity at various temperatures, showing the changes in the zero-shear viscosity range. This range migrated toward higher shear rates with rising temperature. The results were reproducible in the repeated test at 40°C.

These results are not unique. A study of bitumen samples from Nigerian oil sands by Ukwuoma and Ademodi (1999) also suggests that bitumen can behave as a non-Newtonian fluid. However, their data show that the apparent viscosity of bitumen increases with an increasing shear rate, exhibiting a shear-thickening behavior. At temperatures above 70°C, no linear relation between logarithmic viscosity and shear rate was found. These results are different from the results presented here, in that all samples from the Grosmont reservoir show distinct shear-thinning behavior under various temperatures. These differences could be caused by the compositional difference between samples or by an incomplete shear rate sweep (40 s^{-1} to 320

s^{-1}) used in the study of Ukwuoma and Ademodi (1999). Moreover, the nonlinear relationship between viscosity and shear rate at high temperatures (above 80°C) may be due to the evaporation of light ends. As shown in the thermal gravimetric analysis (TGA) in Figure 3.9, the loss of components becomes apparent (>0.2%) even in a “30 years old” bitumen sample (aged for 30 years in a core box) at temperatures higher than 100°C, which is expected to have lost all its light components. It appears inaccurate to monitor the original fluid behavior of bitumen at high temperature (>100°C).

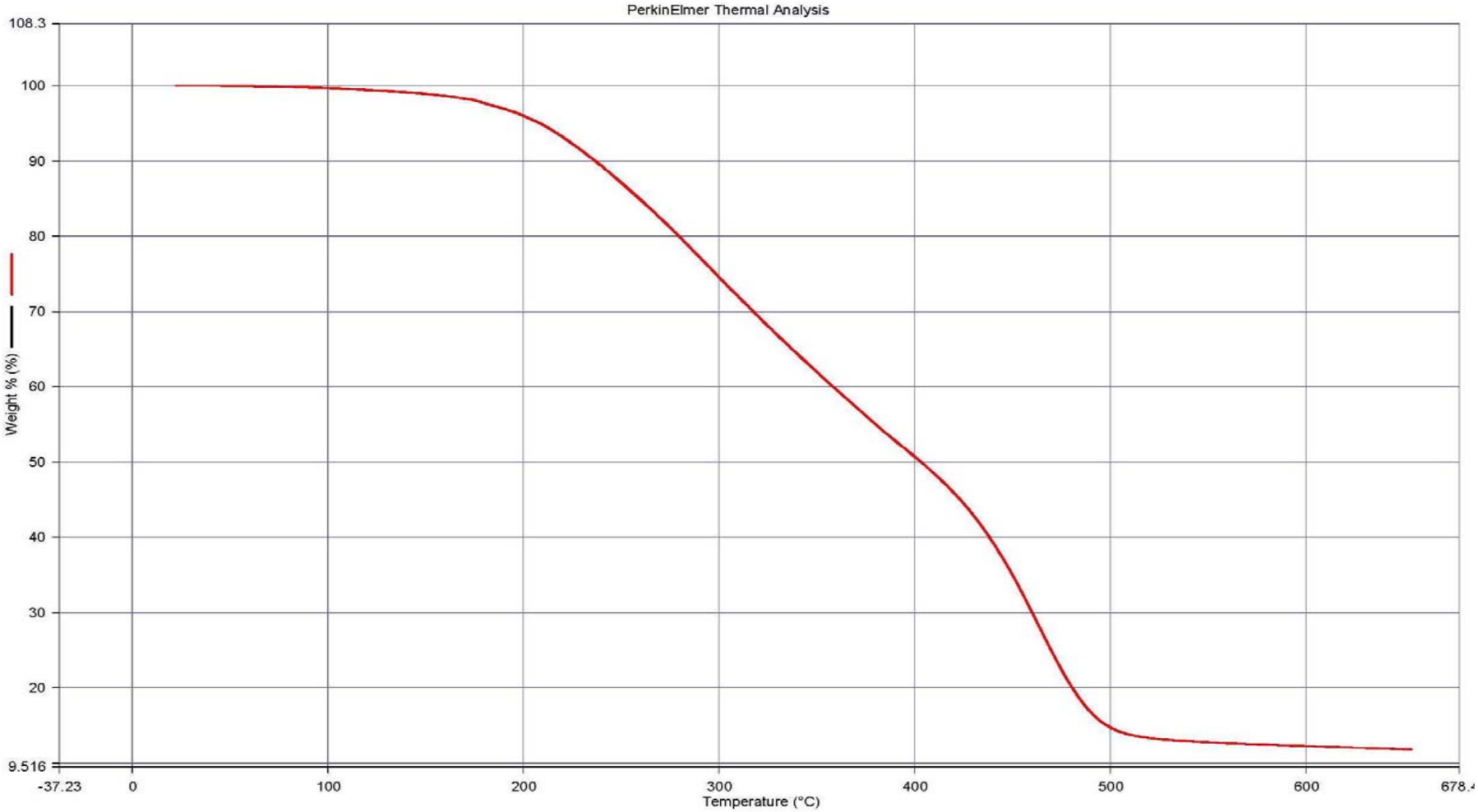

Figure 3.9 Thermal gravimetric analysis of carbonate bitumen, showing no evaporation below 100°C (< 0.2%). Viscosity measurements at higher temperatures are inaccurate because of loss of light components.

3.4.3 The effect of solvents on the rheological properties of carbonate bitumen

Residual solvents like toluene can have a strong influence on bitumen viscosity. In this study, solvents are found to be comparatively minor in importance in viscosity–shear rate relations. For example, sample N-57 (Figure 3.10) has an initial toluene concentration of about 9%. First, the viscosity was measured as a function of shear rate at 40°C, then the shear rate was reduced to the starting point and the measurement repeated (40C-Re curve). The viscosity increased significantly from 106,500 cP to 439,700 cP, a 4-fold increase in 30 mins. In this case, the sample at higher solvent concentration has a better Newtonian behavior and a “gentler” shear-thinning behavior compared to the same sample with less solvent. However, the shear rate limits that yield zero-shear viscosity is about the same for these two measurements. Similar trends were obtained for all other samples at 10%–9%, 1%–2%, and 0% solvent concentrations (e.g., Figure 3.11). Thus, it is clear that the shear rates of zero-shear viscosity stay in a similar range, while the viscosities are rising greatly. This phenomenon is attributed to the Newtonian nature of the applied solvent (toluene in this case), where a higher residual concentration of this solvent make the bitumen more Newtonian-like. The minor effect of solvent on the shear rates of zero-shear viscosity indicates that, at least at these

solvent concentrations, its impact on asphaltene entanglement and molecule aggregation is limited; the solvent probably acts mainly as a lubricant between entanglements and aggregations. Therefore, while the solvent reduces the viscosity significantly, the bitumen maintains similar rheological behavior.

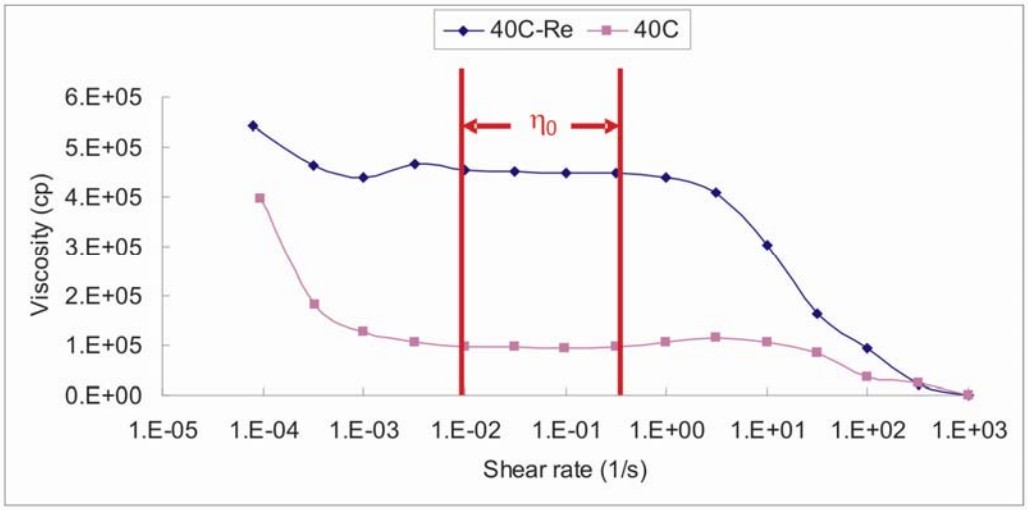

Figure 3.10 Sample N-57 had an initial toluene concentration of 9% and the tests were conducted on the same load of samples at 40°C. Significant changes were observed in viscosity overall, with only minor changes in the zero-shear viscosity shear range. “40C-Re” is the repeated test at 40°C.

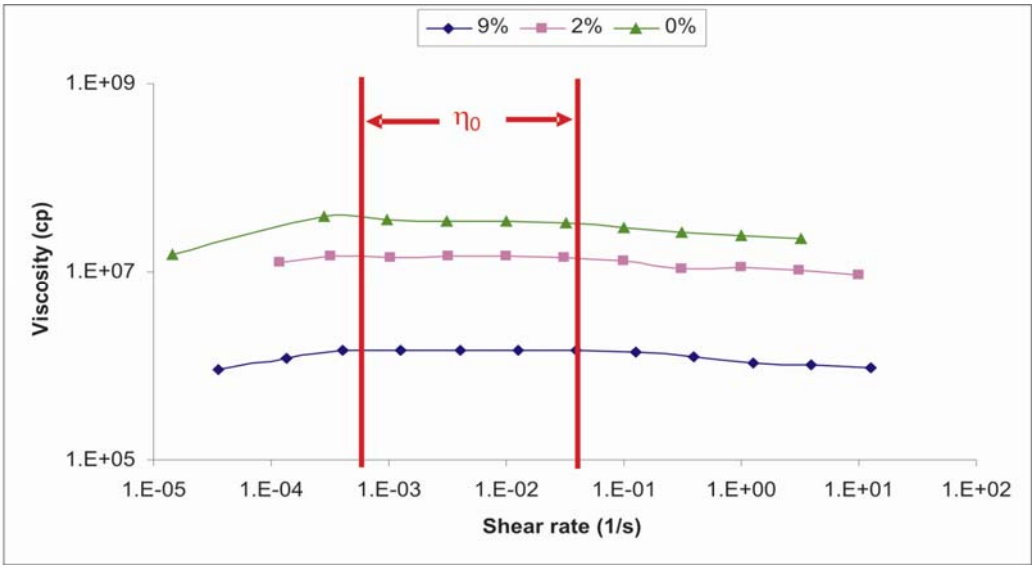

Figure 3.11 The shear rate–viscosity relation of sample UI-87 with different solvent concentrations at 20°C. The viscosity rose one order of magnitude from a 9% solvent concentration sample to the pure sample; the shear rate range of zero-shear viscosity did not change significantly.

3.4.4 The effect of sample origin on the rheological properties of carbonate bitumen

As shown in the previous comparison between Grosmont carbonate bitumen and Athabasca siliciclastic bitumen, the rheological behavior of bitumen samples from different resources may be quite different. Based on the data collected, bitumen samples from the Nisku, Upper Ireton, and the Grosmont formations exhibit similar shear rate–viscosity trends regardless of the depth, location, and stratigraphic unit. However, consistent differences can be found between legacy samples (20–30 years old) and fresh samples (1–2 years old), whereby fresh samples behave more Newtonian-like at the same temperature. As an example,

N-57 and N-77 are Nisku samples collected at similar stratigraphic depths from a legacy well and a fresh well respectively (about 10 km apart) (Figure 3.12). The fresh sample shows a much wider shear rate range of zero-shear viscosity than the legacy sample at 20°C, indicating a significant aging effect on the rheological behavior of the carbonate bitumen. As shown in Figure 3.13, apart from the aging of the samples, the location, depth, formation, host rock type, etc. have no apparent connection to the properties of carbonate bitumen samples collected from the study area.

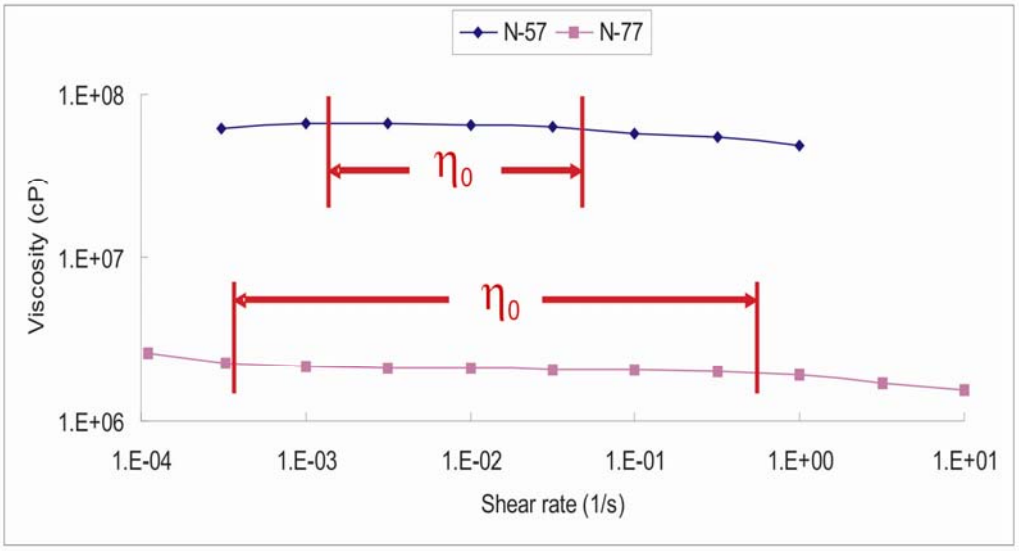

Figure 3.12 Shear rate – viscosity plots at 20°C. The fresh sample (N-77) shows much more Newtonian behavior than the old sample (N-57).

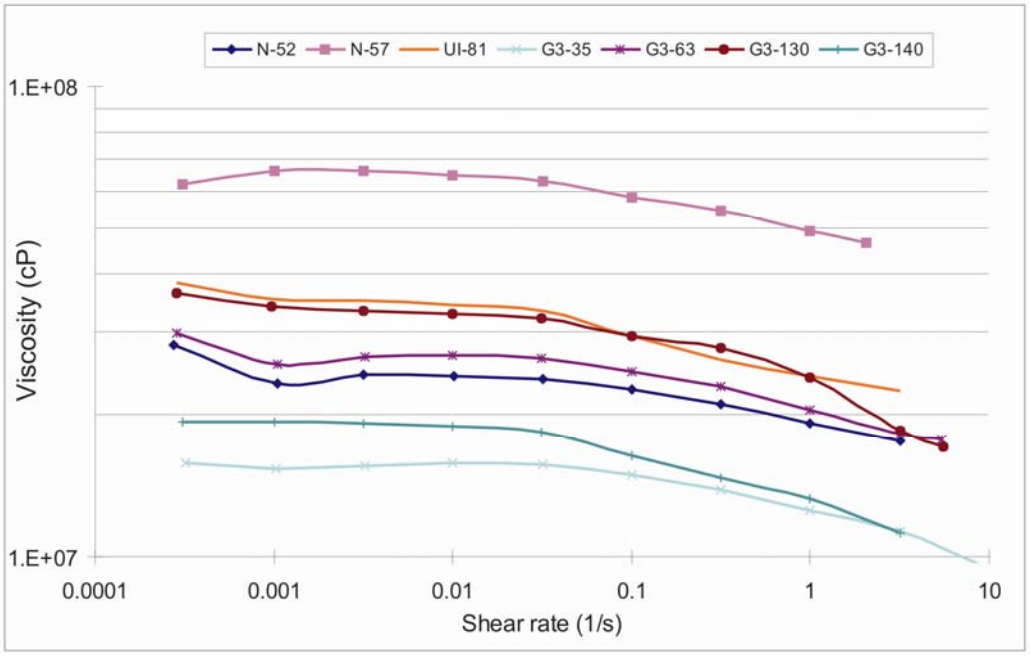

Figure 3.13 Shear rate–viscosity plots at 20°C for a series of legacy samples showing similar shear rate ranges of zero-shear viscosity (0.004–0.04 s^{-1}). Data can be found in Appendix 2.

3.5 Conclusions

All the carbonate bitumen samples studied behave like non-Newtonian fluids at low temperatures (<40°C), exhibiting a distinctive shear-thinning behavior. This is best explained as a disentanglement and disaggregation process of bitumen macromolecules under various shear rates.

Bitumen viscosity and other rheological properties are highly temperature-dependent. Decreasing the temperature of bitumen from 80°C to 20°C in this investigation rapidly changes the samples from a Newtonian to a non-Newtonian fluid. Consequently, it is concluded that

Grosmont bitumen behaves as a non-Newtonian fluid in nature under reservoir conditions (~11°C). Caution should be taken when measuring viscosity under low temperatures, and the shear rate applied should always be included when presenting viscosity data under such condition.

Processes that cause structural changes in the bitumen matrix, such as solvent concentration and aging effects, can alter bitumen's rheological character while leaving its shear-thinning behavior intact.

CHAPTER 4

BITUMEN VISCOSITY

4.1 Introduction

Heavy oils and bitumens are characterized by their high viscosity. Viscosity can vary significantly with depth and location in heavy oil and bitumen reservoirs (e.g., Ward and Clark, 1950; Erno et al., 1991; Miller et al., 1995; Larter et al., 2006) and variations in oil viscosity greatly influence the effectiveness of the chosen oil recovery process. As a result, viscosity is one of the most valued criteria in characterizing heavy oil and bitumen reservoirs and it is critical to map out the viscosity distribution in the reservoir. This task faces three major challenges: 1) how to obtain oil samples representative of the *in-situ* reservoir condition, 2) how to measure the viscosity correctly, and 3) how to predict the viscosity variations in the reservoir.

In this study, the samples are limited to the cores that are publicly accessible in the Core Research Centre, Calgary and their ages vary from 2 to more than 30 years old after drilling. It is fully recognized that the bitumen will go through a series of modifications after the initial coring, such as the loss of its gas fraction when the bitumen was

brought to surface and further weathering during storage. Thus, the viscosity analysis in this study is actually conducted on “dead oil” (contains no gas) with various degree of aging (challenge 1). By incorporating viscosity data obtained from direct measurement, geological concepts, and tools like geochemical data (Larter et al., 2006) and NMR logs (Bryan et al., 2005), viscosity variations in the reservoir can be at least partially predicted, monitored, and explained (challenge 3). However, viable interpretation is always based on accurately measured viscosity data (challenge 2). Indeed, until now, large discrepancy in viscosity measurements from different laboratories is still a common problem in heavy oil and bitumen reservoir characterization (e.g. Miller et al., 1995; Adams et al., 2008). In this study, bitumen samples were processed in 3 different laboratories for viscosity measurements and comparisons.

The objectives of this chapter are: 1) Quality control of the viscosity data, including comparing intra- and inter-laboratory viscosity results, and quantifying the extent of aging. All bitumen viscosities need to be corrected into one standard before examining the viscosity distribution in the Grosmont reservoir. 2) Investigation of the viscosity distribution characteristics and its controlling factors in the Grosmont reservoir, including vertical and lateral variations.

4.2 The Characteristics of Bitumen Viscosity

It is well documented that bitumen viscosity is very sensitive to factors such as temperature, solvent residue concentration, and asphaltene content (e.g., Ward and Clark, 1950; Adams et al., 2008). These factors can be summarized into two categories: 1) bitumen composition, and 2) physical alteration. Bitumen composition involves sample sources, sample aging and contamination, solvent residue in the samples etc., which are factors that are hard to control. On the other hand, physical alteration can be comparatively well manipulated in the laboratory, and include extraction and evaporation methods, experimental temperature and pressure, equipment and geometry, and analytical procedure. As shown in Chapter 3, shear rate and temperature play critical roles in determining the value of zero-shear viscosity, which is used as the defining viscosity of Grosmont bitumen in this study. The effects of temperature and solvent concentration on the zero-shear viscosity of Grosmont bitumen are quite similar to their effects on the viscosities of other heavy oils and bitumens, due to their similar composition. These effects are briefly described below.

It is well documented that bitumen viscosity decreases exponentially with increasing temperature (e.g., Ward and Clark, 1950). This trend is also observed in the zero-shear viscosities of Grosmont bitumens. For example, the viscosity of the 0% solvent sample of UI-81 declines from

3.44E+07 cP at 20°C to 9.95E+03 cP at 80°C, a 3000-fold decrease in a 60°C temperature range (Figure 4.1). Similar to the heavy oils and bitumens elsewhere, the Grosmont bitumen viscosity is also highly sensitive to solvent concentration. As shown in Figure 4.1, at 20°C, the viscosity at 9% solvent concentration is an order of magnitude lower than the viscosity at 1% solvent concentration, and 30 times smaller than the viscosity at zero solvent concentration. With increasing temperature, the viscosity difference between these samples becomes smaller, indicating that the temperature has a greater effect on higher viscosity samples. However, at 80°C, the viscosity of the zero-solvent sample is still 2 to 3 times larger than the 9% solvent sample. The viscosity of bitumen from the Grosmont reservoir is generally the highest as compared to the other bitumens from the Western Canada Sedimentary Basin (Figure 4.2).

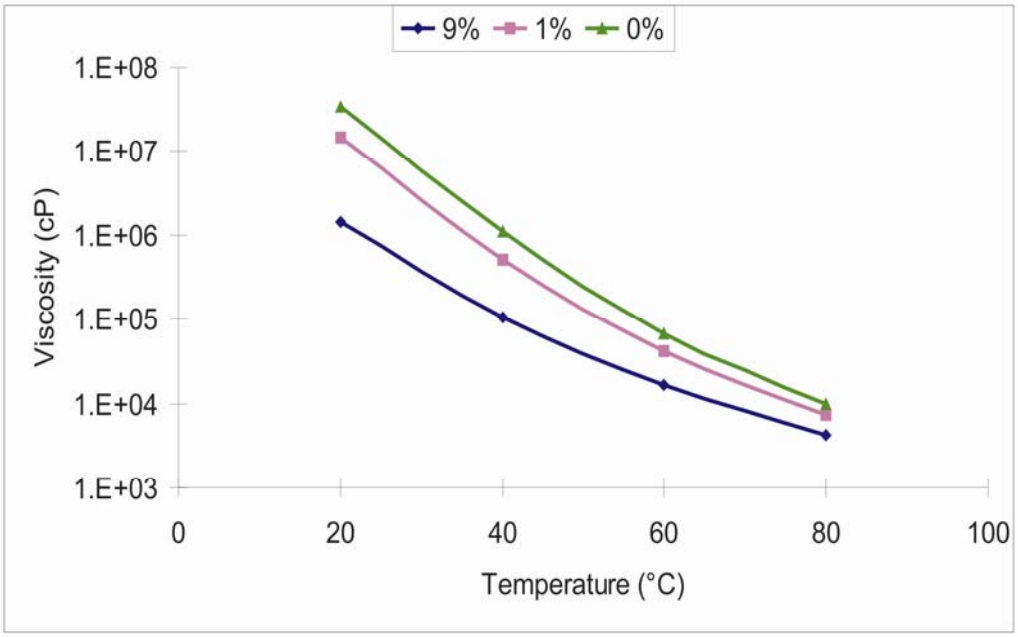

Figure 4.1 Temperature–Viscosity relations of sample UI-81 at various solvent concentrations.

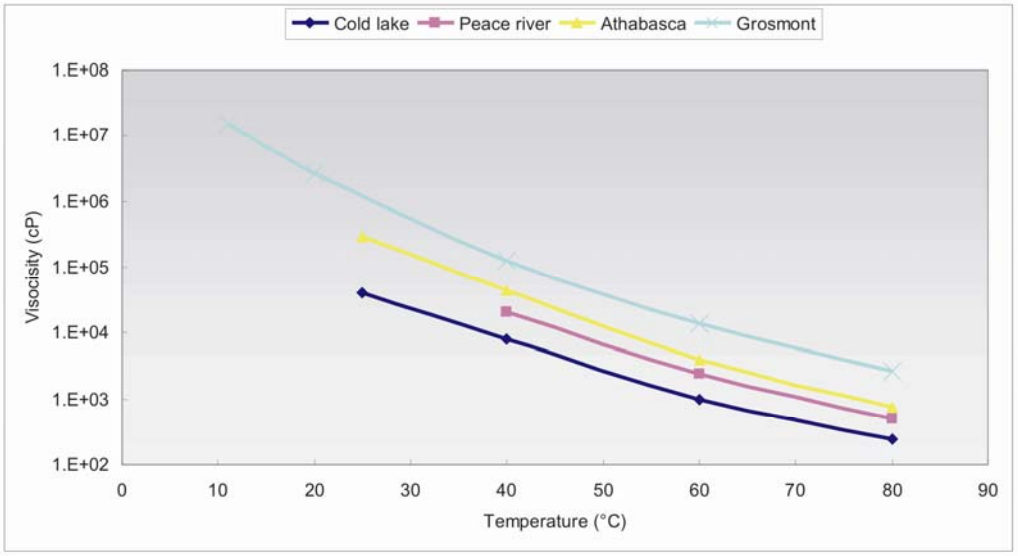

Figure 4.2 Temperature–Viscosity relations for bitumens from Cold Lake, Peace River, Athabasca, and the Grosmont Formations. Viscosities of Grosmont bitumen plotted here were measured on samples extracted from a 1.5 year old core. The viscosities of fresh samples from Grosmont are expected to be lower but still would be the highest viscosity examined. The other viscosities are measured on fresh bitumens (Hepler and Chu, 1989).

4.3 Intra-laboratory Comparisons of Viscosity Measurements

In the design of the viscosity measurement, several procedures were used to minimize the analytical error and improve the consistency of results. First, viscosity was routinely measured at 20°C, 40°C, 60°C, and 80°C. Some samples were also measured at 11°C and/or 30°C for calculating viscosities at in-situ condition (11°C) and for inter-laboratory comparisons (30°C). After a complete run at all 4 temperatures, the viscosity measurement was repeated at 40°C on the same load of samples. The results were accepted to be valid only if the difference between the two measurements at 40°C was less that 10%. This criterion was proved to be practical in this study.

Whenever the difference between the two runs at 40°C was larger than 10%, the operator could still smell the residual solvent (i.e., toluene) in the sample. Thus, the invariably lower viscosity from the first 40°C run is attributable to residual toluene, which was dried out during the higher temperature runs. Also, the solvent concentration can be monitored by GC-MS. In this study, 5 μL of DCM (dichloromethane, also known as methylene chloride) were added to 10.00 mL of toluene (10 mL volumetric glassware was used) as a standard solution. An accurately weighed bitumen sample (± 0.1 microgram) was placed into a 2 mL GC autosampler vial. Using a class A volumetric pipette, 1.00 mL of toluene was added to the vial and the sample was completely dissolved (sample

solution). The sample weight used was in the range of 25 mg. Then, 1 μL of each solution was injected into the GC-MS. The area of the resulting peak of dichloromethane (Figure 4.3) was compared with the standard as shown in Table 4.1. In this particular example, the sample with 20% difference between the two viscosity measurements at 40°C was estimated to have a dichloromethane concentration of about 0.8% (Table 4.1), so samples with less than 10% difference between the two 40°C measurements would contain negligible solvent.

In addition to eliminating samples with too much residual solvent, the accuracy of the machine was routinely calibrated by standard mineral oil provided by Cannon Instruments Inc. and the equipment error was kept to be less than 5% at various temperatures and shear rates. Also, several bitumen samples were retested in a time period of 1 to 2 weeks, and the viscosity results obtained were very close (Table 4.2). This excellent repeatability proves the reliability of the viscosity measurements.

.

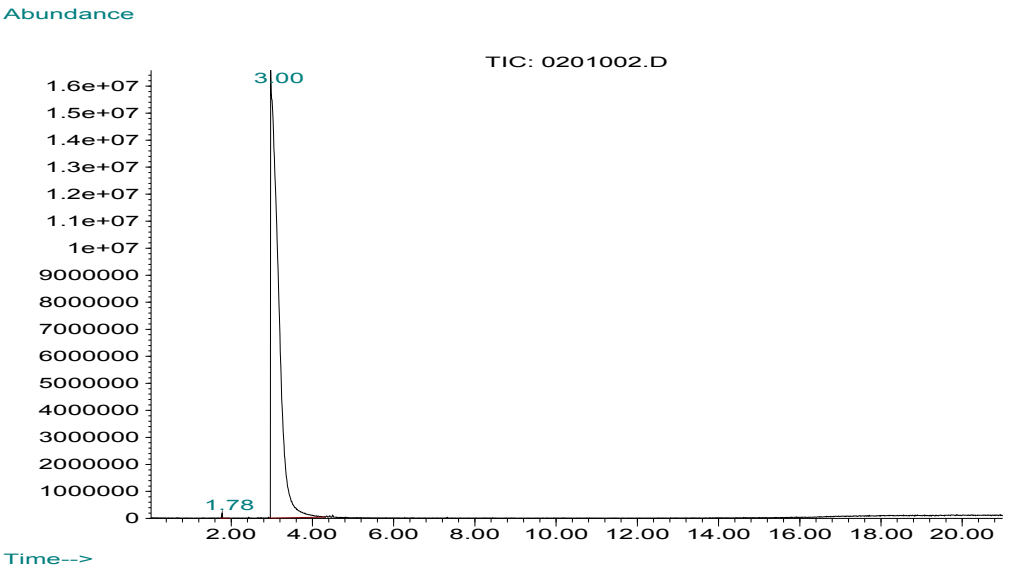

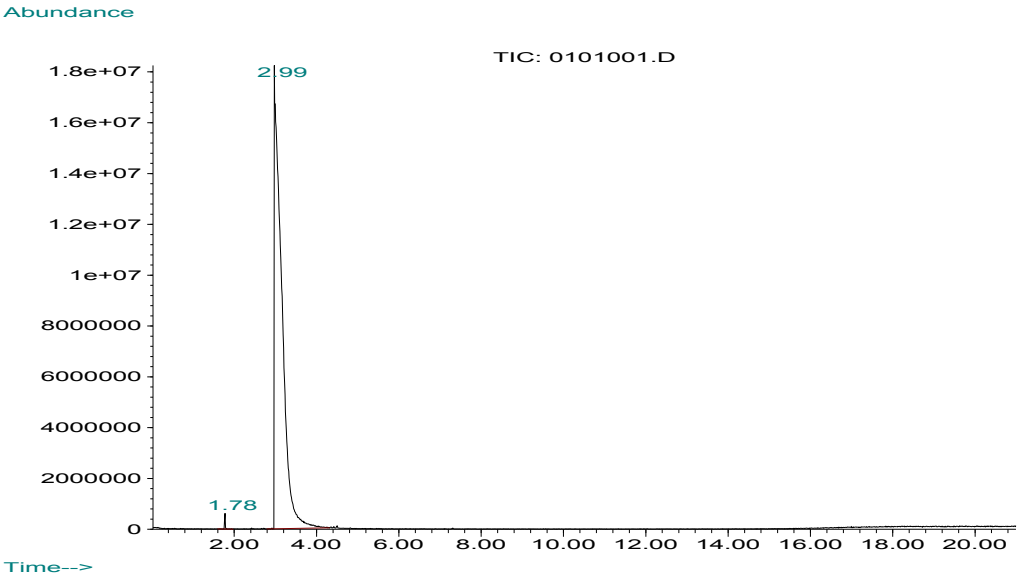

Figure 4.3 Chromatograms of standard solution (above) and unknown sample (below). Note the different abundance of these two samples (y-axis). The small peak areas are dichloromethane, the large peak areas are toluene.

Table 4.1 Example of the applied procedure for calculating the dichloromethane content in the sample.

Standard Solution:	5 μL DCM in 10 mL of toluene	
DCM Density[1]	1.33	g/mL
DCM Volume[2]	0.005	mL
Standard DCM Concentration[3]	0.665	mg/mL of DCM in toluene
DCM Peak Area[4]	5953966	= 0.665 (Standard DCM Concentration)
Sample Solution:	G6	
DCM Peak Area[5]	1576463	= **X** (Sample DCM Concentration[6])
Standard Solution/Sample Solution:		
5953966	=	0.665 (Standard DCM Concentration)
1576463		**X** (Sample DCM Concentration)
X=0.176076 mg/mL (Sample DCM Concentration)		
Mass of DCM in Sample:		
Sample Concentration[7]	21.6732	mg in 1 mL of toluene
Sample DCM Concentration/Sample Mass = **0.812411%** of DCM in Sample Solution		

1. The density of dichloromethane at room temperature (~25℃), a known value.
2. The unit volume of dichloromethane in 1 mL of toluene of the standard solution, a known value.
3. The concentration of dichloromethane in the standard solution (DCM density× DCM volume).
4. The abundance of dichloromethane of the standard solution obtained from GC-MS (the small peak area from the first chromatogram of Figure 4.3).
5. The abundance of dichloromethane of the sample solution obtained from GC-MS (the small peak area from the second chromatogram of Figure 4.3).
6. The concentration of dichloromethane in the sample solution (the unknown “X” that need to be calculated).
7. The concentration of sample in the sample solution, a known value.

Table 4.2. Viscosities of samples G6 and G2 measured under various shear rates at 40°C. The applied shear rates picked are in the zero-shear viscosity range.

Sample ID @ Testing Temperature	**Initial Data[1]**		**Repeated Data[2]**		**Retested Data[3]**	
	shear rate (1/s)	viscosity (cP)	shear rate (1/s)	viscosity (cP)	shear rate (1/s)	viscosity (cP)
G6@40°C	1.00E-1	9.75E+5	3.16E-2	9.57E+5	1.00E-1	9.81E+5
	3.16E-1	9.62E+5	1.00E-1	9.53E+5	3.16E-1	1.00E+6
	1.00E+0	9.35E+5	1.00E+0	9.25E+5	1.00E+0	9.94E+5
G2@40°C	1.00E-2	5.58E+5	1.00E-1	5.66E+5	1.00E-1	5.29E+5
	3.17E-2	5.51E+5	3.16E-1	5.65E+5	3.16E-1	5.53E+5
	1.00E-1	5.46E+5	1.00E+0	5.57E+5	1.00E+0	5.54E+5
	3.16E-1	5.41E+5	3.16E+0	5.32E+5	3.16E+0	5.35E+5

[1] Initial Data: First 40°C measurement in the series of 20°C , 40°C, 60°C , 80°C, 40°C.

[2] Repeated Data: Second 40°C measurement in the above temperature series.

[3] Retested Data: Viscosities measured only at 40°C on new loaded samples after 1 to 2 weeks.

In many previous studies dichloromethane was the solvent of choice for laboratory extraction of bitumen (e.g., Strausz and Lown, 2003). In this investigation, however, both toluene and dichloromethane are used to extract 5 pairs of samples to test the influence of both solvents on viscosity. It turned out that the differences in viscosities obtained from these two solvents are small in most of the cases, with the viscosities of the toluene-extracted samples generally higher than the DCM-extracted samples (see Table 4.3). Note that samples N-52 and N2 are taken from the same well and almost the same depth. The viscosity measured from

DCM-extracted samples showed a much better repeatability. The different results obtained from toluene-extracted samples and DCM-extracted samples are mainly due to the much higher boiling point of toluene (115.5 °C at atmospheric pressure) as compared to dichloromethane (39.8°C at atmospheric pressure), which would remove more light ends during the extraction and thus artificially raise the sample viscosity. In addition, toluene-extracted samples need longer evaporation time (a week) as compared to DCM-extracted ones (3 days), which may explain some of the observed variations. Based on the data shown in Table 4.3, a linear correlation is introduced to correct the viscosities of toluene extracted bitumens into the viscosities obtained from DCM-extracted samples (Figure 4.4).

Table 4.3 Comparisons between viscosities from toluene-extracted samples and DCM-extracted samples at 20°C.

		Viscosity (cP)			
Well ID	**Sample ID**	**Toluene[1]**	**DCM[2]**	**Corrected[3]**	**Error[4]**
10-29-89-23W4	N-52	2.41E+07	2.04E+07	1.53E+07	0.25
	N2	8.57E+07	3.00E+07	3.14E+07	-0.05
	G2	1.32E+07	1.68E+07	1.24E+07	0.26
06-08-89-23W4	N5	5.86E+06	3.45E+06	1.05E+07	-2.04
	G6	1.32E+07	1.20E+07	1.24E+07	-0.03

[1] Viscosities of toluene-extracted samples

[2] Viscosities of DCM-extracted samples

[3] Viscosities of toluene-extracted samples corrected into viscosities of DCM-extracted samples using correlation developed in Figure 4.4.

[4] Error= $(\text{Viscosity}_{DCM}-\text{Viscosity}_{Corrected})/ \text{Viscosity}_{DCM}$

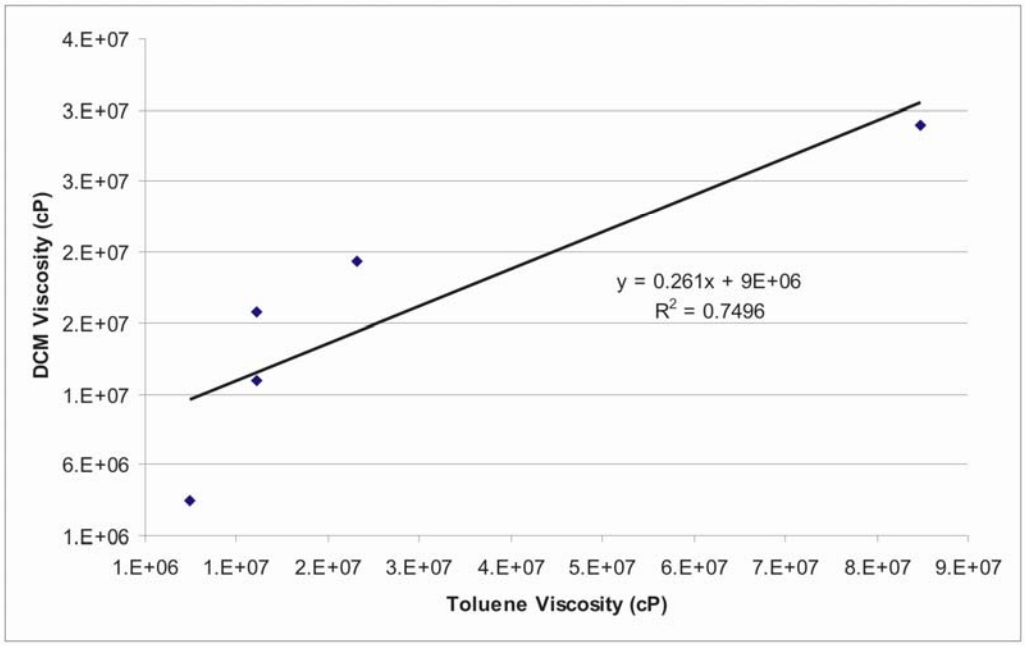

Figure 4.4 Correlation between the viscosities of toluene-extracted bitumens to the viscosities of DCM-extracted bitumen. See Table 4.3 for data source.

4.4 Inter-laboratory Comparisons of Viscosity Measurements

Previous works on Alberta heavy oils have shown large ranges in viscosity data between different laboratories. For example, Miller et al. (2006) obtained viscosities that ranged from 36,000 to 86,000 cP at 20°C for the same sample in a comparison of few commercial laboratories. Even in the same laboratory, ranges as large as 40% were obtained from repeat viscosity measurements of the same sample. The bitumen viscosities used in this project are received from several sources. Thus, it is critical to evaluate the viability of data obtained from various laboratories before handling. The present study offers the first

inter-laboratory viscosity comparison to be conducted and/or published for Grosmont bitumen.

Duplicates of 11 samples were sent to commercial laboratories (Lab A and Lab B), and were also extracted and examined in-house at University of Alberta (Lab C). 4 samples are duplicates of samples tested in Lab A, including 2 fresh samples and 2 legacy samples. The other 7 samples are duplicates of samples tested in Lab B, including 4 legacy samples and 3 fresh samples (Table 4.4).

The two commercial laboratories provided different formats for viscosities. Lab A measured viscosity from 0 to 150°C, with a viscosity point every 0.7 to 1.5°C. Lab B only provided a single viscosity measurement. Moreover, although the requested temperature for the viscosity measurement in Lab B is 20°C, 10 out of 12 legacy samples were actually measured at 30°C, as the laboratory reported that the viscosities were too high to be measured at 20°C using their particular analytical procedure (Appendix 2).

As documented in Table 4.4, no matter whether the samples are “fresh” or “legacy”, viscosities obtained from Lab A are about 2 to 7 times higher than viscosities from Lab C. Also, data are still incommensurate with each other at 60°C (Table 4.5), where viscosities drop down to the range of 10^4 cP and are numerically similar to heavy oil viscosities obtained by Miller et al. (2006). At 60°C, the errors range

from 48% to 217%, which are also close to the range reported by Miller et al. (2006).

The viscosities of 4 legacy samples measured at 30°C (i.e., samples N2, N3, UI3, and G2) in Lab B are approximately 1 to 7 times larger than the viscosities measured in Lab C (Table 4.4). This ratio is expected to be even higher at 20°C, if measurements were available at that temperature for these samples. The viscosities of the 3 fresh samples are reported and compared at 20°C. Two of them have much smaller ratios than the ones obtained from the legacy samples (-0.16 and 0.37). However, the third sample (sample G7) shows a large disparity between the viscosity results from these two laboratories, indicating that the errors of viscosity measurements are inconsistent.

Based on these observations, no consistent correlation could be found between Labs A, B, and C. Therefore, no direct “mixing” of data from Labs A, B, and C was conducted. Rather, in this study, bitumen viscosities from Lab C were used as a standard and corrections are introduced to normalize the viscosity data from the other laboratories to this standard.

Using the data from Table 4.4, a linear correlation was developed to correct the viscosities obtained from Lab A at 20°C into the standard viscosity at 20°C, as shown in Figure 4.6. Similarly, the viscosities of legacy samples measured at 30°C in Lab B were converted into

standard viscosity at 30°C using the linear correlation plotted in Figure 4.6. Since most of the viscosities are available at 20°C instead of 30°C, these data were further corrected into standard viscosities at 20°C using the correlation developed from the standard viscosities (Figure 4.7). The viscosities used in this correlation are from the same samples used in the viscosity correction from Lab B to Lab C at 30°C (i.e. samples N2, N3, UI3, and G2 in Table 4.4). Overall, the relative errors of most of the corrected viscosities are in the range of one fold at 20°C (i.e. column "Error" in Table 4.6), which are illustrated in Figure 4.8.

Two legacy samples from Lab B were originally measured at 20°C (i.e. samples N1, UI1). They had to be first corrected into 30°C using the correlation from Figure 4.7, and then corrected into standard viscosities at 30°C by the correlation from Figure 4.6. Lastly, these two viscosities were corrected into the standard viscosities at 20°C by applying the correlation from Figure 4.7 again.

Most of the viscosities of fresh samples from Lab B and Lab C are similar, so no correlation was used for these samples. The final standard viscosities of all the samples used in this study are summarized in Table 4.8.

Table 4.4 Inter-laboratory comparisons of viscosities from duplicate samples.

Well ID	Sample ID	Depth	Formation	Solvent	Viscosity (cP)			Ratio*	Fresh/Legacy @ tested Temperatures
					Lab A	Lab B	Lab C		
16-13-89-23W4	N-1	289.3	Nisku	DCM	1.48E+08	—	2.02E+07	6.34	Legacy @ 20°C
	G3-4	344.0	UGM3	DCM	6.19E+07	—	1.97E+07	2.15	Legacy @ 20°C
08-01-89-23W4	GRM 127	325.8	UGM3	DCM	2.16E+07	—	2.74E+06	6.88	Fresh @ 20°C
	GRM 129	343.65	UGM3	DCM	8.60E+06	—	2.27E+06	2.78	Fresh @ 20°C
10-29-89-23W4	N2	265-267	Nisku	Mixed	—	8.90E+06	4.50E+06	0.98	Legacy @ 30°C
	N3	305.3-307.4	Nisku	Mixed	—	4.83E+07	9.27E+06	4.21	Legacy @ 30°C
	UI3	327.35-328.1	UIreton	Mixed	—	1.73E+07	2.07E+06	7.35	Legacy @ 30°C
	G2	346-349	UGM3	Mixed	—	1.00E+07	2.60E+06	2.85	Legacy @ 30°C
06-08-89-23W4	N5	270.6-280.6	Nisku	Mixed	—	2.91E+06	3.45E+06	-0.16	Fresh @ 20°C
	G6	322.8-324.2	UGM3	Mixed	—	1.64E+07	1.20E+07	0.37	Fresh @ 20°C
07-26-85-19W4	G7	350.2-350.8	UGM3	Mixed	—	5.89E+07	3.16E+06	18.6	Fresh @ 20°C

*Ratio= $(Viscosity_{Lab\ A}-Viscosity_{Lab\ C})/ Viscosity_{Lab\ C}$ or Ratio= $(Viscosity_{Lab\ B}-Viscosity_{Lab\ C})/ Viscosity_{Lab\ C}$

Table 4.5 Inter-laboratory comparison of viscosities from duplicate samples at 60°C.

Well ID	Sample ID	Depth	Formation	Solvent	Viscosity at 60°C		Ratio*	Other
					Lab A	Lab C		
16-13-89-23W4	N-1	289.3	Nisku	CH2CL2	7.29E+04	4.92E+04	0.48	Legacy @ 60°C
	G3-4	344.0	UGM3	CH2CL2	6.09E+04	4.87E+04	0.25	Legacy @ 60°C
08-01-89-23W4	GRM 127	325.8	UGM3	CH2CL2	4.71E+04	1.49E+04	2.17	Fresh @ 60°C
	GRM 129	343.65	UGM3	CH2CL2	3.35E+04	1.34E+04	1.49	Fresh @ 60°C

*Ratio= $(Viscosity_{Lab\ A}-Viscosity_{Lab\ C})/ Viscosity_{Lab\ C}$

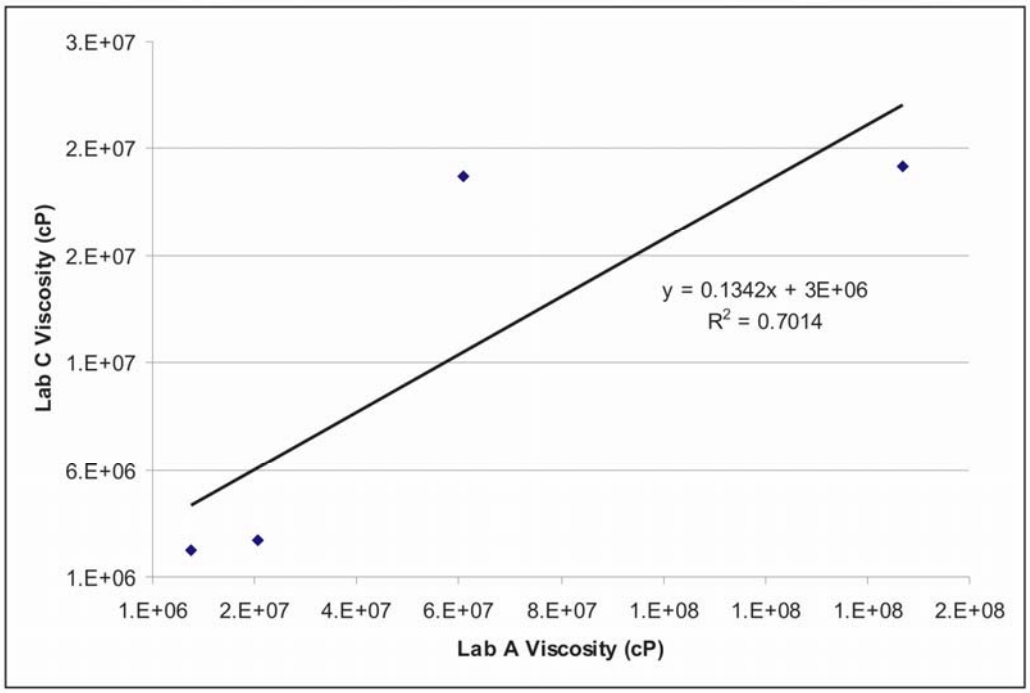

Figure 4.5 Correlation between Lab A viscosities and standard viscosities from Lab C. Please see Table 4.4 for data source.

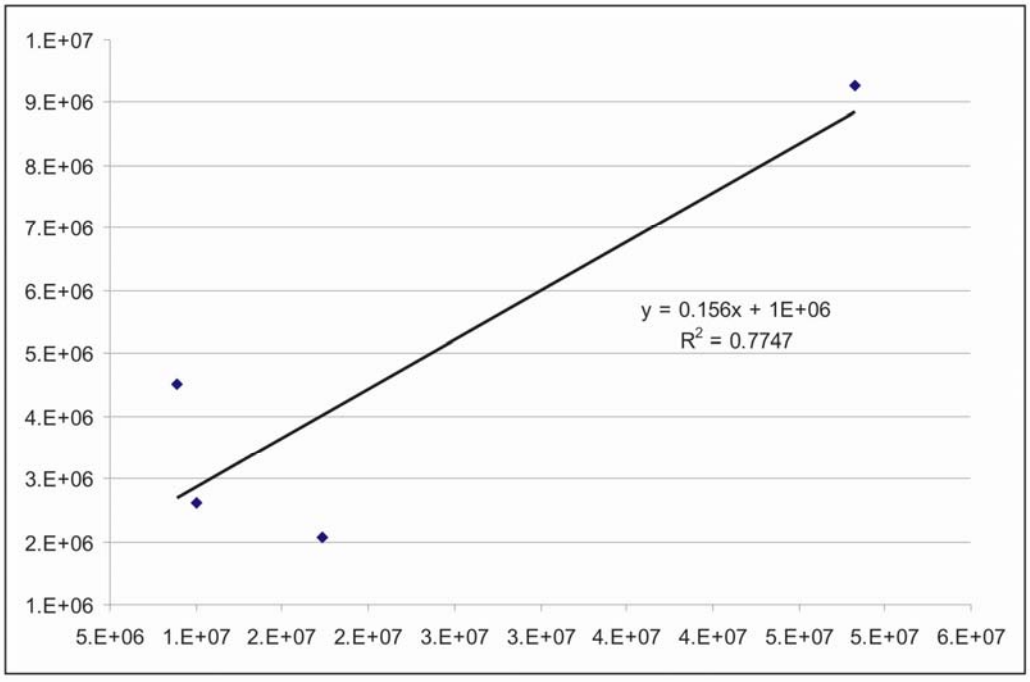

Figure 4.6 Correlation between Lab B viscosities and standard viscosities from Lab C. Data is based on the legacy samples tested at 30°C. Please see Table 4.4 for data source.

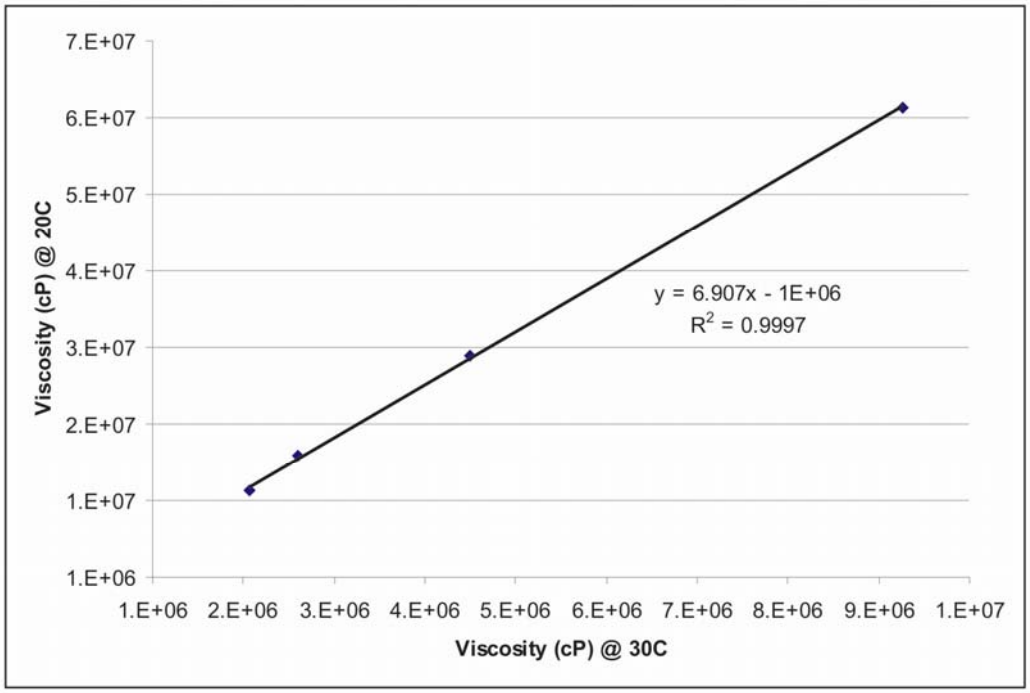

Figure 4.7 Correlation between standard viscosities at 30°C and standard viscosities at 20°C. The data are the measured viscosities of samples N2, N3, UI3, G2 in Table 4.4.

Table 4.6 Comparison of corrected and standard viscosities.

Sample ID	Commercial Labs Viscosity (cP)	Standard Lab Viscosity (cP) @ 20˚C	Equations Corrected Viscosity (cP) @ 20˚C	Error*
N-1	1.48E+08	2.02E+07	2.29E+07	-0.13
G3-4	6.19E+07	1.97E+07	1.13E+07	0.43
GRM 127	2.16E+07	2.74E+06	5.90E+06	-1.15
GRM 129	8.60E+06	2.27E+06	4.15E+06	-0.83
N2	8.90E+06	3.00E+07	1.55E+07	0.48
N3	4.83E+07	2.53E+07	5.79E+07	-1.29
UI3	1.73E+07	1.22E+07	2.45E+07	-1.01
G2	1.00E+07	1.68E+07	1.67E+07	0.01

*Error= $(viscosity_{standard}-viscosity_{equation})/viscosity_{standard}$

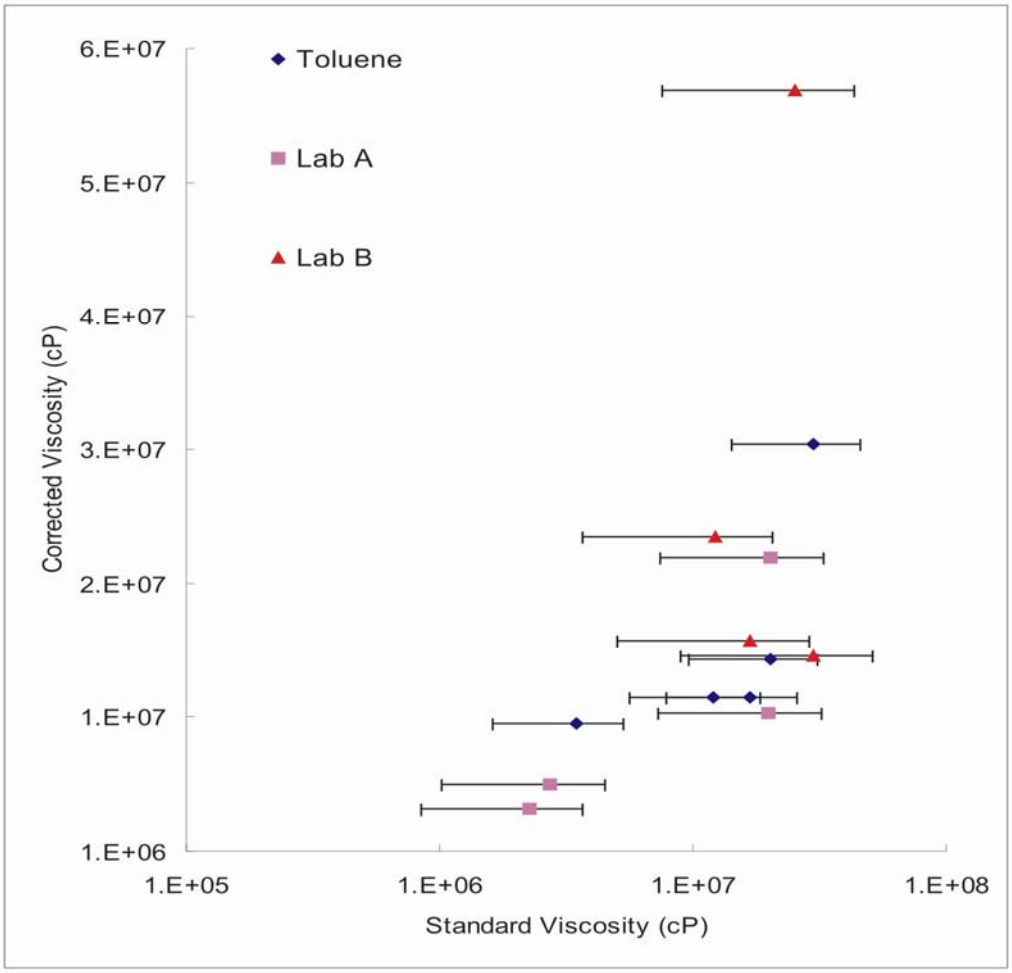

Figure 4.8 The averaged errors of the corrected viscosities at 20˚C from toluene-extracted bitumens (Legend "Toluene"; Table 4.3 for data source), Lab A (Table 4.6 for data source) and lab B (Table 4.6 for data source) as compared to standard viscosities (viscosities of DCM-extracted bitumens from Lab C) at 20˚C.

4.5 Aging Effect

Aging is caused by oxidation and/or loss of volatile components that lead to variations in chemical composition and structural changes (Mastrofini and Scarsella, 2000). Asphalt studies suggested that aging decreases the saturate and aromatic content and increases the content of resins and asphaltene (e.g., Lu and Isacsson, 2002). These chemical changes alter the rheological properties, and the asphalt becomes more

solid-like.

Aging phenomena were also observed in the natural bitumen used in this study. Rather than using the American Society for Testing and Materials (ASTM) standard aging tests like the thin-film oven test (TFOT, ASTM D-1754) and the rolling thin-film oven test (RTFOT, ASTM D-2872), the available legacy samples and fresh samples provided a natural aging experiment in a time gap of 20 to 30 years under room temperature and atmospheric pressure.

In the study area, wells 10-29-89-23W4 (completed in 1983) and 8-33-90-23W4 (completed in 2007) provided the most closely spaced pair of legacy and fresh wells (10 km apart), with high bitumen saturation in 3 studied formations (Nisku, Upper Ireton, and Grosmont). Elemental analysis (Table 4.7) of samples from these two wells show that carbon (C), hydrogen (H), and hydrogen-carbon atomic ratios (H/C atomic) are higher in the fresh samples, whereas nitrogen (N), sulfur (S), and non-NCSH (mainly oxygen) are higher in the legacy samples. These numbers suggest the successive loss of saturates and aromatics and an increase in the weight percentage of resins and asphaltenes.

Table 4.7 Elemental compositions of legacy and fresh samples.

Sample Status	Sample ID	Depth (m)	N	C	H	S	Non-NCSH	H/C Atomic
Legacy	N-52	264.75	0.59	81.78	9.83	5.93	1.87	1.44
Legacy	UI-81	315.45	0.55	81.44	9.83	5.82	2.36	1.45
Legacy	G3-35	349.65	0.52	82.16	10.10	6.13	1.59	1.47
Fresh	N-79	277.25	0.46	82.41	10.13	5.84	1.16	1.48
Fresh	UI-129	305.55	0.46	82.68	10.29	5.15	1.43	1.49
Fresh	G3-245	339.6	0.45	82.19	10.32	5.51	1.54	1.51

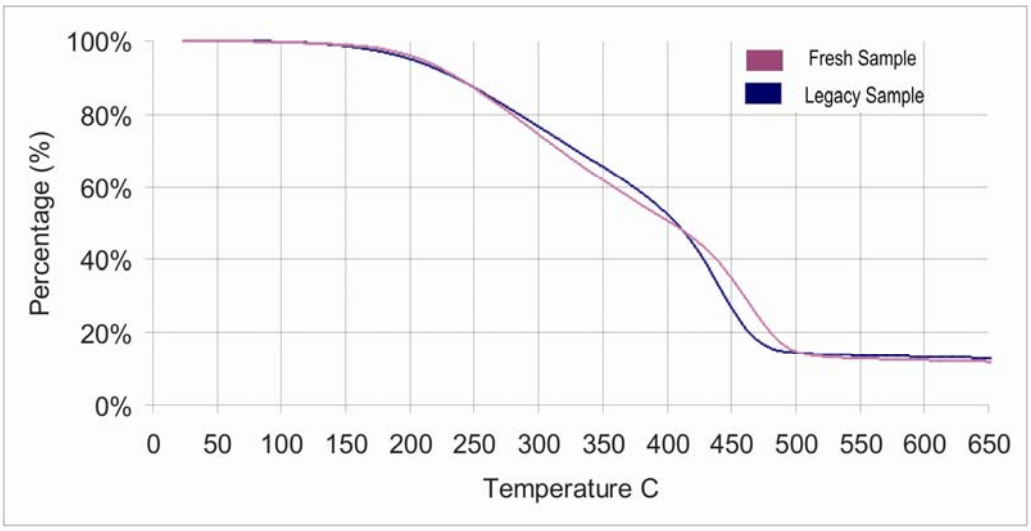

Figure 4.9 Comparison of thermal gravimetric analysis results from fresh sample and legacy samples.

Indeed, the thermal gravimetric analysis (TGA) results from fresh samples and legacy samples clearly show that the fresh samples have higher amount of low-carbon-number hydrocarbons (boiling point from roughly 270°C to 410°C), while the legacy samples have a higher abundance of hydrocarbons with higher carbon numbers (boiling points ranging 410°C to 500°C) (Figure 4.9).

The viscosity difference between legacy samples and fresh samples is evident from the data obtained from all three laboratories, regardless of the large differences in inter-laboratory comparisons (Table 4.9). The viscosities of samples from well 10-29-89-23W4 and well 8-33-90-23W4 are listed in Table 4.8. These viscosities were all determined in the “standard” Laboratory (Lab C), and all the viscosities measured on toluene-extracted samples have been corrected into viscosities of DCM-extracted samples. Table 4.8 is divided into 3

sections. The samples from roughly the same stratigraphic depth are compared in the first section. The viscosity ratios of samples from well 10-29-89-23W4 (legacy) to samples from well 8-33-90-23W4 (fresh) ranges from about 3 to 34, with the majority of the ratios being smaller than 7.

Viscosities of samples from the similar depths are compared in the second section of Table 4.8. This data set shows a fairly similar ratio range for each formation as compared to the data obtained from the first set, with viscosities from shallower rock units exhibiting more significant changes from fresh samples to legacy samples (i.e., from 13.90 to 4.87 in the column “Ratio” in Table 4.8).

The averaged viscosities of each formation and grand total for both legacy and fresh samples are listed in the third section of Table 4.8. There is no obvious correlation in the viscosity changes between fresh samples and legacy samples. Therefore, in order to avoid any alterations of the original sequence of the viscosity value in the legacy samples, a constant coefficient of 8.38 was used to correct the legacy samples to fresh ones (obtained from the “Total Ave” in Table 4.7).

Table 4.8 Comparisons of legacy and fresh standard viscosities in a pair of wells at 20°C.

10-29-89-23W4 (legacy)			8-33-90-23W4 (fresh)			
Sample ID	**Depth (m)**	**Viscosity**	**Sample ID**	**Depth (m)**	**Viscosity**	**Ratio***
Section 1						
N-52	264.75	2.04E+7	—	—	—	—
N2	265-267	3.00E+7	—	—	—	—
N-57	295.45	2.60E+7	N-77	274.55	2.07E+6	12.56
N3	305.3-307.5	2.53E+7	N-79	277.25	4.81E+6	5.26
UI-81	315.45	1.80E+7	UI-122	285.25	2.87E+6	6.27
UI3	327.4-328.1	1.22E+7	UI-125	295.13	1.87E+6	6.52
UI-90	334.2	4.97E+7	UI-129	305.55	1.47E+6	33.81
G3-33	344	9.74E+6	G3-240	316.05	3.11E+6	3.12
G2	346-349	1.68E+7	G3-243	321.4	2.72E+6	6.18
G3-35	349.65	1.30E+7	G3-245	339.6	2.88E+6	4.51
—	—	—	G3-246	343.84	2.00E+6	—
Section 2						
N-57	295.45	2.60E+7	UI-125	295.13	1.87E+6	13.90
N3	305.3-307.5	2.53E+7	UI-129	305.55	1.45E+6	17.45
UI-81	315.5	1.80E+7	G3-240	316.05	3.12E+6	5.77
G3-33	344	9.74E+6	G3-246	343.84	2.00E+6	4.87
Section 3						
Nisku Ave	264.8-307.5	2.54E+7	Nisku Ave	274.6-277.3	3.46E+6	7.39
Ireton Ave	305.3-334.2	2.66E+7	Ireton Ave	285.3-305.6	2.05E+6	12.87
UGM Ave	344-349.6	1.32E+7	UGM Ave	316.1-343.8	2.68E+6	4.92
Total Ave	264.5-349.5	2.21E+7	Total Ave	274.5-343.8	2.64E+6	8.38

Ratio= $Viscosity_{legacy}$ / $Viscosity_{fresh}$

To this end, all the viscosities measured in the 3 laboratories were corrected into one standard, that is, the viscosities measured on DCM-extracted “fresh” samples in Lab C at 20°C. Based on the viscosity data from well 8-33-90-23W4, a correlation of standard viscosities from 20°C to 11°C is introduced (Figure 4.10). Therefore, all

the viscosities are now also available at the current *in-situ* temperature of the Grosmont reservoir. The original viscosities and corrected viscosities for all samples are documented in Table 4.9.

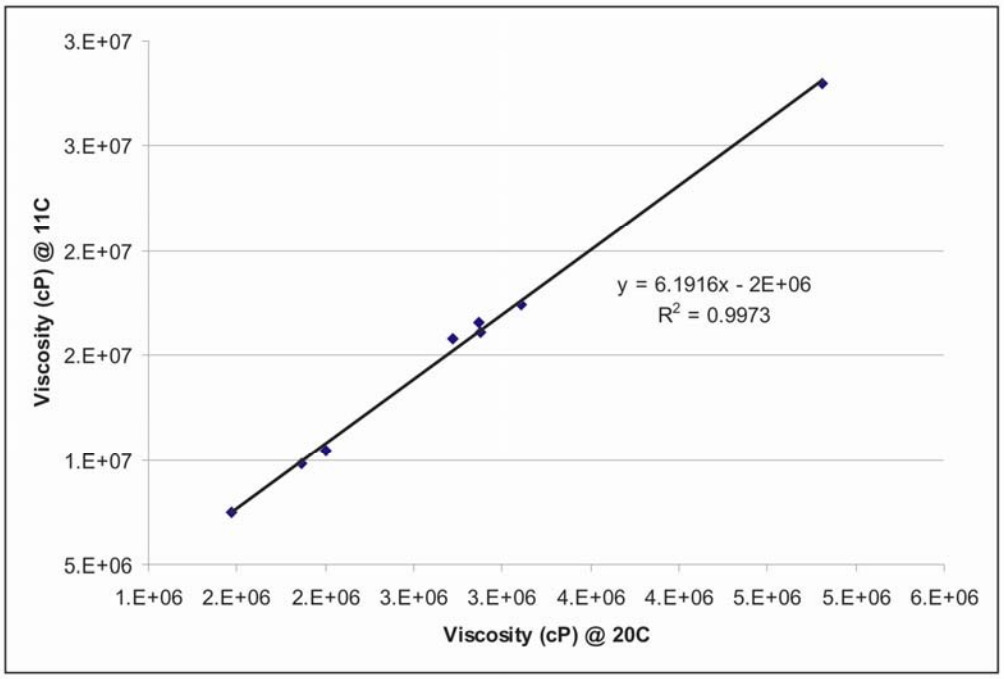

Figure 4.10 Correlation between viscosity at 20°C and viscosity at 11°C. Data are from the measured standard viscosities of samples from well 8-33-90-23W4. Please see Appendix 2 for data source.

Table 4.9 Summary of viscosities from 3 different laboratories and the corrected standard viscosities used in this study.

Source	Well ID	Sample ID	Depth (m)	Formation	Labs A/B Viscosity	Lab C Viscosity		Standard[3]	Fresh[4]	11°C[5]
						T[1]	DCM[2]			
Batch 1/Lab A										
Legacy	16-13-89-23W4	N-1	289.3	Nisku	1.41E+08	–	2.02E+07	2.02E+07	2.41E+06	1.29E+07
		N-5	298.8	Nisku	1.29E+08	–	–	2.03E+07	2.42E+06	1.30E+07
		G3-3	343.1	UGM3	7.25E+07	–	–	1.27E+07	1.52E+06	7.41E+06
		G3-4	344.0	UGM3	6.18E+07	–	1.97E+07	1.97E+07	2.35E+06	1.25E+07
	7-34-90-23W4	N-15	278.3	Nisku	6.32E+08	–	–	8.78E+07	1.05E+07	6.29E+07
		N-18	281.6	Nisku	2.45E+08	–	–	3.59E+07	4.28E+06	2.45E+07
Fresh	08-01-89-23W4	GRM 124	298.4	Nisku	9.30E+06	–	–	4.25E+06	4.25E+06	2.43E+07
		GRM 125	290.4	Nisku	8.62E+06	–	–	4.16E+06	4.16E+06	2.38E+07
		GRM 126	336.1	UGM3	1.19E+07	–	–	4.60E+06	4.60E+06	2.65E+07
		GRM 127	325.8	Ulreton	2.13E+07	–	2.74E+06	2.74E+06	2.74E+06	1.50E+07
		GRM 128	294.0	Nisku	6.67E+06	–	–	3.90E+06	3.90E+06	2.21E+07
		GRM 129	343.65	UGM3	8.65E+06	–	2.27E+06	2.27E+06	2.27E+06	1.21E+07
		GRM 130	331.5	Ulreton	8.55E+06	–	–	4.15E+06	4.15E+06	2.37E+07
Batch 2/Lab C										
Legacy	10-04-94-23W4	G3-130	518.1	UGM2	–	3.31E+07	–	1.76E+07	2.10E+06	1.10E+07
		G3-140	565.5-566.8	UGM1	–	1.90E+07	–	1.40E+07	1.67E+06	8.32E+06
	10-29-89-23W4	N-52	264.75	Nisku	–	2.41E+07	2.04E+07	2.04E+07	2.44E+06	1.31E+07
		N-57	295.45	Nisku	–	6.51E+07	–	2.60E+07	3.10E+06	1.72E+07
		UI-81	315.45	Ulreton	–	3.44E+07	–	1.80E+07	2.15E+06	1.13E+07
		G3-35	349.65	UGM3	–	1.55E+07	–	1.30E+07	1.56E+06	7.64E+06
	10-29-86-19W4	G3-63	309	UGM3	–	2.63E+07	–	1.59E+07	1.89E+06	9.72E+06
Batch 3/Lab B										
Legacy	11-12-91-24W4	N1	282.5-285.7	Nisku	1.59E+08	–	–	2.27E+07	2.71E+06	1.48E+07
	10-21-92-24W4	UI1	363-366	Ulreton	4.05E+08	–	–	5.57E+07	6.65E+06	3.92E+07
		UI2	377-379	Ulreton	2.80E+06	–	–	8.92E+06	1.06E+06	4.59E+06

Legacy	10-12-93-24W4	G1	444-446.7	UGM3	2.75E+07	–	–	3.55E+07	4.24E+06	2.43E+07
	10-29-89-23W4	N2	265-267	Nisku	8.90E+06	8.57E+07	3.00E+07	3.00E+07	3.58E+06	2.02E+07
		N3	305.3-307.45	Nisku	4.83E+07	6.24E+07	–	2.53E+07	3.02E+06	1.67E+07
		UI3	327.35-328.1	UIreton	1.73E+07	1.23E+07	–	1.22E+07	1.46E+06	7.02E+06
		G2	346-349	UGM3	1.00E+07	1.32E+07	1.68E+07	1.68E+07	2.00E+06	1.04E+07
	6-10-87-23W4	N4	349.4-358.2	Nisku	3.00E+06	–	–	9.14E+06	1.09E+06	4.75E+06
	11-26-87-20W4	UI4	263.4-267	UIreton	2.80E+06	–	–	8.92E+06	1.06E+06	4.59E+06
	10-29-86-19W4	G3	283-283.3	UGM3	3.64E+07	–	–	4.51E+07	5.39E+06	3.13E+07
		G4	303-303.6	UGM3	1.50E+07	–	–	2.21E+07	2.63E+06	1.43E+07
Fresh	11-26-91-24W4	UI5	316.8-319	UIreton	1.27E+06	–	–	1.27E+06	1.27E+06	5.87E+06
		G5	335.25-336.4	UGM3	5.26E+06	–	–	5.26E+06	5.26E+06	3.05E+07
	06-08-89-23W4	N5	270.6-280.6	Nisku	2.91E+06	5.86E+06	3.45E+06	3.45E+06	3.45E+06	1.94E+07
		G6	322.8-324.2	UIreton	1.64E+07	1.32E+07	1.20E+07	1.20E+07	1.20E+07	7.23E+07
	07-26-85-19W4	UI6	325-326.2	UIreton	1.73E+07	–	–	1.73E+07	1.73E+07	1.05E+08
		G7	350.2-350.8	UGM3	5.89E+07	–	3.14E+06	3.14E+06	3.14E+06	1.74E+07
Batch 4/Lab C										
Legacy	10-29-89-23W4	UI-90	334.2	UIreton	–	–	4.97E+07	4.97E+07	5.93E+06	3.47E+07
		G3-33	344	UGM3	–	–	9.74E+06	9.74E+06	1.16E+06	5.19E+06
Fresh	8-33-90-23W4	N-77	274.55	Nisku	–	–	2.07E+06	2.07E+06	2.07E+06	1.08E+07
		N-79	277.25	Nisku	–	–	4.81E+06	4.81E+06	4.81E+06	2.78E+07
		UI-122	285.25	UIreton	–	–	2.87E+06	2.87E+06	2.87E+06	1.58E+07
		UI-125	295.13	UIreton	–	–	1.87E+06	1.87E+06	1.87E+06	9.55E+06
		UI-129	305.55	UIreton	–	–	1.47E+06	1.47E+06	1.47E+06	7.10E+06
		G3-240	316.05	UGM3	–	–	3.11E+06	3.11E+06	3.11E+06	1.73E+07
		G3-243	321.4	UGM3	–	–	2.72E+06	2.72E+06	2.72E+06	1.49E+07
		G3-245	339.6	UGM3	–	–	2.88E+06	2.88E+06	2.88E+06	1.58E+07
		G3-246	343.84	UGM3	–	–	2.00E+06	2.00E+06	2.00E+06	1.04E+07

[1] Viscosities measured on toluene extracted samples.
[2] Viscosities measured on dichloromethane extracted samples.
[3] Viscosities corrected to standard (Lab C) at 20°C.
[4] Viscosities of legacy samples corrected into viscosities of fresh samples.
[5] Viscosities at 11°C.

4.6 Viscosity Distribution

The frequency distribution of the standard viscosity values at calculated *in-situ* temperature (11°C) is shown in Figure 4.11. For the total 49 measurements, two-thirds (67.35% or 33 out of 49) are lower than 2E+07 cP. Viscosities of almost half of the samples are in the range of 1E+07 to 2E+07 cP. Only 7 viscosities are higher than 2E+07 cP.

In Figure 4.12, these data are plotted according to sample elevation. It can be seen that the viscosities from the Nisku are clustered at an elevation of 210 m to 250 m, which is due to the limited distribution of the Nisku Formation in the study area. The viscosities of the Nisku samples are mostly between 1E+07 to 2E+07 cP, with the highest and the lowest values obtained from the shallowest and deepest samples, respectively. The viscosity results from Upper Ireton are scattered in this plot but can be divided into three “zones” (10-20 m thick) according to elevation. This distribution probably is an artifact controlled mainly by the oil saturated zones in this rock unit, where most of the samples were taken. Compared to the Nisku, the Upper Ireton viscosities have a wider range in each zone (from 1E+06 to 1E+08 cP). Lastly, the viscosities of Grosmont samples show a very rough decrease with increasing depth. Also, the Grosmont has the largest range in elevation (about 100 m), but its viscosities have a smaller range than the data from the Upper Ireton.

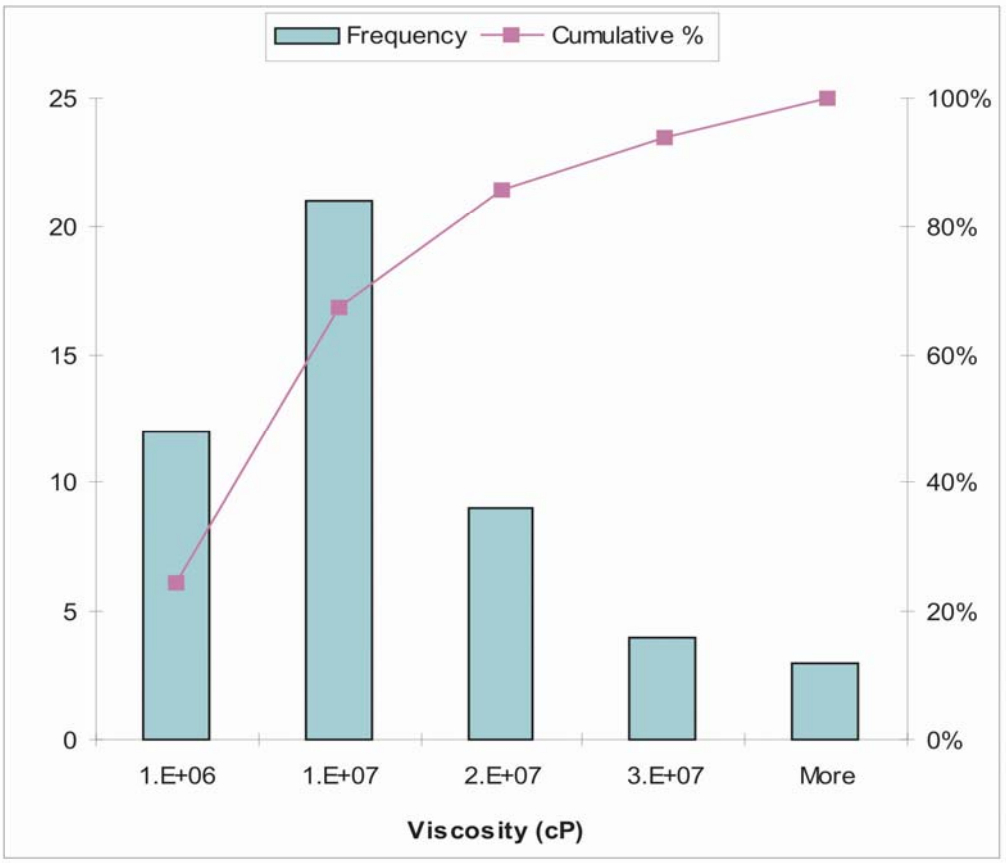

Figure 4.11 Histogram showing the viscosity distribution at 11°C of all the samples.

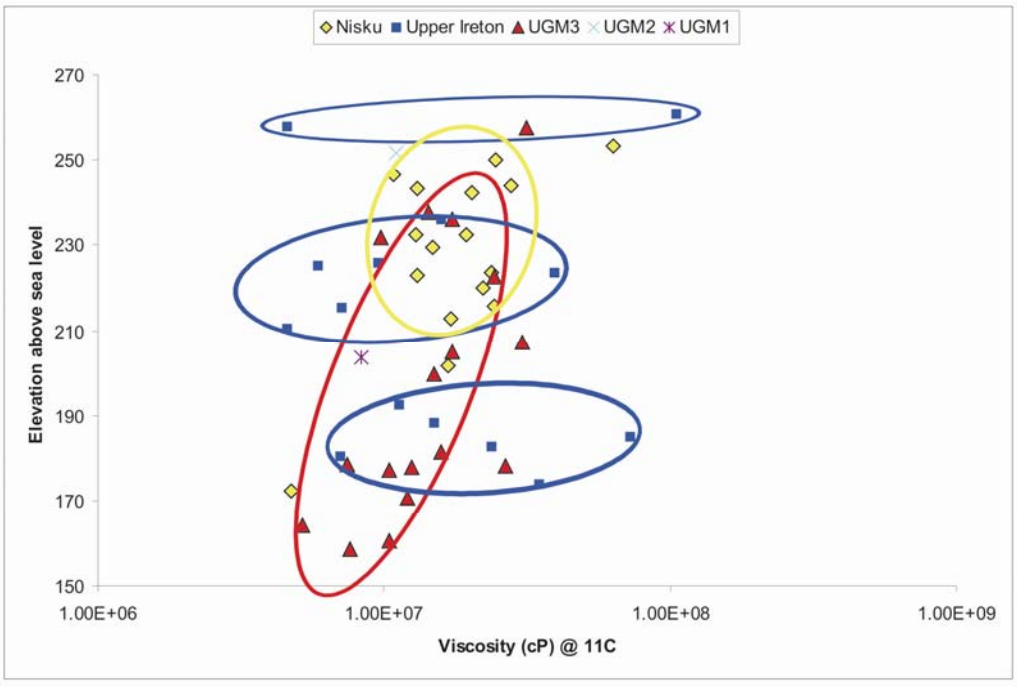

Figure 4.12 Standard viscosities variation along elevation from all samples under in-situ conditions (11°C).

4.6.1 Vertical distribution

The variation of reservoir properties (permeability, porosity, oil saturation) and bitumen viscosity along depth from a single well 10-29-89-23W4 are plotted in Figure 4.13. This well was chosen because of its abundance of viscosity measurements. The viscosity variation is generally independent of the other three reservoir properties in this well. For example, while the Upper Ireton Formation exhibits uniformly high porosity and oil saturation, the viscosity shows a sinusoidal trend with increasing depth in this 30 m thick unit (310 m to 340 m).

For comparison, Figure 4.14 is a plot of vertical viscosity variation in wells 10-29-89-23W4 and 08-33-90-23W4 (see Table 4.8 for data source) at 20°C. The viscosity logs exhibit zigzag curves with increasing depth in these two wells, and the viscosity tends to be highest near the boundaries between the formations, as indicated by different colors. These two wells are close to each other (about 10 km apart), and the viscosity variation in each formation is overall quite similar: the viscosity in the Nisku Formation increases along the depth; the viscosity profile from the Upper Ireton Formation has a bow trend. These similarities suggest that the viscosity distribution is probably related to or controlled by stratigraphy. The reason(s) for the observed patterns are under further investigation. Possibilities include 1) oil-water contacts migrating up and down over time; 2) oil migration and/or biodegradation controlled by aquitards that divide the reservoir into stratigraphically separated units; and 3) differences in microbial activity, i.e., aerobic versus

anaerobic, possibly controlled by the level of oxygenation over time.

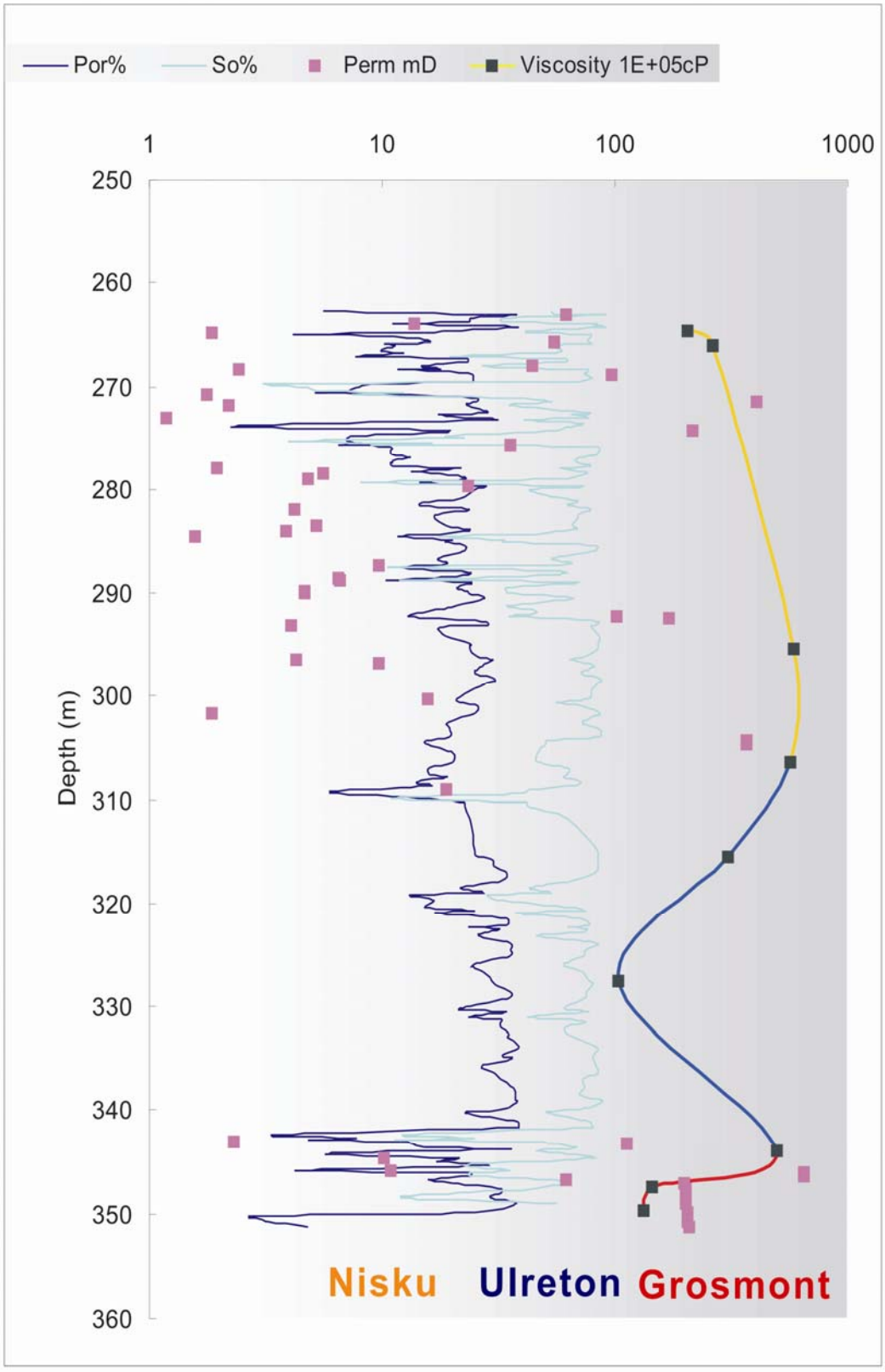

Figure 4.13 Porosity, oil saturation, permeability, and viscosity (20°C) variations along depth from well 10-29-89-23W4.

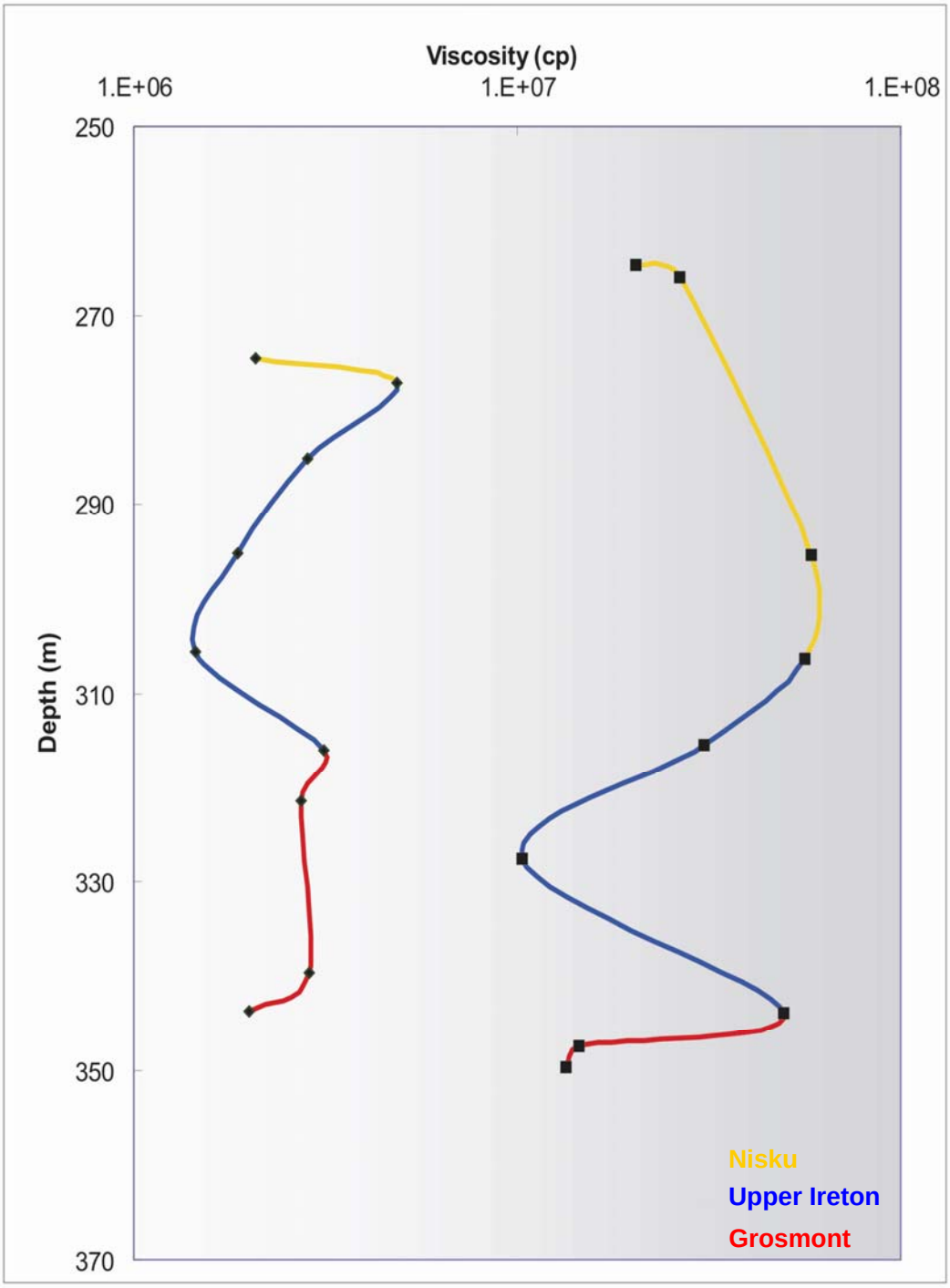

Figure 4.14 Viscosity comparisons along depth of fresh well (left) and legacy wells (right) at 20°C. Nisku, Upper Ireton, and Grosmont formations are represented by different colors.

4.6.2 Lateral distribution

A strike cross section was constructed to illustrate the regional bitumen viscosity distribution (Figures 4.15 and 4.16). The wells for this cross section were chosen upon the available viscosity measurements. Gamma ray logs were used for correlating the stratigraphic unit. A vertical exaggeration of approximately 120X was used.

The cross section shown in Figure 4.16 includes the Nisku Formation, Upper Ireton Formation, and all 3 Grosmont units. The Nisku Formation is only present in the middle part of the cross section, due to erosion. The Upper Ireton Formation is truncated on the north and south edges of the cross section. Because the strata dip toward the southwest, and the control wells at each end of the cross section are located more northeast as compared to wells in the central regions, thus strata at these locations had experienced more erosion (Figure 4.15).

Within the limited presence of the Nisku Formation, the lateral variation of viscosity exhibits a uniform pattern. The viscosities along the top of the Nisku Formation are in the range of 1E+7 cP to 2E+7 cP and they increase with increasing depth. The highest viscosities (> 2E+7 cP) are found in wells 08-33-89-23W4, 10-29-89-23W4, and 7-34-90-24W4 near the bottom of the Nisku Formation, where the Nisku stratum is the thickest (Figure 4.16).

The viscosity distribution in the Upper Ireton can be separated into three zones with depth. Each zone can be correlated laterally across area (Figure 4.16). The top and bottom zones contain more viscous bitumen with average viscosity of ~1.5E+7 cP, whereas middle zone

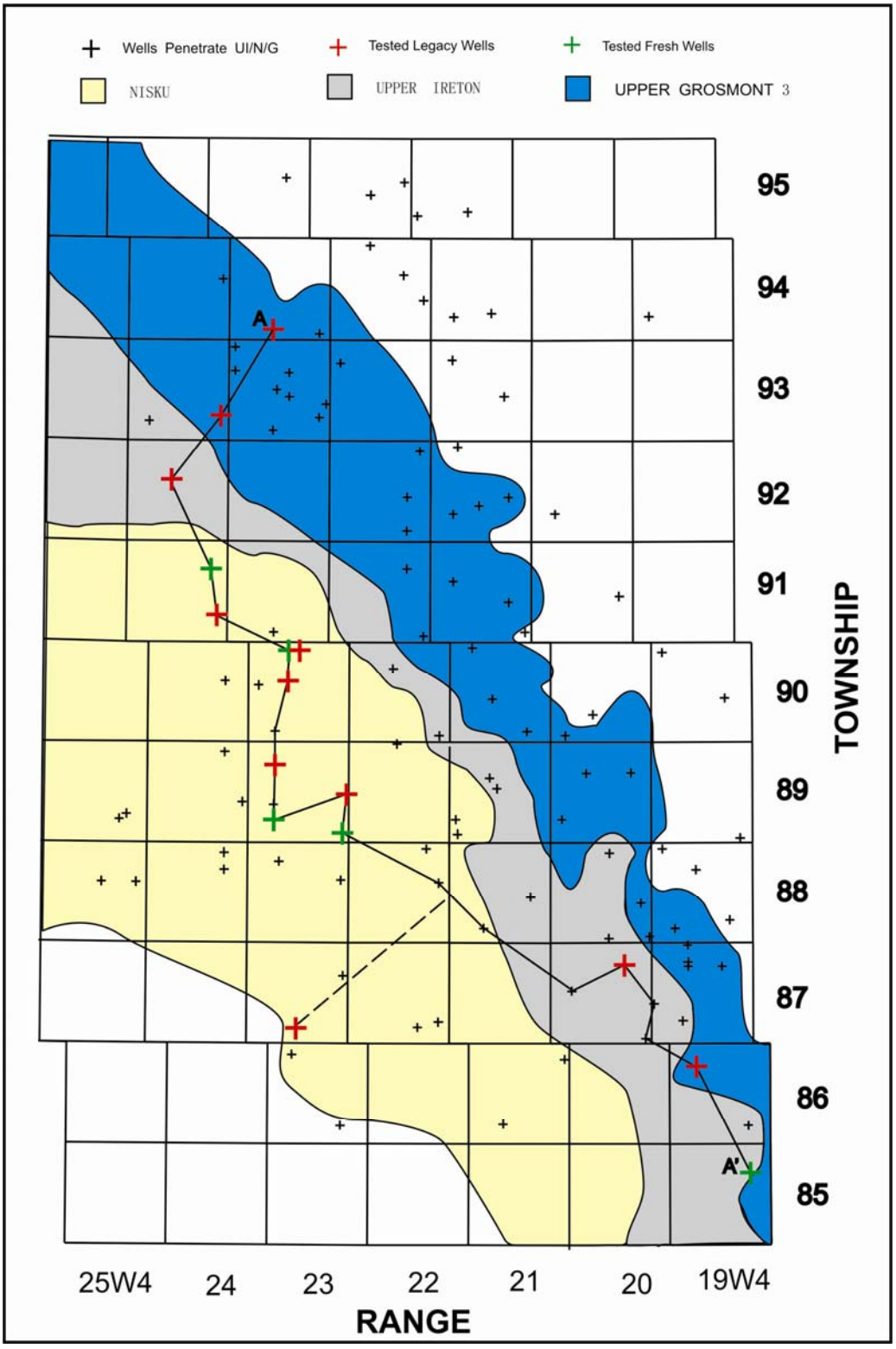

Figure 4.15 Strike cross section (AA`) using all the wells that have viscosity measurements in the study area. The subcrops of Nisku, Upper Ireton, and Upper Grosmont 3 are shown by different colors (modified from Dembicki, 1994). The dotted line is a projection line for the cross section.

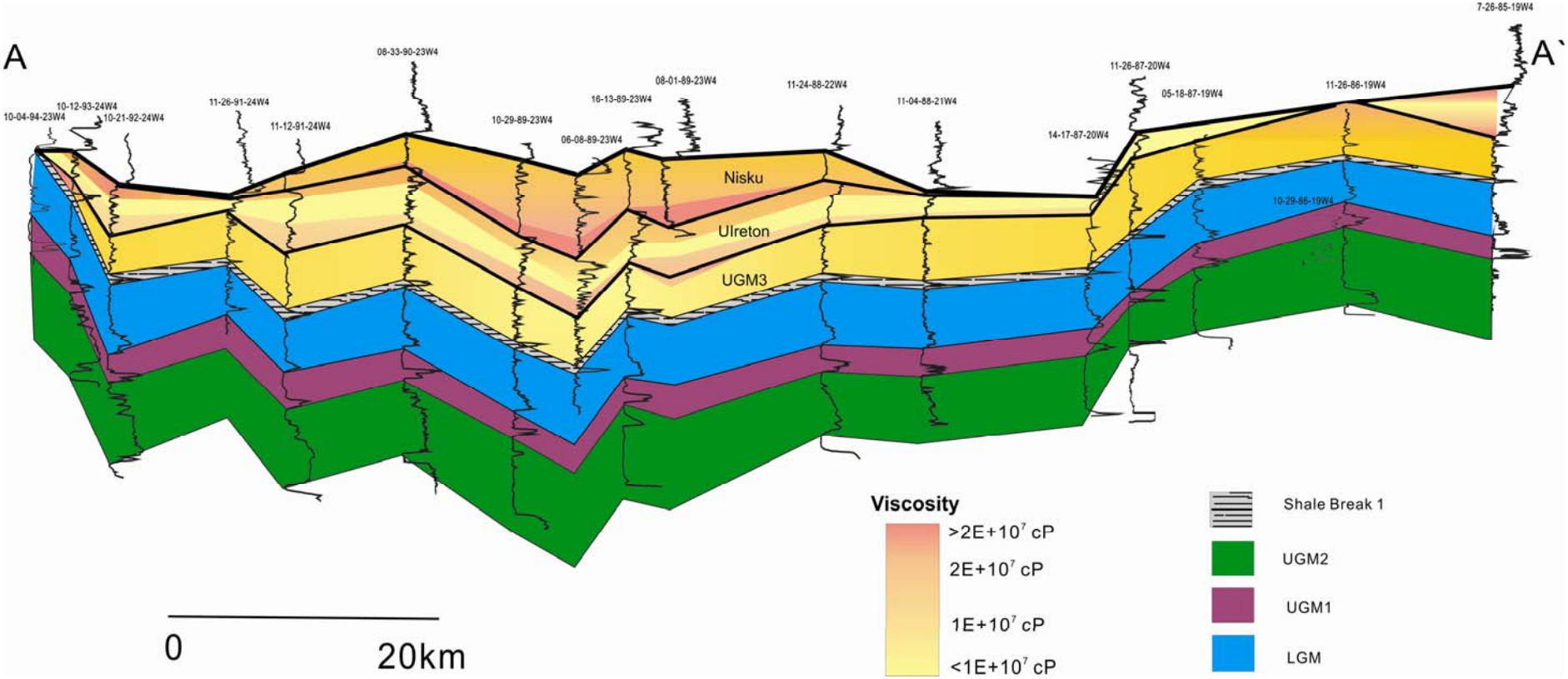

Figure 4.16 Strike cross section in the study area illustrating the viscosity variation in Nisku, Upper Ireton, and UGM 3. The standard viscosity at 11˚C is used (the column “11˚C” in Table 4.9).

samples have comparatively lower viscosities of less than 1E+7 cP.

In the Upper Grosmont 3, the bitumen is less viscous in the central area of the cross section, where the thickness of this rock unit is also the highest (e.g. well 10-29-89-23W4 in Figure 4.16). The viscosities increase away from the middle of the section and are mostly in the range of 1E+7 cP to 2E+7 cP. In few locations, the viscosities exceed 2E+7 cP. These bitumens were all sampled near the Upper Ireton-Grosmont boundary. The viscosity variations in the UGM 2 and UGM 1 were not mapped in this cross section, as only one or two measurements were available for each unit.

These observed lateral distribution patterns match the vertical variations (Figure 4.14) and the viscosity statistic results shown in Figure 4.11 and Figure 4.12.

4.7 Conclusions

The results from inter-laboratory comparisons indicate that viscosity measurements obtained from different laboratories on the same samples can be quite different and result can vary far above analytical errors. This is due to different methods of preparing samples, different procedures applied, and different equipment used in each laboratory. Furthermore, neglecting to consider non-Newtonian nature of Grosmont bitumen in the commercial laboratories (Lab A and B) likely is another factor that causes inconsistency with in-house measurement (Lab C).

The results from intra-laboratory comparisons show that consistency

in viscosity measurements can be reached by the procedures designed in this study. Therefore, this study leads the way to a detailed and practice-tested industry standard of viscosity measurement.

Distinct differences in “aging” were observed between bitumen samples extracted from legacy and fresh cores. A viscosity difference by one order of magnitude is not uncommon. Therefore, viscosity data from legacy cores must be corrected accordingly.

The viscosity distribution in the Grosmont reservoir is complex and varies cyclically with depth, commonly in one order of magnitude. Moreover, viscosity seems stratigraphic-related, as similar trends are observed in samples from adjacent wells in the Nisku, Upper Ireton, and the Grosmont Formations. Lateral variations of viscosity support the observation from vertical viscosity variation. Each rock unit probably has its own viscosity distribution pattern, with the high viscosity zones normally formed in the rock unit boundaries.

CHAPTER 5

BIODEGRADATION

5.1 Introduction

It is estimated that the amount of biodegraded oil in the earth exceeds that of conventional oil (Tissot and Welte, 1984). Major petroleum accumulations in the Western Canada Sedimentary Basin (WCSB), such as Athabasca, Cold Lake, Peace River, and the Grosmont are confirmed to be heavily to severely biodegraded hydrocarbons (heavy oil and bitumen deposits). Petroleum biodegradation is the alteration of crude oil by microorganisms, such as bacteria, yeast, and fungi (Connan, 1984; Blanc and Connan, 1994). Compared with conventional oil, biodegraded oil generally has a lower American Petroleum Institute (API) gravity, higher viscosity, and higher nitrogen, sulfur, oxygen (NSO) contents (Barker 1979). These changes reduce oil value and negatively affect the oil production and refining operation. Therefore, it is very important to measure and predict the extent of the biodegradation during exploration.

Biomarkers, or biological markers, are complex molecular fossils derived from biochemicals in once-living organisms (Peters et al., 2005).

In petroleum exploration, different biomarker compound classes, especially the steranes and triterpanes, have been widely studied and applied in oil and source rock correlation, oil maturity evaluation, organic-facies indications, and so forth. Because different biomarker parameters have different resistance to biodegradation, they are known to be the best proxies for assessing the level of petroleum biodegradation. Biomarker biodegradation scales have been successfully established to rank the extent of biodegradation of crude oils (e.g., Moldowan et al., 1992; Wenger, 2001; Peters et al., 2005).

Previous organic geochemical studies found that the Cretaceous oil sands and heavy oils in the WCSB are similar to each other, suggesting a common origin (e.g., Vigrass, 1968; Deroo et al., 1977; Mackenzie et al., 1983). Two biomarker studies published in the 1980s are specifically focused on the Grosmont reservoir. Hoffmann and Strausz (1986) studied bitumen samples from the Grosmont Formation and concluded that the maturity and source of Grosmont bitumen is similar to the bitumen in Athabasca deposits but subjected to a higher level of biodegradation. Brooks et al. (1989) examined a group of samples from the so-called “Carbonate Triangle” in northeastern Alberta, including samples from the Nisku, Upper Ireton, and the Grosmont Formations, and found that the Grosmont bitumen was the most biodegraded, followed by Nisku and Upper Ireton bitumen. However, no clear

geographic, stratigraphic or depth pattern to the level of biodegradation was found. This may have been due to the limited number of samples examined and their scattered distribution.

This chapter reports the biomarker results of 18 bitumen samples from the Nisku, Upper Ireton and the Grosmont Formations (Table 5.1 and Table 5.2). The complete geochemical data for all the samples are documented in the Appendix 3. The objective of this work is to: 1) characterize samples from the Nisku, Upper Ireton, and the Grosmont Formations in the study area according to their biomarker content; 2) explore the possible differences imprinted in biomarkers between fresh samples and legacy samples; and 3) quantify the extent of biodegradation, and characterize the relation of biodegradation to viscosity.

5.2 Methods

As described in Chapter 1, biomarker analysis was conducted on Batch 3 consisting of 18 samples from 10 wells in the study area (Table 5.1). Batch 3 included 5 samples from the Nisku Formation, 7 samples from the Upper Ireton Formation, and 6 samples from the Grosmont Formation. Among these samples, 12 were from legacy wells and 6 were from newly drilled wells that are adjacent to the legacy wells

(Figure 5.1).

Bitumens were extracted from the core samples with dichloromethane in a soxhlet apparatus. Gas chromatography-mass spectrometry (GC-MS) was performed on the saturated hydrocarbons using a Hewlett Packard 5890 chromatograph (splitless injection) interfaced to a HP 5970B quadrupole mass selective detector (electron input energy 70 eV, source temperature 250°C). The gas chromatograph was equipped with a HP-5MS capillary column (30 m x 0.25 mm i.d., 0.25 μm film thickness; J&W Scientific; helium carrier gas). Separation was achieved with an oven temperature program of 40°C for 5 min, increasing to 300°C at 4°C/min, then held at 300°C for 20 min. Further details of instrumental operation are also documented in Appendix 3.

Data were collected by single ion monitoring (SIM). Steranes and diasteranes were identified from the m/z 217 fragmentograms. Tricyclic terpanes (also known as tricyclics) and pentacyclic terpanes (primarily hopanes) were quantified from the m/z 191 fragmentograms. The m/z 177 ion fragmentograms were used for the analysis of 25-norhopanes (Peters et al., 2005).

Table 5.1 Location, depth, stratigraphic interval and the presence of selected biomarker compounds of the samples in this study.

Source	Well ID	Sample ID	Depth (m)	Formation	Steranes	Dia-steranes	Hopanes	25-Nor-hopanes	28,30-Bisnorhopane	Gamma-cerane	Nor-moretane
	11-12-91-24W4	N1	282.5-285.7	Nisku	—	minor	√	√	—	√	√
Legacy	10-21-92-24W4	UI1	363-366	Upper Ireton	—	minor	√	√	—	√	√
		UI2	377-379	Upper Ireton	—	√	√	√	—	√	√
	10-12-93-24W4	G1	444-446.7	UGM3	—	minor	√	√	—	√	√
	10-29-89-23W4	N2	265-267	Nisku	—	—	√	√	—	√	√
		N3	305.3-307.5	Nisku	—	√	√	√	—	√	√
		UI3	327.4-328.1	Upper Ireton	—	√	√	√	√	√	√
		G2	346-349	UGM3	—	√	√	√	√	√	√
	6-10-87-23W4	N4	349.4-358.2	Nisku	—	√	√	√	√	√	√
	11-26-87-20W4	UI4	263.4-267	Upper Ireton	—	√	√	√	√	√	√
	10-29-86-19W4	G3	283-283.3	UGM3	—	√	√	√	√	√	√
		G4	303-303.6	UGM3	—	√	√	√	√	√	√
Fresh	11-26-91-24W4	UI5	316.8-319	Upper Ireton	—	√	√	√	√	√	√
		G5	335.3-336.4	UGM3	—	√	√	√	√	√	√
	06-08-89-23W4	N5	270.6-280.6	Nisku	√	√	√	√	√	√	√
		G6	322.8-324.2	UGM3	—	√	√	√	—	√	√
	07-26-85-19W4	UI6	325-326.2	Upper Ireton	—	minor	√	√	—	√	√
		G7	350.2-350.8	UGM3	—	√	√	√	√	√	√

Table 5.2 The distribution of selected compound classes and the representative biomarker ratios in the samples.

Well ID	Drilled year	Sample ID	Viscosity[1] (cP)	Hopanes distribution	H30/ H29[2]	Ts/ Tm[3]	Tricyclics distribution	C23/ H29[4]	25-norhopanes distribution	N29/ H29[5]	N28/ H29[6]
11-12-91-24W4	1980	N1	1.59E+08	minor[7]	0.09	0.39	minor	0.03	medium[9]	0.18	0.30
10-21-92-24W4	1980	UI1	4.05E+08	minor	0.08	0.34	minor	0.05	minor	0.04	0.03
		UI2	2.80E+06	minor	0.05	0.35	major	0.50	medium	0.10	0.14
10-12-93-24W4	1981	G1	2.75E+07	minor	0.08	0.33	minor	0.06	minor	0.04	0.03
10-29-89-23W4	1983	N2	8.90E+06	minor	0.08	0.39	minor	0.06	medium	0.16	0.28
		N3	4.83E+07	minor	0.09	0.36	major	0.73	medium	0.20	0.32
		UI3	1.73E+07	minor	0.16	0.39	major	1.79	major	1.43	2.62
		G2	1.00E+07	major[8]	1.01	0.41	major	2.12	major	3.38	7.60
6-10-87-23W4	1978	N4	3.00E+06	major	0.81	0.44	major	2.19	major	2.04	4.16
11-26-87-20W4	1980	UI4	2.80E+06	major	1.42	0.39	major	0.89	minor	0.03	0.04
10-29-86-19W4	1975	G3	3.64E+07	major	0.98	0.36	major	0.65	minor	0.05	0.06
		G4	1.50E+07	major	1.10	0.34	major	0.86	medium	0.16	0.24
11-26-91-24W4	2007	UI5	1.27E+06	major	1.27	0.33	major	0.65	minor	0.05	0.03
		G5	5.26E+06	major	1.12	0.37	major	0.66	minor	0.05	0.03
06-08-89-23W4	2007	N5	2.91E+06	major	1.61	0.28	major	0.76	minor	0.07	0.07
		G6	1.64E+07	minor	0.13	0.30	major	0.94	major	1.17	2.15
07-26-85-19W4	2007	UI6	1.73E+07	minor	0.13	0.34	major	0.79	major	1.16	2.16
		G7	5.89E+07	major	0.99	0.29	major	0.22	medium	0.33	0.63

1. UI2 to G4 are measured at 30°C, rest of the samples are measured at 20°C. Data obtained from Lab B. 2. 17α(H)-hopane/17α(H)-norhopane.
3. 18α(H)-trisnorhopane/17α(H)-trisnorhopane. 4. C23 tricyclic terpane/17α(H)-norhopane. 5. C29 17α(H) 25-norhopane/17α(H)-norhopane.
6. C28 17α(H) 25, 30-bisnorhopane /17α(H)-norhopane. 7-9. Indications of the relative abundance for each biomarker class.

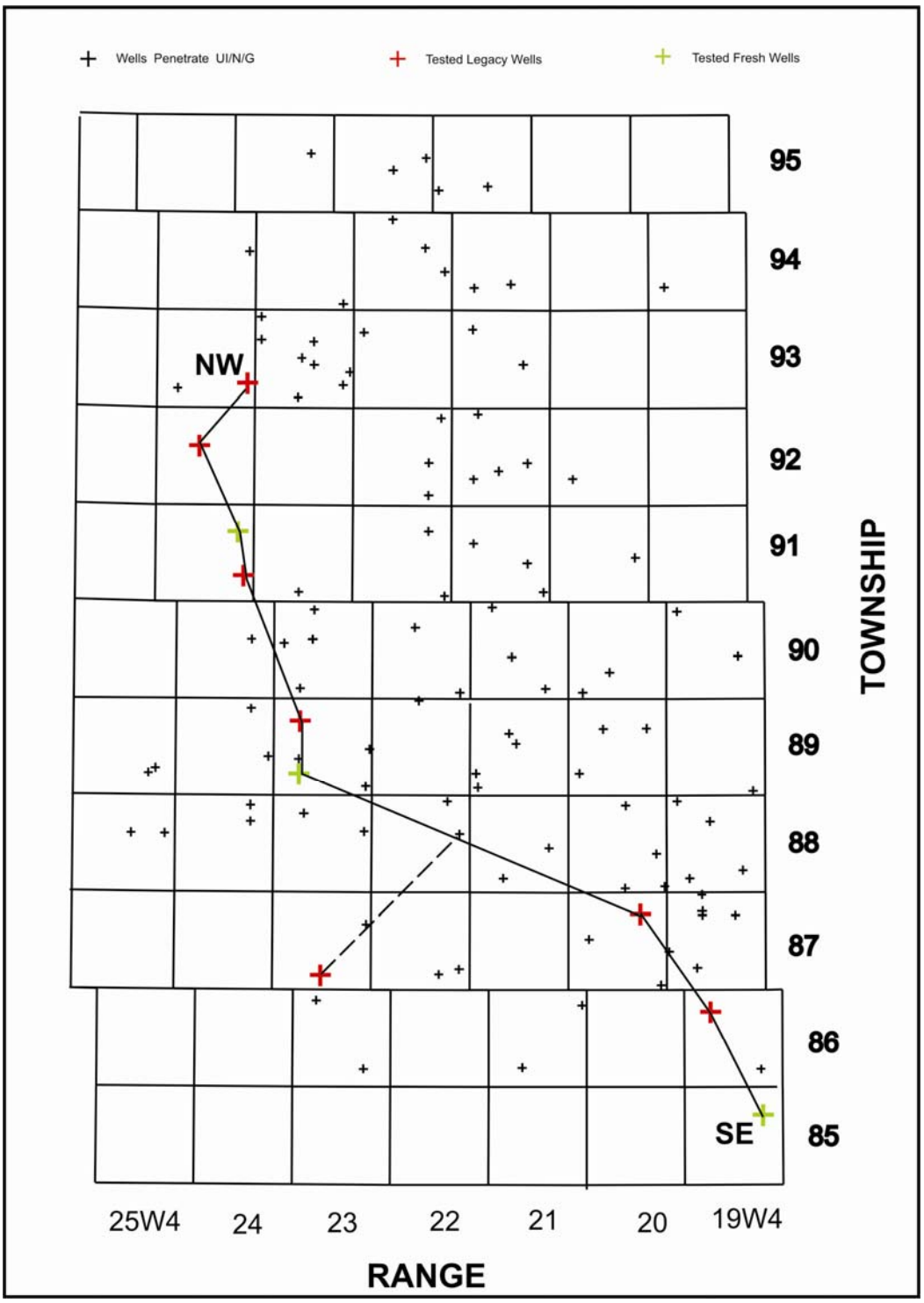

Figure 5.1 Well control map of the study area showing the locations of the wells with biomarker analyses. The legacy wells and fresh wells are highlighted in red and green. The dotted line is the projection line of well 6-10-87-23W4 for cross section NW-SE shown in Figure 5.8.

5.3 Biomarker Distributions

As shown in Table 5.1, regular steranes are completely missing in 17 of the 18 samples analyzed. This is in agreement with the results from previous studies, i.e., regular steranes are almost all biodegraded in the bitumens from the Nisku, Upper Ireton and the Grosmont Formations (Brooks et al., 1988, 1989). C27 and C29 diasteranes were detected in most of the samples from the m/z 217 fragmentograms, but in many cases the quantities appear to be highly reduced, such as in samples G1 and UI6. No diasteranes were found in sample N2.

Regular hopanes are present in all 18 samples analyzed herein; however, their distributions were not the same but roughly form two groups, noted as “major” and “minor” in the column “Hopanes distribution” in Table 5.2. The “major” group includes 9 samples that have a full set of homohopanes (i.e., C31–C35), like samples G2, N4, and UI4. This group is normally dominated by C29 17α(H)-norhopane (H29 for short) and/or C30 17α(H)-hopane (H30 for short) with a ratio (H29/H30) that ranges from 0.81 to 1.61 (Table 5.2). The “minor” group includes the rest of the samples that are dominated by C29 17α(H)-norhopane and generally have highly biodegraded C30–C33 hopanes. For example, in several samples, only traces of C31–C33 hopanes were detectable in the m/z 191 fragmentograms (e.g., samples N1, UI6, and G6) while the C34 and C35 extended hopanes remain.

The H29/H30 ratios are in the range of 0.05 to 0.16 in this group.

The distribution of tricyclic terpanes can also be separated into two groups, noted as “major” and “minor” in the column “Tricyclics distribution” in Table 5.2. The “major” group consists of 14 samples that have abundant tricyclics and have a fairly high peak at C23 tricyclic terpane (C23 for short) in the m/z 191 fragmentograms, with the C23/H29 ratio ranging from 0.22 to 2.19 (Table 5.2). The other 4 samples (samples N1, UI2, G1, N2) in the “minor” group lack C23 tricyclic terpane (C23/H29<0.06), and all the other tricyclic terpanes are approximately equally distributed.

The distributions of 25-norhopanes in the samples examined are characterized by the presence and absence of certain 25-norhopane members in the m/z 177 fragmentograms. Accordingly, the 18 samples can be separated into three groups, noted as “major”, “medium”, and “minor” in the column “25-norhopanes distribution” in Table 5.2. The “major” group consists of 6 samples that have a series of 25-norhopanes from C28 to C33; with only one of them having a discernible peak of C34 (i.e., sample G2). These samples also have very high concentrations of C28 17a(H)-25,30 bisnorhopane (N28 for short), which is usually the largest peak in the m/z 177 fragmentograms (N28/H29 ranges from 0.63–7.60), such as in samples UI3 and N4 (Table 5.2). The “medium” group consists of 5 samples that exhibit only

fairly low amounts of 17a(H)-25,30 bisnorhopane and 17a(H)-25 norhopane, and they lack all the extended 25-norhopanes. The N28/H29 ratio varies from 0.28 to 0.32. The “minor” group includes the other 7 samples that have very low concentrations or even absence of 25-norhopanes, with N28/H29 ratios range from 0.03 to 0.07.

28, 30-bisnorhopane was detected in 10 of the 18 samples (e.g., samples N4, UI3, G2 in Table 5.1). Quite similar to the previous results, this compound is not consistently present in the carbonate samples. Gammacerane that was previously found in all the samples examined (Brooks et al 1988, 1989), was also detected in the samples here (Table 5.1). Similarly, another highly bioresistant compound, normoretane, is detected in all samples and exhibits a high concentration in all m/z 177 fragmentograms.

5.4 Biodegradation Characteristics

Useful scales to assess the extent of biodegradation have been proposed and developed by many workers (e.g., Brooks et al., 1988, 1989; Moldowan et al., 1992; Wenger et al., 2001; and Peters et al., 2005). Brooks et al. (1988, 1989) suggested the following order of susceptibility to biodegradation for the heavy oil, oil sands, and carbonate bitumen in the WCSB: n-alkanes > acyclic isoprenoids >

regular steranes > hopanes > rearranged steranes > tricyclic terpanes, which fit the general order of biodegradation scale. In addition, the susceptibility of individual compounds within each class was characterized by Peters et al. (2005). Variations in these sequences depend on the oil source, the complex and largely unknown microbial population in the subsurface, and reservoir conditions.

From the biomarker distributions described above, it is clear that all the bitumen samples analyzed herein are severely biodegraded. Specifically, the m/z 217 fragmentograms of samples N5, G1, and N2 in Figure 5.2 show the distribution of steranes and diasteranes of severe levels of biodegradation. In sample N5, the regular steranes has already been biodegraded. However, most of the samples examined in this study show more severe biodegradation; even the levels of diasteranes were heavily reduced (e.g., sample G1) or completely missing (e.g., sample N2). Moreover, these fragmentograms display a preferential loss of diasteranes of C27R > C27S > C29R > C29S, which agrees with the general order of biodegradation that the lower homologs and R isomer of diasteranes are biodegraded preferentially (Peter et al., 2005).

Figure 5.3 shows the m/z 191 fragmentograms from samples UI4, UI2, and N1 with an increasing level of biodegradation. It can be seen that sample UI4 has a relatively unaffected distribution of hopanes and

tricyclic terpanes with an abundance of C30 17α(H)-hopanes and C23 tricyclic terpanes. There appears to be some preferential degradation of the 22R relative to the 22S diastereoisomer of the C31–C35 17α(H)-hopanes. In samples UI2 and N1 in Figure 5.3, all the peaks from C30 to C33 are highly reduced, as the microbes appear to favor C30–C33 > C34–C35 17α(H)-hopanes. This is similar to the biodegradation pathway observed by Peters and Moldowan (1991) for homohopanes with the presence of 25-norhopanes. Moreover, it is interesting to note that the 22S C34 hopane (peak “w” in Figure 5.3) and 22R C35 hopane (peak “x” in Figure 5.3) are preserved in the m/z 191 fragmentograms, indicating that at least the 22R diastereoisomer of C35 hopane is more bioresistant than its 22S counterpart. This is an unusual sequence of biodegradation, as in most cases the 22R isomers are easier to be biodegraded than 22S isomers (e.g., Peters et al., 2005).

In the m/z 191 fragmentogram of sample UI2, the hopanes are heavily biodegraded, but the distributions of tricyclic terpanes are relatively unaltered, indicating a higher level of bioresistance. From Table 5.1 and Table 5.2, it is also evident that tricyclic terpanes are more bioresistant than hopanes and even diasteranes (e.g., samples G6 and UI6). This is inconsistent with some proposed biodegradation scales (e.g., Wenger et al., 2002) but is in agreement with the previous

investigation in the Grosmont reservoir (e.g., Brooks et al., 1989).

The m/z 191 fragmentogram of sample N1 (Figure 5.3) shows an affected distribution of tricyclic terpanes, displayed by an almost complete removal of C23 and heavily reduced concentrations of C21, C22, and C24 tricyclic terpanes. This suggests a general order of susceptibility to biodegradation of tricyclic terpanes: C23, C24 > C21, C22 > C25 > C20, C26–C30. This biodegradation pathway implies that the microbes prefer to consume the high abundance low-carbon-number homologs of tricyclic terpanes. Also, the relative concentrations of 22S C34 and 22R C35 hopanes were not affected, even after the removal of tricyclic terpanes, indicating a higher resistance to biodegradation of these two homohopanes as compared to the tricyclics.

The distribution of 25-norhopanes can be divided into three groups according to their abundance. The m/z 177 fragmentograms of representive samples from these groups are shown in Figure 5.4. It can be seen that these three samples exhibit a stepwise reduction in concentration of 25-norhopanes from high-carbon-number homologs to low-carbon-number ones. A biodegradation pathway of this pattern was observed by Bost et al. (2001) under aerobic conditions in the laboratory. Nevertheless, it does not necessarily mean that the distributions of 25-norhopanes in these samples are caused by aerobic biodegradation.

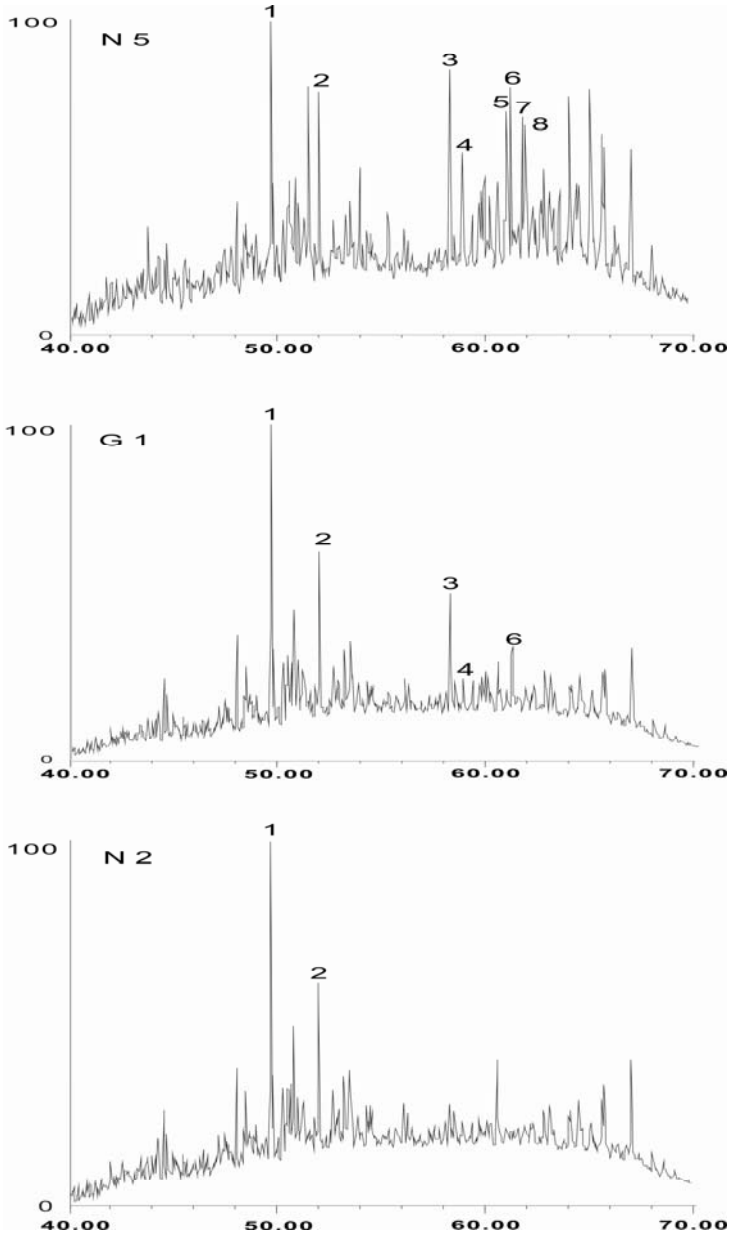

Figure 5.2 m/z 217 fragmentograms of the sterane distribution of the samples showing increasing biodegradation. Peaks are identified in Table 5.3.

Table 5.3 Compounds identified in the m/z 217 fragmentograms.	
Peak #	**Compound**
1	C21 sterane
2	C22 sterane
3	13β(H), 17a(H) -diacholestane(20S) or C27 diasterane (20S)
4	13β(H), 17a(H)-diacholestane(20R) or C27 diasterane (20R)
5	5a(H), 14a(H), 17a(H)-cholestane (20S) or C27 sterane (20S)
6	24-ethyl-13β(H), 17a(H)-diacholestane (20S) or C29 diasterane (20S)
7	5a(H), I4 a(H), 17 a(H)-cholestane(20R) or C27 sterane (20R)
8	24-ethyl-13β(H),17 a(H)-diacholestane(20R) or C29 diasterane (20R)

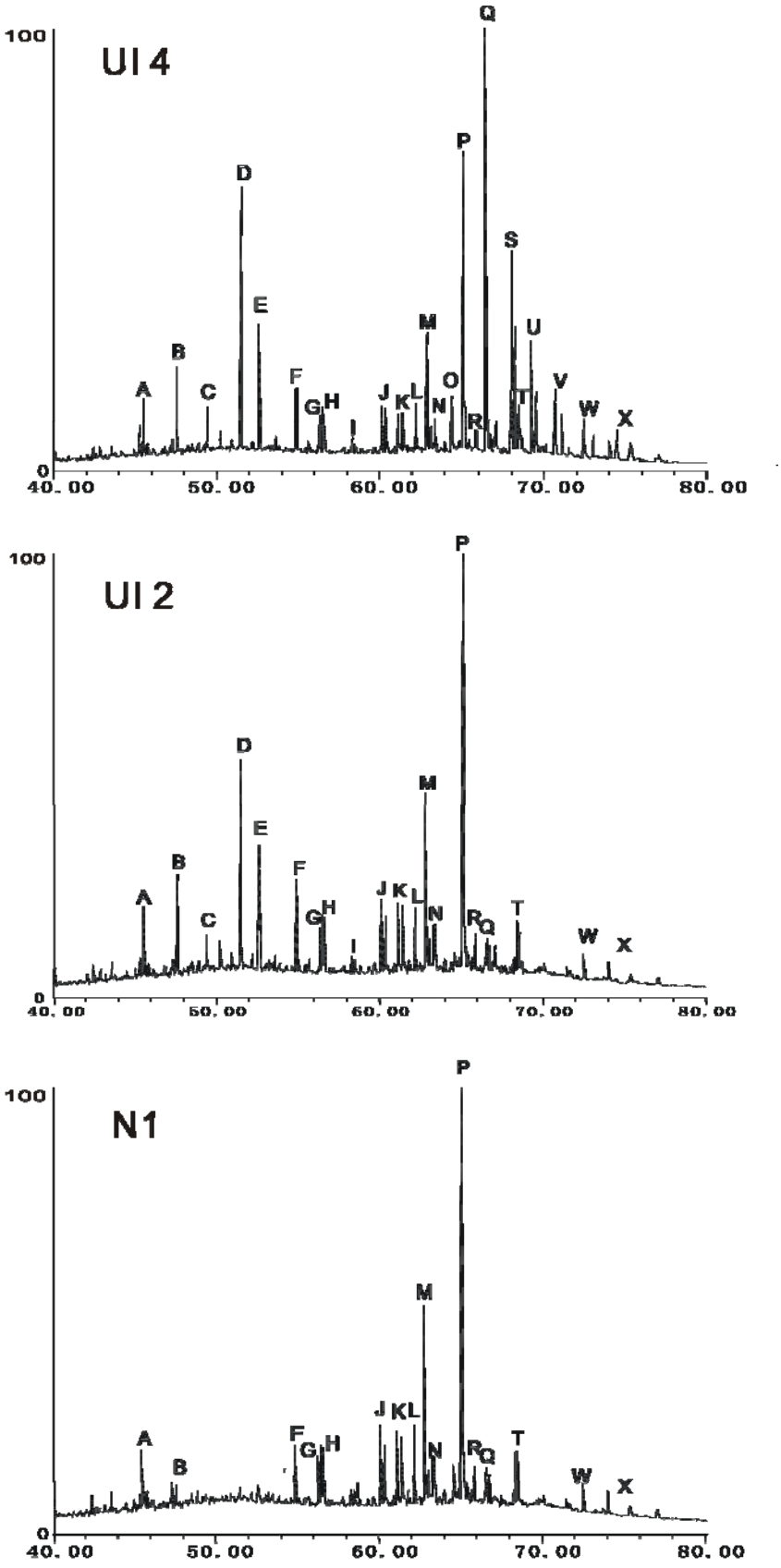

Figure 5.3 m/z 191 fragmentograms of the triterpanes distributions showing an increasing level of biodegradation. Peaks are identified in Table 5.4.

The origin and the enrichment of the 25-norhopanes in biodegraded oil have been controversial for many decades. Several hypotheses have been proposed for the origins of these compounds, and the prevailing idea is that the 25-norhopanes are derived from the demethylation of their hopane counterparts (e.g., Peters et al., 2005). Unfortunately, no definite conclusion can be derived from the present set of samples by comparing the distributions of hopanes and 25-norhopanes (Table 5.2). Taking Figure 5.4 as an example, these three samples have quite different abundance of 25-norhopanes, yet their hopanes distributions are similar (Table 5.2). Also, as shown in Figure 5.5, the preferential removal of C30 to C34 hopanes and the presence of C29 to C33 25-norhopanes suggest that the 25-norhopane is likely derived from the conversion of their hopanes counterpart. However, there is no selective rise of the 22S C34 25-norhopanes to reflect the selective loss of 22S C35 hopane. Indeed, a close examination of the distribution of hopanes and 25-norhapanes from Table 5.2 reveals that the presence and absence of 25-norhopanes do not match with the biodegradation degree as indicated by the hopanes. That is, the distribution of 25-norhopanes is independent of the distribution of hopanes in the samples examined here.

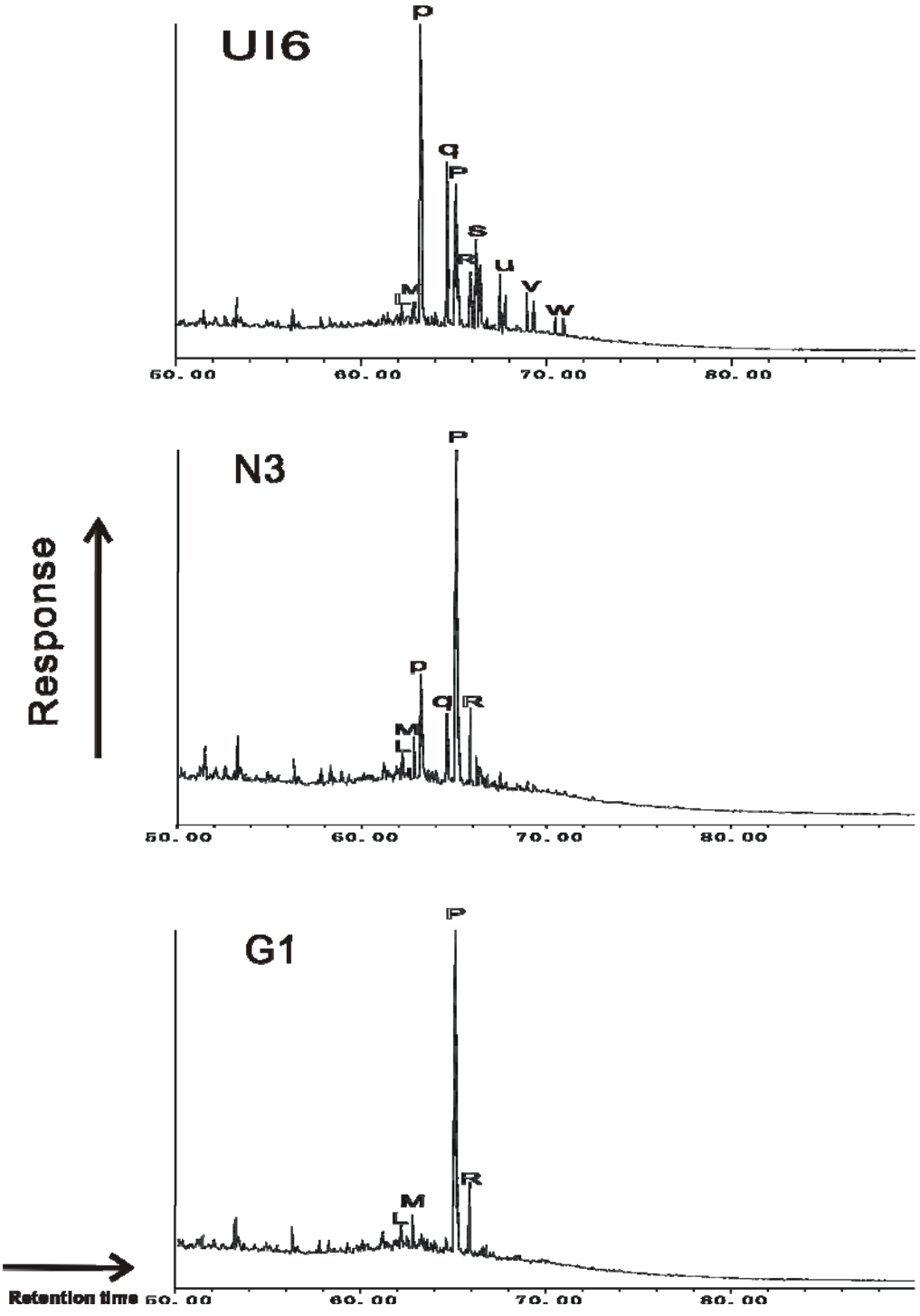

Figure 5.4 m/z 177 fragmentograms showing the distribution of demethylated hopanes. Note the presence and absence of 25-norhopanes. Peaks identified in Table 5.4.

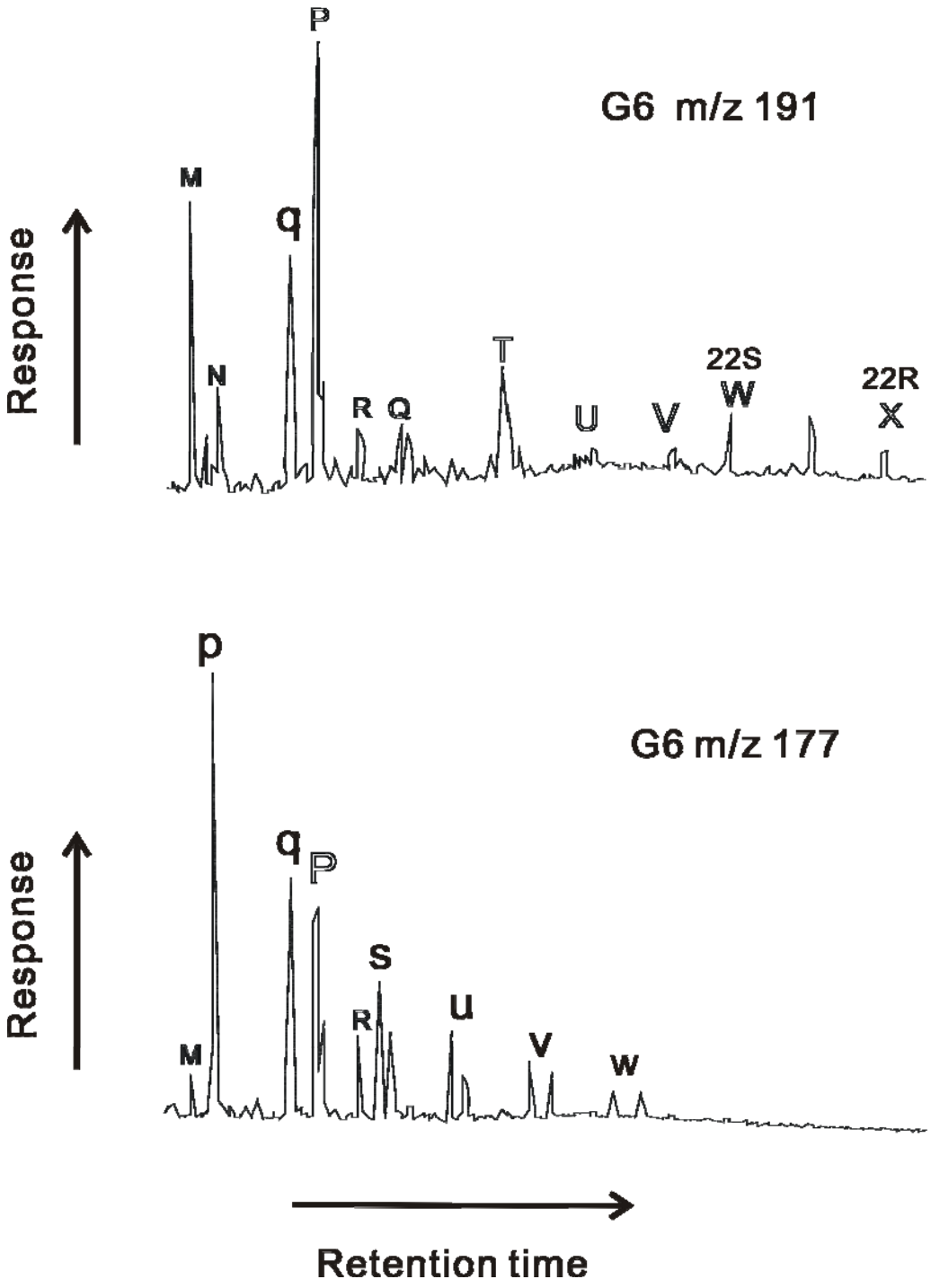

Figure 5.5 Comparison of the m/z 191 fragmentogram and the m/z 177 fragmentograms showing the distribution of hopanes and 25-norhopanes. Peaks identified in Table 5.4.

Normoretane, which is not mentioned in the previous studies, can be found in both m/z 191 and m/z 177 fragmentograms of all the samples. Its abundance in severely biodegraded samples (e.g., sample N1) indicates that normoretane is more bioresistant than most hopanes, 25-norhopanes and tricyclic terpanes.

Previous studies had reported the presence of 28, 30-bisnorhopane in all the samples from heavy oil, oil sands (Brooks et al., 1988), and part of the samples from the Grosmont reservoir (Brooks et al., 1989). Brooks et al. (1989) believed that 28,30-bisnorhopane was an oil source indicator, and concluded that there were at least two oil sources for the bitumen deposit in the Grosmont reservoir, based on the absence and presence of 28, 30-bisnorhopane. If this is true, then the results obtained here support their idea. However, it needs to be noted that for all the samples that lack 28, 30-bisnorhopane, their hopanes are also severely biodegraded, and all these samples belong to the group previously classified as “minor” in the “hopanes distribution” (Table 5.1 and Table 5.2). In this group, 28, 30-bisnorhopane is detected in only one sample (i.e., sample UI3). Moreover, its H30/H29 ratio is the highest (0.16) as compared to the other samples (as low as 0.05), indicating that this sample is less biodegraded than the others in the “minor” group. As shown in Table 5.1 and Table 5.2, the presence and absence of 28, 30-bisnorhopane are directly related to the abundance of hopanes. A

similar relationship can also be observed from the data presented by Brooks et al (1989). Therefore, it can be concluded that for the 18 samples examined here, the 28, 30-bisnorhopanes are altered and depleted at about the same rank of biodegradation as the hopanes. As a result, it is more likely that the 28, 30-bisnorhopane was widely present in the Grosmont reservoir before biodegradation but had been severely biodegraded to an undetectable level, rather than the previous conclusion that there were two oil families in the Grosmont reservoir (i.e., Brook et al., 1989). If this argument is valid, then it supports the hypothesis that the bitumen from the Grosmont reservoir was sourced from the same stratigraphic units as the overlying Cretaceous heavy oil and oil sands deposits.

Table 5.4 Compounds identified in the m/z 191and m/z 177 fragmentograms.	
Peak	**Compound**
A	C20 tricyclic terpane
B	C21 tricyclic terpane
C	C22 tricyclic terpane
D	C23 tricyclic terpane
E	C24 tricyclic terpane
F	C25 tricyclic terpane
G	C24 tetracyclic terpane
H	C26 tricyclic terpane isomers
I	C27 tricyclic terpane isomers
J	C28 tricyclic terpane isomers
K	C29 tricyclic terpane isomers
L	18a(H)-trisnorhopane(Ts)
M	17a(H)-trisnorhopane(Tm)
N	C30 tricyclic terpane isomers
O	28,30-bisnorhopanes
P	17α(H),21β(H)-norhopane
Q	17α(H) 21β(H)-hopane
R	17β(H), 21α(H)-normoretane
S	(20S) and 20(R) 17α(H), 21β(H)-homohopanes
T	gammacerane
U	(20S) and 20(R) 17α(H), 21β(H)-bishomohopanes
V	(20S) and 20(R) 17α(H), 21β(H)-C33 hopanes
W	(20S) and 20(R) 17α(H), 21β(H)-C34 hopanes
X	(20S) and 20(R) 17α(H), 21β(H)-C35 hopanes
p	17α(H)-25,30 bisnorhopane
q	17α(H)-25 norhopane
s	(20S) and 20(R) 17α(H)-25 norhomohopanes
u	(20S) and 20(R) 17α(H)-25 norbishomohopanes
v	(20S) and 20(R) 17α(H)-25 nor C32 hopanes
w	(20S) and 20(R) 17α(H)-25 nor C33 hopanes

5.5 The Levels of Biodegradation in the Grosmont Reservoir

Similar to the biodegradation sequence observed by Brooks et al. (1988, 1989), the susceptibility of different compound classes in this study generally decreases in the following order: steranes > hopanes > diasteranes > tricyclic terpanes > gammacerane and normoretane. However, several samples do not follow this trend. For example, samples G2 and N4 have a fairly low concentration of C29 30-norhopane compared to the abundance of C23 tricyclic terpane and other hopane compounds (C30 to C35). Sample G7, on the other hand, has very low concentration of C23 tricyclic terpane while the hopanes and 25-norhopanes are present, which was opposite to the general sequence of biodegradation. The reasons for these unusual distributions are not clear. Only these three samples have high concentrations of both hopanes and 25-norhopanes, suggesting that the source of these samples might be different from the others. Other possibilities include different microbial populations under disparate reservoir conditions, or unknown manners of oil mixing, etc.

The extent of biodegradation of the other 15 samples is differentiated by combining several biomarker ratios. Among them, two combinations work very well. One combined the ratios of 17α(H)-hopane/17α(H)-norhopane, C23 tricyclic terpane/17α(H)-norhopane, and 17α(H)-trisnorhopane/17α(H)-norhopane together,

based on the increasing bioresistance from 17α(H)-hopane to 17α(H)-trisnorhopane (commonly known as Tm). The other combination is 17α(H)-hopane/17α(H)-trisnorhopane, 17α(H)-norhopane/17α(H)-trisnorhopane, and C23 tricyclic terpane/17α(H)-trisnorhopane, based on the increased in bioresistance from 17α(H)-hopane to C23 tricyclic terpane and the stable concentration of 17α(H)-trisnorhopane in all the samples. As shown in ternary plots (Figure 5.6 and Figure 5.7), both combinations successfully separate the samples into three groups, reflecting their relative level of biodegradation. These results fit the actual biomarker distribution, as indicated by the presence and absence of certain tricyclic and hopane compounds (Table 5.1 and Table 5.2).

These considerations lead to a simple 3-level biodegradation pattern. Level A has the highest extent of biodegradation, in which the tricyclics are heavily degraded. Level B has medium extent of biodegradation and is characterized by a reduced distribution of hopanes and 25-norhopanes. Level C has minor extent of biodegradation that includes the samples with relatively unaltered triterpanes. As shown in Table 5.5, the two combinations yield the same results for all the samples with regard to the proposed levels of biodegradation.

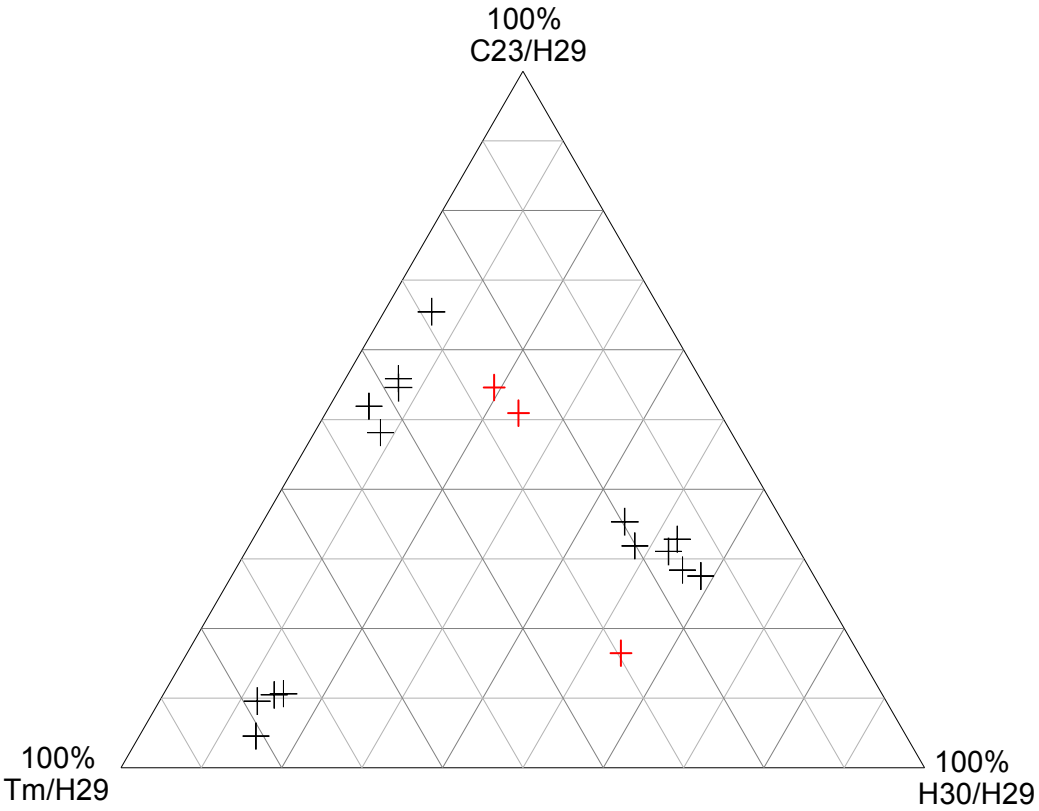

Figure 5.6 Ternary diagram showing the different extent of biodegradation of the 18 samples based on the normalized ratios of H30/H29[1], C23/H29[2], and Tm/H29[3]. Three abnormal samples, i.e., samples G2, N4, and G7, were highlighted in red and are not used in the plot. Please see Table 5.5 for data source and footnotes.

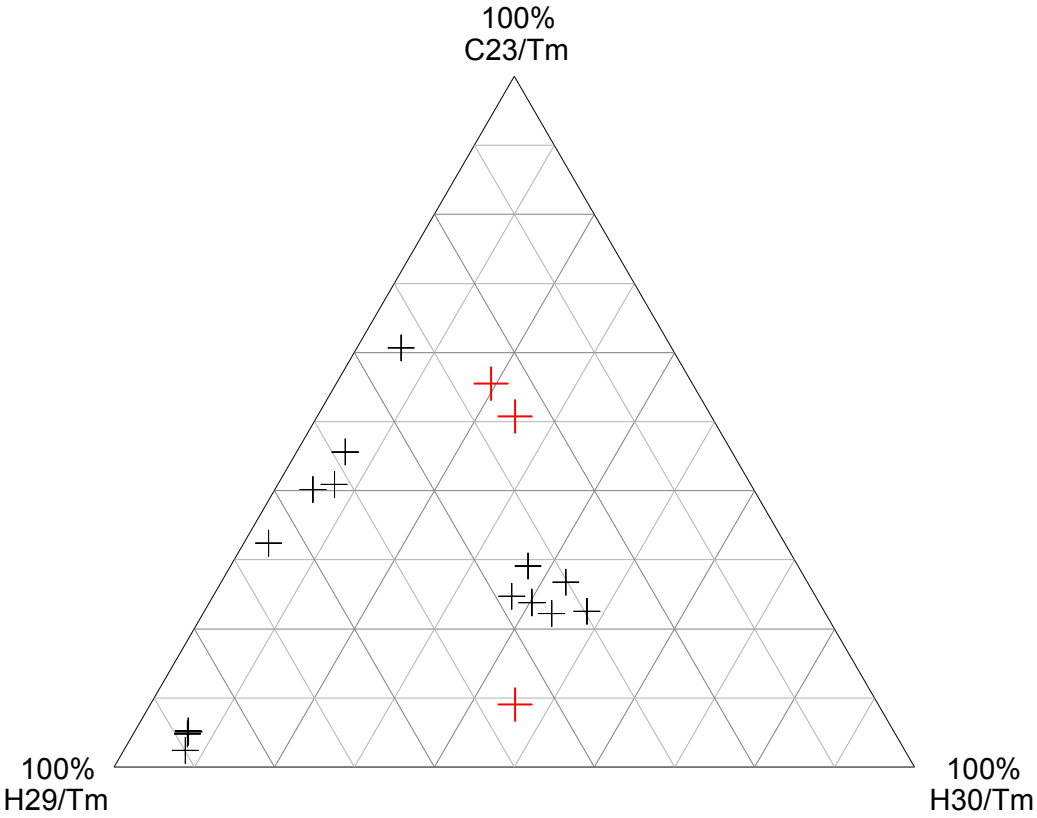

Figure 5.7 Ternary diagram showing the different extent of biodegradation based on the normalized ratios of H30/Tm[5], C23/Tm[6], and H29/Tm[7]. A comparison with Figure 5.7 shows that both plots successively separate the samples into three major groups, reflecting the extent of biodegradation. Please see Table 5.5 for data source and footnotes. Three abnormal samples, i.e., samples G2, N4, and G7, were highlighted in red and were not used in the plot.

Table 5.5 The calculated ratios of the biomarker parameters and normalized percentages used in the ternary plots for characterizing the biodegradation.

Sample ID	H30/ H29[1]	C23/ H29[2]	Tm/ H29[3]	Sum[4]	H30/ H29%*	C23/ H29%*	Tm/ H29%*	Bdn Level+	C23/ Tm[5]	H29/ Tm[6]	H30/ Tm[7]	Sum[8]	C23/ Tm%*	H29/ Tm%*	H30/ Tm%*
N1	0.09	0.03	0.47	0.59	14.5%	4.5%	80.9%	A	0.06	2.11	0.18	2.35	2.4%	90.0%	7.7%
UI1	0.08	0.05	0.38	0.51	14.9%	10.6%	74.5%	A	0.14	2.63	0.20	2.97	4.8%	88.5%	6.7%
UI2	0.05	0.50	0.42	0.97	4.9%	51.9%	43.2%	B	1.20	2.39	0.11	3.71	32.4%	64.5%	3.1%
G1	0.08	0.06	0.42	0.55	13.8%	10.5%	75.7%	A	0.14	2.39	0.18	2.71	5.1%	88.2%	6.7%
N2	0.08	0.06	0.48	0.62	12.2%	9.6%	78.3%	A	0.12	2.07	0.16	2.34	5.2%	88.2%	6.6%
N3	0.09	0.73	0.49	1.31	6.6%	55.9%	37.6%	B	1.49	2.04	0.17	3.70	40.2%	55.1%	4.7%
UI3	0.16	1.79	0.78	2.74	5.9%	65.4%	28.6%	B	2.29	1.27	0.21	3.77	60.7%	33.8%	5.5%
G2	1.01	2.12	0.93	4.06	24.9%	52.3%	22.8%	C	2.29	1.08	1.09	4.46	51.3%	24.2%	24.5%
N4	0.81	2.19	1.04	4.04	20.1%	54.3%	25.6%	C	2.12	0.97	0.78	3.86	54.9%	25.0%	20.1%
UI4	1.42	0.89	0.39	2.70	52.8%	32.8%	14.4%	C	2.29	2.58	3.68	8.54	26.8%	30.2%	43.0%
G3	0.98	0.65	0.41	2.04	48.0%	31.9%	20.1%	C	1.58	2.43	2.38	6.40	24.7%	38.0%	37.3%
G4	1.10	0.86	0.48	2.45	45.0%	35.3%	19.7%	C	1.80	2.08	2.29	6.16	29.1%	33.7%	37.1%
UI5	1.27	0.65	0.36	2.28	55.7%	28.4%	15.9%	C	1.78	2.75	3.49	8.02	22.2%	34.2%	43.5%
G5	1.12	0.66	0.35	2.13	52.6%	31.1%	16.3%	C	1.90	2.87	3.22	7.98	23.8%	35.9%	40.3%
N5	1.61	0.76	0.39	2.76	58.4%	27.5%	14.1%	C	1.96	2.57	4.15	8.68	22.5%	29.7%	47.8%
G6	0.13	0.94	0.66	1.73	7.2%	54.6%	38.2%	B	1.43	1.52	0.19	3.14	45.6%	48.4%	6.0%
UI6	0.13	0.79	0.71	1.63	8.2%	48.1%	43.6%	B	1.10	1.40	0.19	2.69	40.9%	52.0%	7.0%
G7	0.99	0.22	0.47	1.68	59.0%	13.1%	27.9%	C	0.47	2.14	2.13	4.73	9.9%	45.2%	44.9%

1. 17α(H)-hopane / 17α(H)-norhopane.
2. C23 tricyclic terpane / 17α(H)-norhopane.
3. 17α(H)-trisnorhopane / 17α(H)-norhopane.
4. Sum of the ratios from 1, 2, 3.
5. 17α(H)-hopane / 17α(H)-trisnorhopane.
6. 17α(H)-norhopane / 17α(H)-trisnorhopane,.
7. C23 tricyclic terpane / 17α(H)-trisnorhopane.
8. Sum of the ratios from 5, 6, 7.

*. Normalized percentages.

+. The defined biodegradation levels for evaluating the biodegradation extent of the samples.

Based on the presence or absence of specific biomarker compounds and certain biomarker ratios, Brooks et al. (1989) concluded that the succession from most biodegraded to least biodegraded was Grosmont Formation > Nisku Formation > Upper Ireton Formation. Other than this general biodegradation scheme, they found no clear geographic, stratigraphic, or depth pattern to biodegradation.

The strike cross section in Figure 5.8 can be used to illustrate the regional distribution of biodegradation in the study area (section line is highlighted in Figure 5.1). A vertical exaggeration of approximately 520X was used. Several general trends can be observed from this cross section. 1) The northwest of the study area seems to have suffered more severe biodegradation than the southeast region. 2) The samples that exhibit the highest level of biodegradation (level A) are observed in the northwest and central areas. 3) Most of the samples having biodegradation levels of A or B are obtained from intervals near the Formation boundaries (both above and below). 4) The samples from fresh wells, highlighted in green in Figure 5.8, appear less biodegraded compared to legacy samples from adjacent wells, which may be due to a lesser extent of exposure in the air (aging). Yet no firm conclusions can be made due to the limited data. 5) One single well, 10-29-89-23W4, shows a decreasing biodegradation with depth. Other than this, no clear depth pattern to biodegradation was found in those wells. This may due to the limited sample points in each well.

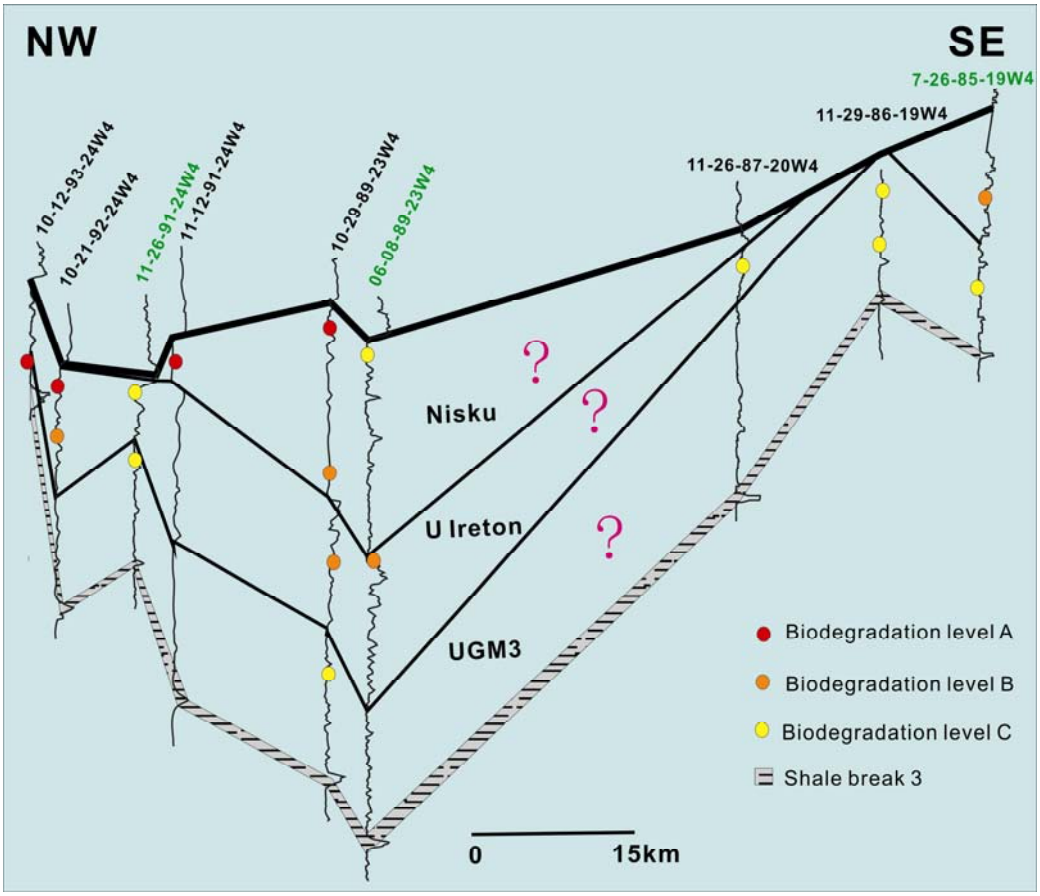

Figure 5.8 A cross-section from northwest to southeast of the study area to illustrate the biodegradation pattern. The question marks indicate areas that lack sample control. Fresh wells are highlighted in green.

5.6 The Relationship of Aging and Viscosity to Biodegradation

In the previous chapter, the aging of bitumen was observed as increasing viscosity and heteroatom content from fresh samples to legacy samples. Adams et al. (2008) compared the total ion current GC-MS fragmentograms for two sets of bitumen samples that have been stored for different periods of time. They showed that the fresh samples contain more light end compounds than legacy samples and concluded that evaporation of light end fraction over storage time was responsible for the increase in bitumen viscosity. Similar results were obtained in this study by comparing samples from a legacy well and a nearby fresh well. Figure 5.9 shows that the fresh sample (sample UI5) contains a substantial quantity of light ends compared to the legacy sample (sample UI4), and the fresh sample has a lower viscosity than the legacy sample (Table 5.2).

Although it is obvious that legacy bitumens have smaller light end fraction and higher viscosities, the fresh samples and the legacy samples could exhibit a similar extent of biodegradation (Table 5.1 and Table 5.2). Therefore, the difference between fresh samples and legacy samples cannot be identified from their biomarker characteristics solely. Fresh samples and legacy samples with quite different viscosities might have similar biomarker distributions and could be present in the same biodegradation level (Table 5.2 and Table 5.5). This indicates the high resistance of the biomarkers to evaporation. Thus, the biomarker data obtained here suggest that the loss of lower molecular weight hydrocarbons by evaporation over time, i.e. physical aging rather than

biological aging, is mainly responsible for the higher viscosities of legacy samples.

The effect of long time surface exposure (>20 years) on the biomarkers of the bitumen is hard to explain. On one side, as shown in Figure 5.8, the legacy samples generally have higher levels of biodegradation than the fresh ones. Four samples missing tricyclics (i.e., samples N1, UI1, G1, and N2) are all from legacy wells, and this could be a result of further biodegradation after coring. On the other side, as shown in Table 5.2, even some fresh samples have level B biodegradation (loss of hopanes, i.e., samples G6 and UI6), indicating that subsurface biodegradation is capable of reaching the extreme.

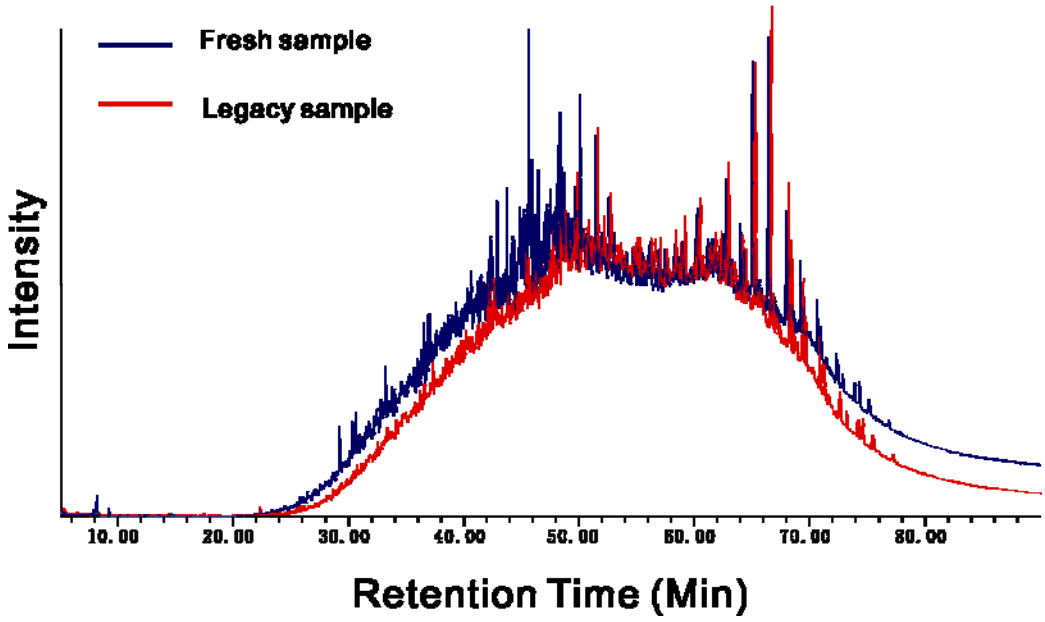

Figure 5.9 Comparison of total ion current GC-MS fragmentograms from legacy sample UI4 and fresh sample UI5 under the same intensity scale (y axis). The two wells are drilled 30 years apart, and the fresh sample exhibits substantially more light compounds with retention time less than 50 minutes. Their biodegradation level is about the same based on the selected biomarker parameters (Table 5.5).

There might be a correlation between biomarker biodegradation parameters and physical degradation parameters like oil viscosity. Based on their study in a heavy oil field in California, McCaffrey et al. (1996) successfully established a relationship between these two factors. A similar approach has been applied in other areas for viscous oil quality prediction, such as in Alaska (Smally et al., 1997), Venezuela (Guthrie et al., 1998), and China (Koopmans et al., 2002). However, due to the different extent of biodegradation in each oil field and the diversity of biomarkers, the recorded relationship between geochemical parameters and oil viscosity are not generally applicable. For example, McCaffrey et al. (1996) found that the C35 homohopane index (C35 homohopanes/ΣC31–C35 homohopanes) and the compound ratio 22R, 25-nortrishomohopane/2R-trishomohopane correlated best with viscosity in the heavy oil reservoir studied (R^2=0.88). These ratios were useful because the hopanes were decreasing with increasing 25-norhopanes in this specific reservoir. This is not the case in the samples examined here, however, in which such conversion was not seen. Therefore, it is crucial to examine the local biomarker distribution and biodegradation characteristics and develop the biomarker biodegradation parameters individually for each study area.

Considering that two combinations developed in section 5.5 in this study (Table 5.5) efficiently characterized the degree of biodegradation in each sample, potential correlations might exist between these biomarker parameters and viscosity. The viscosities of the samples were provided by Lab B with a single temperature measurement

technique (20°C or 30°C). Several duplicates were retested in Lab C (the standard laboratory) at 20°C, 30°C, 40°C, 60°C, and 80°C. In Figure 5.10 and Figure 5.11, viscosities of legacy samples and fresh samples are plotted separately with the biodegradation parameters from the two combinations. Although the viscosity data comes from the same laboratory with the same preparation and measurement method, the correlations with the biodegradation parameters are quite different. While no clear relationship is seen between the legacy sample viscosities and all the applied biodegradation parameters (Table 5.6), viscosities from the fresh samples correlate very well with the ratios of H30/H29, H29/Tm, H30/Tm, and (C23+H29+H30)/Tm: correlation coefficiencies of R^2 >0.9 (Table 5.7), higher than the biodegradation parameters used by McCaffrey et al. (1996) was determined.

There is a large discrepancy between the viscosities of legacy samples and the biodegradation parameters. For example, the viscosity of sample UI2 at 30°C was around 2.8E+06 cP, which is the lowest among all the legacy samples. The hopanes and 25-norhopanes in the fragmentograms of sample UI2, however, are all heavily reduced (e.g., Figure 5.3), indicating Level B biodegradation in this sample (Table 5.5). In comparison, viscosities of the same legacy samples obtained from Lab C were plotted versus biodegradation parameters in Figure 5.12. It shows an almost perfect correlation with the biodegradation parameters ($R^2 \approx 1$, Table 5.8), even more promising than the correlations obtained from the fresh samples of Lab B. These facts suggest inaccuracy of the viscosity measurements from Lab B, especially on the legacy samples.

Possibly due to such inconsistencies between the biodegradation and viscosity measurements, no correlation was found between the viscosities converted into in-situ conditions (fresh sample at 11 °C) and the available biodegradation parameters (Figure 5.13 and Table 5.9). However, the correlations from fresh samples of Lab B and legacy samples from Lab C indicate that biodegradation parameters H30/H29 and H30/Tm have the best potential to be used to correlate with bitumen viscosity from the Grosmont reservoir in the study area.

In conclusion, there are several limitations in attempting to correlate viscosity and biodegradation parameters. First, incorrect viscosity data will always lead to no or wrong correlations between these factors. Second, the age of the samples plays an important role in the correlations, that is, the aging effect on oil viscosity and biodegradation is difficult to quantify. Third, several samples (i.e., samples G2, N4, and G7) did not quite follow the same route of biodegradation. Correlations did not include these abnormal data.

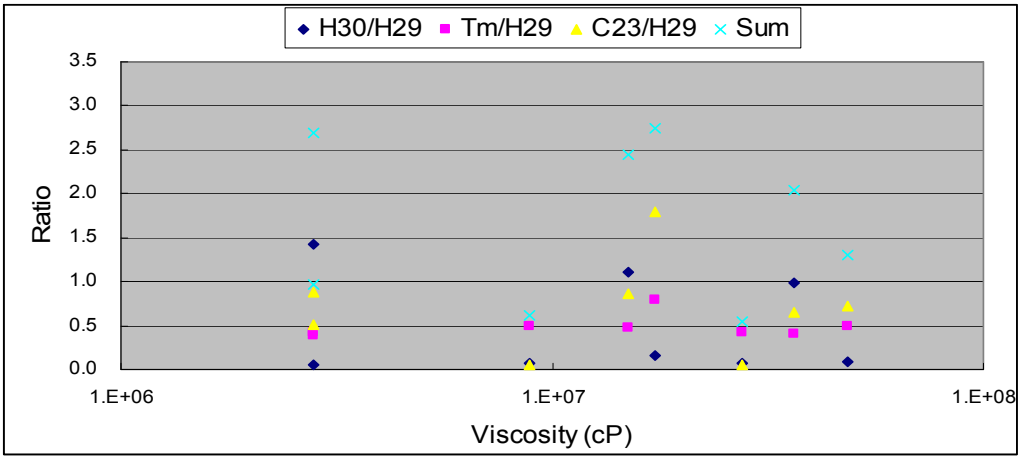

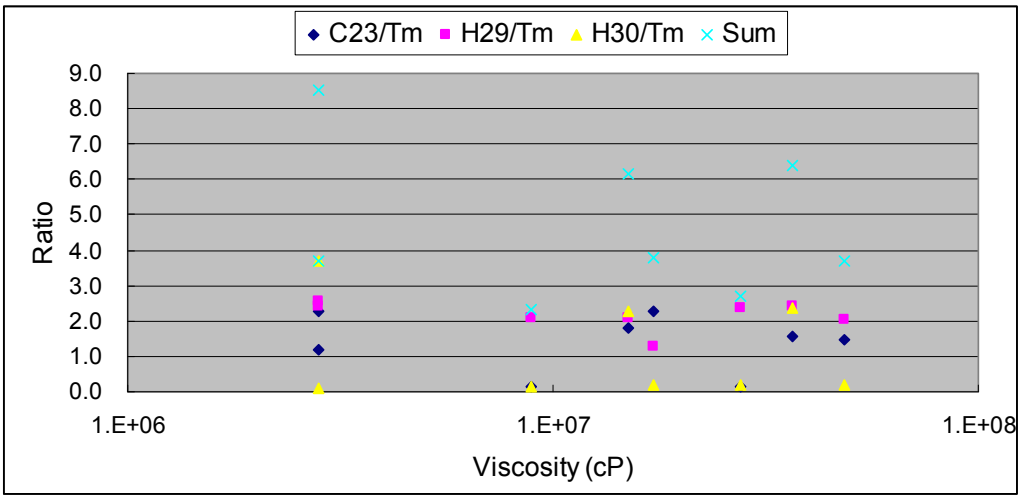

Figure 5.10 The relationship between biomarker parameters and the viscosity of legacy sample at 30°C. No linear correlation is noticed, shown in Table 5.7. Data from three abnormal samples, i.e. G2, N4, and G7, were not used in the plot.

Table 5.6 Correlations between biomarker parameters and viscosities of legacy samples obtained from Lab B.

Biomarker Parameter (y)		**Linear Regression of Cross Plot with Viscosity (x) at 30°C**	**Correlation Coefficiency (R^2)**
Combination 1	H30/H29	y = -7E-09x + 0.6271	0.0364
	C23/H29	y = -7E-10x + 0.7062	0.0004
	Tm/H29	y = 3E-10x + 0.4791	0.0012
	Sum	y=-7E-09x + 1.8124	0.0158
Combination 2	H30/Tm	y = -2E-08x + 1.4912	0.0398
	C23/Tm	y = -3E-09x + 1.427	0.0039
	H29/Tm	y = -3E-09x + 2.2062	0.0101
	Sum	y = -2E-08x + 5.1245	0.0309

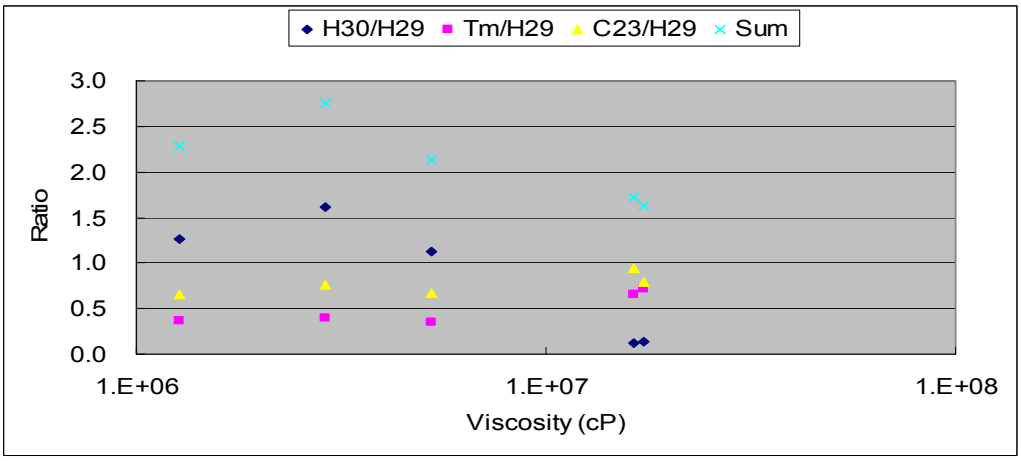

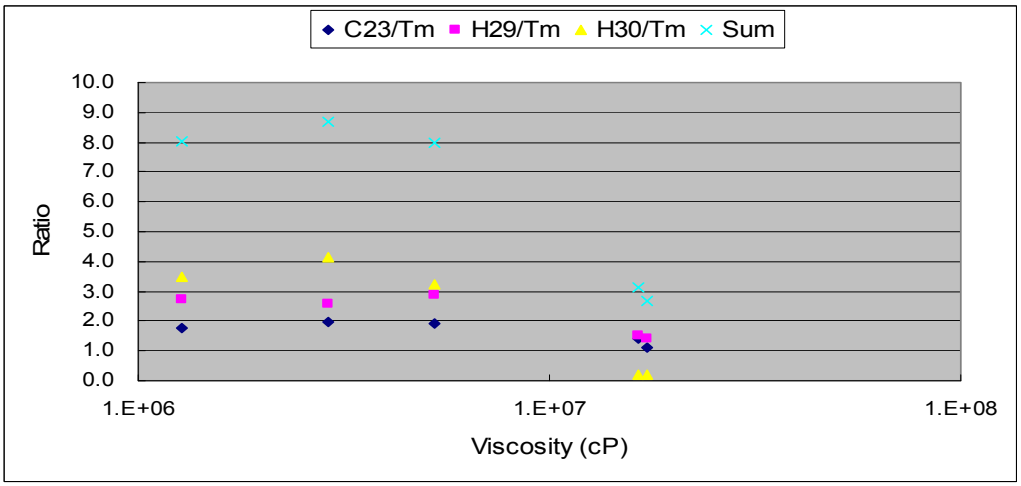

Figure 5.11 The relationship between biomarker parameters and the viscosity of fresh sample at 20°C. Notice the good correlation between viscosity and H30/H29, Tm/H29, H30/Tm, H29/Tm, and Sum of Combination 2 (shown in Table 5.8). Data from three abnormal samples, i.e. G2, N4, and G7, were not used in the plot.

Table 5.7 Correlations between biomarker parameters and viscosities of fresh samples obtained from lab B.

Biomarker Parameter (y)		**Linear Regression of Cross Plot with Viscosity (x) at 20°C**	**Correlation Coefficiency (R^2)**
Combination 1	H30/H29	y = -9E-08x + 1.5983	0.9349
	C23/H29	y = 1E-08x + 0.6573	0.5969
	Tm/H29	y = 2E-08x + 0.3018	0.9415
	Sum	y = -5E-08x + 2.5573	0.768
Combination 2	H30/Tm	y = -2E-07x + 4.354	0.9582
	C23/Tm	y = -4E-08x + 2.0041	0.8246
	H29/Tm	y = -9E-08x + 2.9819	0.918
	Sum	y = -4E-07x + 9.34	0.962

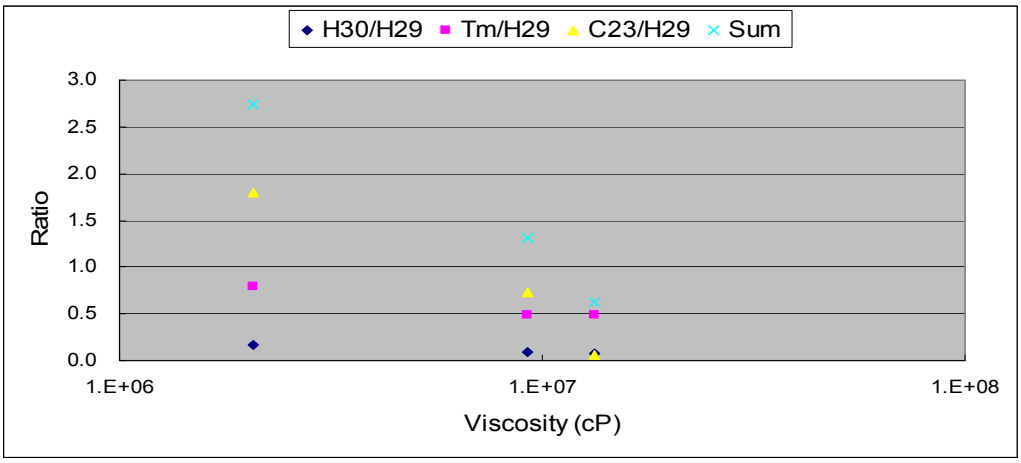

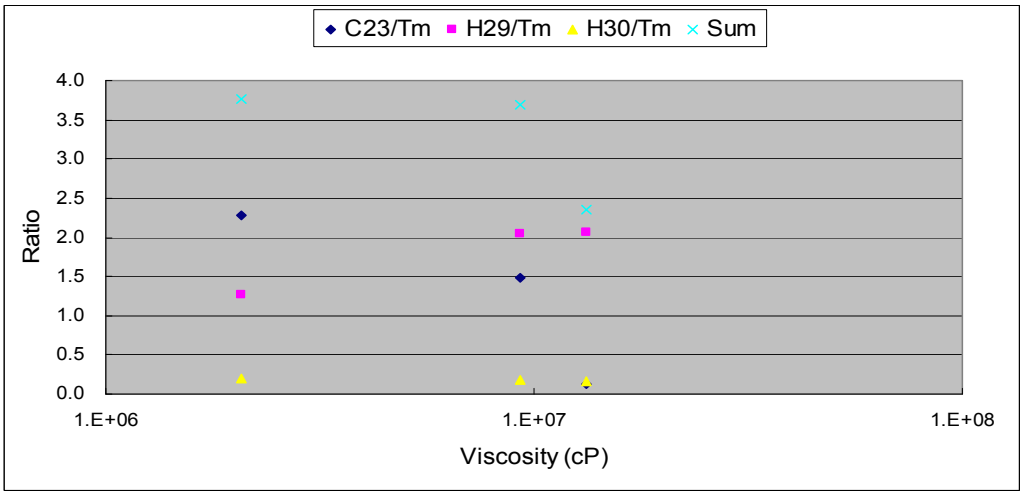

Figure 5.12 The relationship between biomarker parameters and the viscosity of legacy samples obtained from Lab C (standard laboratory) at 30°C. Notice the excellent correlation between viscosity and C23/H29, Sum of Combination 1, H30/Tm (shown in Table 5.8). Data from three abnormal samples, i.e. G2, N4, and G7, were not used in the plot.

Table 5.8 Correlations between biomarker parameters and viscosities of legacy samples obtained from standard lab.

Biomarker Parameter (y)		**Linear Regression of Cross Plot with Viscosity (x) at 30°C**	**Correlation Coefficiency (R^2)**
Combination 1	H30/H29	y = -8E-09x + 0.1748	0.9389
	C23/H29	y=-2E-07x + 2.1253	0.9989
	Tm/H29	y = -3E-08x + 0.8205	0.8884
	Sum	y = -2E-07x + 3.1205	0.9986
Combination 2	H30/Tm	y = -5E-09x + 0.2171	0.9997
	C23/Tm	y = -2E-07x + 2.8039	0.9054
	H29/Tm	y = 7E-08x + 1.1781	0.8959
	Sum	y = -1E-07x + 4.199	0.6394

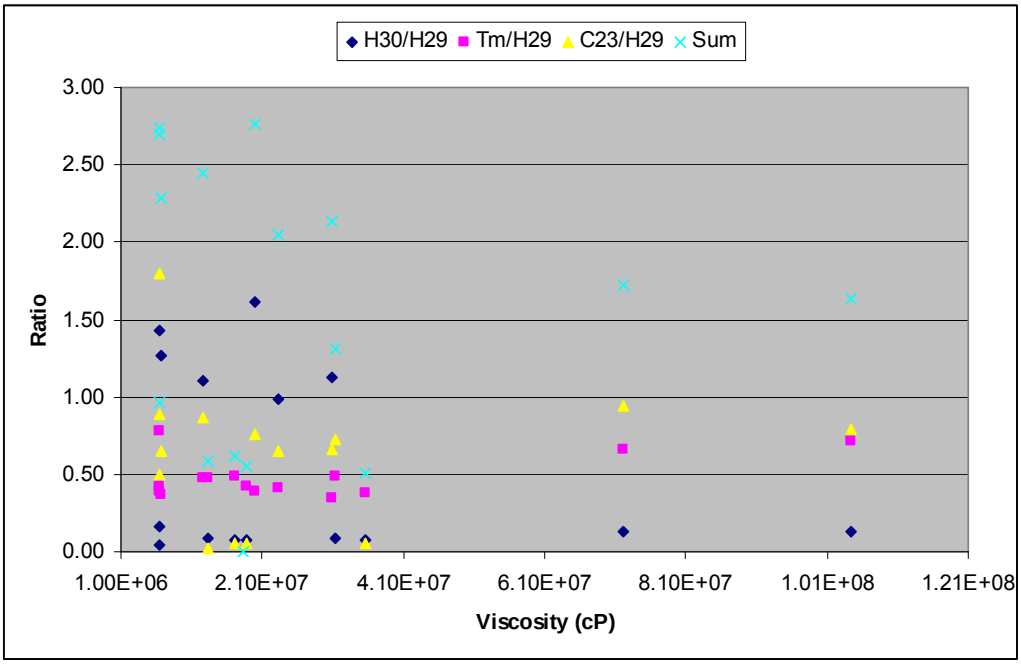

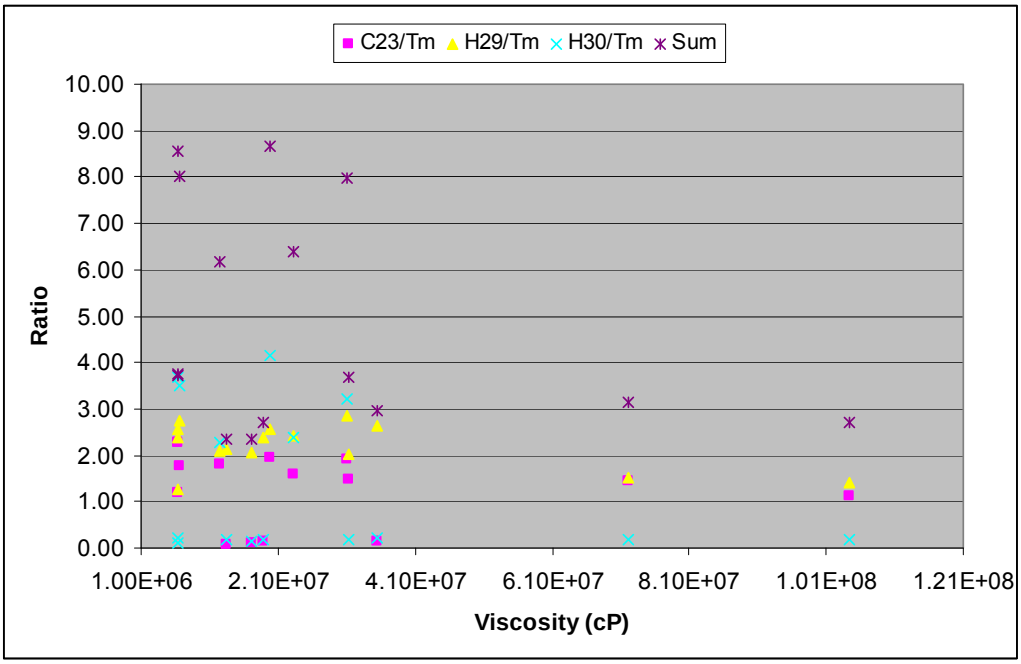

Figure 5.13 The relationship between biomarker parameters and the viscosity converted to in-situ conditions (fresh sample at 11 °C). No linear correlation is noticed, shown in Table 5.9. Data from three abnormal samples, i.e. samples G2, N4, and G7, were not used in the plot.

Table 5.9 Correlations between biomarker parameters and viscosity converted to in-situ conditions (fresh sample at 11 °C).

Biomarker Parameter (y)		Linear Regression of Cross Plot with Viscosity (x) at 11°C	Correlation Coefficiency (R2)
Combination 1	H30/H29	y = -7E-09x + 0.7445	0.0967
	C23/H29	y = 9E-10x + 0.6048	0.0027
	Tm/H29	y = 2E-09x + 0.414	0.2508
	Sum	y = -2E-09x + 1.6217	0.004
Combination 2	H30/Tm	y = -2E-08x + 1.8847	0.0993
	C23/Tm	y = -4E-09x + 1.3863	0.0163
	H29/Tm	y = -9E-09x + 2.444	0.2394
	Sum	y = -3E-08x + 5.715	0.1186

5.7 Conclusions

Based on the biomarker information from the 18 samples analyzed, the Nisku, Upper Ireton, and Grosmont Formations were subjected to severe levels of biodegradation. Regular steranes are generally missing from our samples, and the distributions of hopanes are strongly affected in at least half of the samples. Even the tricyclics and diasteranes are found to be heavily biodegraded in 4 samples.

Most of the biomarker distributions and biodegradation characteristics are typical for the examined compound classes. The order of susceptibility to biodegradation in the Grosmont reservoir is steranes > hopanes > diasteranes > tricyclic terpanes > gammacerane and normoretane, which is in agreement with the previous study by Brooks et al. (1989).

Some special biomarker characteristics are found in this investigation. The biodegradation distribution shows that the microbes favored tricyclic terpane homologs with high abundance and low carbon numbers. 22S C34 and 22R C35 hopanes are found to be more bioresistant than other hopanes, as well as most of the other compound class examined, such as the tricyclic terpanes and the diasteranes. The conversion from hopanes to 25-norhopanes is not evident in the samples examined here, possibly because severe biodegradation affected the distribution of 25-norhopanes, or this conversion does not exist at all.

The source-oriented biomarker, 28, 30-bisnorhopane, is found to be biodegraded at about the same biodegradation level of hopanes.

Therefore, it is likely that the absence of 28, 30-bisnorhopane in the Grosmont reservoir is due to the extreme biodegradation. This finding is very important, as it supports the notion that the Devonian Grosmont bitumen and the overlying Cretaceous heavy oil and oil sands deposits share the same oil source, all of them contain the uncommon biomarker 28, 30-bisnorhopane.

Biodegradation parameters are successfully identified (i.e. H30/H29, C23/H29, and Tm/H29; C23/Tm, H29/Tm, and H30/Tm) to differentiate the extent of biodegradation of each sample examined. A 3-level biodegradation pattern catered to the Grosmont reservoir has been derived. It shows that biodegradation is related to stratigraphy and, more specifically, appears enhanced at formation boundaries.

Aging is found to have minor effect on the biomarker distributions in this study, probably due to the severe degree of biodegradation the bitumens had experienced in the subsurface. Some biodegradation parameters (i.e., H30/H29 and H30/Tm) show great potential for correlating with bitumen viscosities to predict oil quality at *in-situ* conditions. However, more data with accurate viscosity measurements are needed to examine this possibility.

CHAPTER 6

CONCLUSIONS AND FUTURE WORK RECOMMENDATIONS

The main objective of this thesis is to generate useful petrophysical data of bitumen, especially bitumen viscosities, in the Grosmont reservoir to assist future exploitation in the study area. This goal is approached by investigating the bitumen properties of 49 samples from 15 wells along a NW-SE strike cross section in the study area. The main conclusions and recommended future work can be summarized as follows.

1) Bitumen from the Grosmont reservoir is essentially a non-Newtonian fluid with a shear-thinning behavior, especially at low temperature (<40°C). This behavior is related to and/or controlled by the composition and internal structure of the bitumen. Caution should be taken when measuring bitumen viscosity under low temperature, and the shear rate applied should always be included when presenting viscosity data. A method to calculate the zero-shear viscosity of Grosmont bitumen has been developed in this study.

Recommended future work: The study of bitumen rheology shows that both zero-shear viscosity and the corresponding shear rate are

temperature-dependent. It is likely that there is a correlation between these two factors, which should be independent of temperature. If such a correlation exists and is established, it can be used for choosing the shear rate range for zero-shear viscosity measurements, as long as the approximate viscosity of the tested sample at the temperature of interest is known. This will greatly improve the efficiency of viscosity measurements as the input of the shear rate range becomes predictable.

2) The results of inter-laboratory comparison show that the viscosity measurements from different laboratories are not interchangeable. The observed inconsistencies are possibly due to the different methods of preparing samples, different procedures applied, and different equipment used. A practice-tested standard laboratory procedure for viscosity measurement is urgently needed by the oil industry. The intra-laboratory comparisons show that consistency of viscosity measurement can be achieved by the procedure designed in this study.

Aging effects can be identified in the Grosmont bitumen by comparing legacy samples to the adjacent fresh samples. The viscosities of legacy samples are commonly one magnitude higher than the viscosities of fresh ones. Therefore, the viscosity data from legacy samples have to be corrected for use as reservoir proxies. The viscosity distribution in the Grosmont reservoir is complex, varying cyclically with

depth, and is probably stratigraphically related, as similar trends are observed from adjacent wells and along the constructed strike cross section. Viscosity tends to increase toward stratigraphic unit boundaries, which implies more extensive biodegradation in those areas.

Recommended future work: Due to the limit of time, the viscosity distribution has examined only along one strike section in the study area. This is not enough for characterizing the whole reservoir. Viscosity data along several dip cross sections and along some additional strike cross sections are needed.

3) The biomarker results from the 18 samples analyzed indicate that the Nisku, Upper Ireton, and Grosmont Formations were subjected to extreme level of biodegradation, featured by the loss of regular steranes, strongly biodegraded hopanes, and affected distributions of tricyclics and diasteranes. Based on the biomarker distributions and biodegradation characteristics, the samples can be grouped into 3 biodegradation levels. No firm correlation between viscosity and biodegradation parameters has been found so far. This is at least partially due to: (i) the different biodegradation and evaporation rates between bulk oil and the biomarkers, and (ii) the inaccuracy of viscosity data.

Recommended future work: Similar to the shortage of viscosity measurements, more biomarker analyses are needed to establish a

detailed description on the extent of biodegradation in the study area. With the limited data, the viscosities measured from the standard laboratory (Lab C) correlated well with several biodegradation parameters. Viscosity measurements using the standard procedure from Lab C should be carried out on the rest of the 18 samples to prove the validity of these correlations. If these correlations are valid, then they could be used for predicting bitumen viscosities of the Grosmont reservoir.

BIBILIOGRAPHY

Adams, J., Jiang, C., Bennett, B., Huang, H., Oldenburg, T., Noke, K., Snowdon, L., Gates, I., and Larter, S., 2008, Viscosity Determination of Heavy Oil and Bitumen: Cautions and Solutions, Proceedings for the World Heavy Oil Congress 2008.

Alvarez, J.M., Sawatzky, R.P., Forster, L.M. and Coats, R.M., 2008, Alberta's bitumen carbonate reservoirs - moving forward with advances R&D. World Heavy Oil Congress, Edmonton 10-12 March 2008, Paper 2008-467.

Asgar-Deen, M., 2008, Towards economic production of Grosmont Formation bitumen: assessing the relative influence of reservoir porosity and permeability, versus bitumen quality, on production potential: Back to exploration – 2008 CSPG CSEG CWLS Convention abstracts, 969-972.

Bahia, H.U. and Anderson, D.A, 1995, The New Proposed Rheological Properties of Asphalt Binders: Why are they required and how do they compare to conventional properties, *in* Hardin, J. C., ed., Physical Properties of Asphalt Cement Binders, Philadelphia, American Society for Testing and Materials, p. 1-27.

Barker, C., 1979, Organic geochemistry in petroleum exploration, AAPG Continuing Education Course Note Series, no. 10, p. 159.

Belyea, H.R., 1952. Notes on the Devonian System of the north-central plains of Alberta. Geological Survey of Canada, Paper 52-27.

Blanc, P. and J. Connan, 1994, Preservation, degradation, and destruction of trapped oil; The petroleum system; from source to trap, AAPG Memoir, vol. 60, p. 237-247.

Buschkuehle, B. E., Hein F. J., and Grobe1 M., 2007, An Overview of the Geology of the Upper Devonian Grosmont Carbonate Bitumen Deposit, Northern Alberta, Canada, Natural Resources Research, V. 16, P3-15.

Brooks, P. W., M. G. Fowler, and MacQueen, R. W., 1988, Biological marker and conventional organic geochemistry of oil sands/heavy oils, Western Canada Basin, Organic Geochemistry, vol. 12, no. 6, p. 519-538.

Brooks, P. W., M. G. Fowler, and MacQueen, R. W., 1989, Biomarker geochemistry of Cretaceous oil sands, heavy oils and Paleozoic carbonate trend bitumens, Western Canada Basin; The Fourth UNITAR/UNDP international conference on Heavy crude and tar sands; Volume 2, Geology, geochemistry, International Conference on Heavy Crude and Tar Sands, vol. 4, p. 593-606.

Bryan, J., Moon, D., and Kantzas, A., 2005, In situ viscosity of oil sands using low field NMR, Journal of Canadian Petroleum Technology, vol. 44, no. 9, p. 23-30.

Connan, J., 1984, Biodegradation of crude oils in reservoirs, *in* Brooks, J. and D. H. Welte, eds., Advances in petroleum geochemistry; Volume 1, United Kingdom (GBR), Acad. Press, London, United Kingdom (GBR).

Cutler, W.G., 1983. Stratigraphy and sedimentology of the Upper Devonian Grosmont Formation, Alberta, Canada. Bulletin of Canadian Petroleum Geology, v.31, p. 282-325.

Dealy, J. M., 1979, Rheological properties of oil sand bitumen, Canadian Journal of Chemical Engineering, vol. 57, p. 677-690.

Cordell, G.M., 1982. Reservoir simulation of a Grosmont carbonate pilot. Presented at Alberta Oil Sands Technology and Research Authority's Third Annual "Advances in Petroleum Recovery & Upgrading Technology Conference". Calgary, Alberta, June 10-11, 1982, 14 p.

Dembicki, E.A., 1994, The Upper Devonian Grosmont Formation: well log evaluation and regional mapping of a heavy oil carbonate reservoir in northeastern Alberta. Unpub. M.Sc. thesis University of Alberta, 221 pp.

Dembicki, E.A., Machel, H.G., and Huebscher, H., 1994, Reservoir characteristics of a heavy-oil carbonate reservoir: the Grosmont Formation, Alberta, Canada. CSPG-CSEG Joint Annual Meeting, Exploration Update

'94, Book of Abstracts, p. 375-376.

Dembicki, E.A., and Machel, H.G., 1996, Recognition and delineation of paleokarst zones by the use of wireline logs in the bitumen-saturated Upper Devonian Grosmont Formation of northeastern Alberta, Canada: American Association of Petroleum Geologists Bulletin, no. 80, 695-712.

Deroo, G., Powell, T. G., Tissot, B., and McCrossan, R. G., 1977, The origin and migration of petroleum in the western Canadian sedimentary basin, Alberta; a geochemical and thermal maturation study, Bulletin - Geological Survey of Canada, no. 262.

Erno, B. P., Chriest, J. R., and Wilson, R. C., 1991, Depth-Related Oil Viscosity Variation in Canadian Heavy Oil Reservoirs, Journal of Canadian Petroleum Technology, vol. 30, no. 3, p. 36-41.

Etherington, J.R., and McDonald, I. R., 2005, Is bitumen a petroleum reserve: Proceedings of SPE Hydrocarbon Economics and Evaluation Symposium, 15-21.

Guthrie, J. M., Walters, C. C., and Peters, K. E., 1998, Comparison of micro-techniques used for analyzing oils in sidewall cores to model viscosity, API gravity, and sulfur content; AAPG international conference and exhibition; abstracts, AAPG Bulletin, vol. 82, no. 10, p. 1921.

Harrison, R.S., 1982. Geology and production history of the Grosmont Carbonate pilot project, Alberta, Canada. Second International Conference on Heavy Crude and Tar Sands, Caracas, Venezuela, February 7-17, 1982, Volume 1.

Harrison, R.S., 1984. The bitumen-bearing Paleozoic carbonate trends of northern Alberta. In: Meyer, R.F., Early, J.W. Barnea, J., and Johnston, R.L. (convs.): Exploration for heavy crude oil and bitumen. American Association of Petroleum Geologists Research Conference, Santa Maria, CA, October 28-November 2, 1984.

Harrison, R.S. and McIntyre, B.G., 1981. The geologic setting of the Grosmont thermal recovery project, northeastern Alberta. Seminar on

Advances in Petroleum Recovery and Upgrading Technology, Calgary, May 24-26, 1981, 11 p.

Head, I. M., Jones, D. M., and Larter, S. R., 2003, Biological activity in the deep subsurface and the origin of heavy oil: Nature, no. 426, 344-352.
Henaut, I., Barre, L., Argillier, J. -., Brucy, F., and Bouchard, R., 2001, Rheological and Structural Properties of Heavy Crude Oils in Relation with Their Asphaltenes Content, SPE International Symposium on Oilfield Chemistry, p. 353-358.

Hein, F. J., 2006, Heavy oil and oil (tar) sands in North America; an overview and summary of contributions, Natural Resources Research (New York, N.Y.), vol. 15, no. 2, p. 67-84.

Hepler, L. G. and Zhu, X., eds., 1989, AOSTRA technical handbook on oil sands, bitumens and heavy oils, Edmonton, Alberta Oil Sands Technology and Research Authority, 376 p.

Hoffmann, C. F. and Strausz, O. P., 1986, Bitumen accumulation in Grosmont Platform complex, Upper Devonian, Alberta, Canada, AAPG Bulletin, vol. 70, no. 9, p. 1113-1128.

Hopkins, J., and Barrett, K., 2008, Reservoir Units within a multi-layered dolostone Formation: Grosmont Formation, Saleski Area: Back to exploration – 2008 CSPG CSEG CWLS Convention core conference abstracts, 105-109.

Huebscher, H. and Machel, H.G., 1995a, Cross-formational fluid flow in Devonian dolostones. The 1st SEPM Congress on Sedimentary Geology, St. Pete Beach, FLA, Congress Program and Abstracts, p. 71.

Huebscher, H. and Machel, H.G., 1995b, Seal quality related to facies distribution and diagenesis, an example from the Woodbend Group, north-central Alberta. CSPG/CWLS Joint Annual Convention, Program and Abstracts, 2 pp.

Huebscher, H. and Machel, H.G., 1997a, Paleokarst in the Grosmont Formation, northeastern Alberta. In: Wood, J. and Martindale, B.

(compilers), CSPG-SEPM Joint Convention, Core Conference, p. 129-151.

Huebscher, H. and Machel, H.G., 1997b, Stratigraphic and facies architecture of the Upper Devonian Woodbend Group, north-central Alberta. CSPG-SEPM Joint Convention, June 1-6, Program with Abstracts, p. 135.

Koopmans, M. P., Larter, S. R., Zhang, Ch., Mei, B., Wu, T., and Chen, Y., 2002, Biodegradation and mixing of crude oils in Eocene Es3 reservoirs of the Liaohe Basin, northeastern China, AAPG Bulletin, vol. 86, no. 10, p. 1833-1843.

Larter, S.R., Adams, J.J., Gates, I.D., Bennett, B., and Huang, H., 2006, The origin, prediction and impact of oil viscosity heterogeneity on the production characteristics of tar sand and heavy oil reservoirs: Journal of Canadian Petroleum Technology, no. 1, 52-61.

Larter, S. R., H. Huang, J. Adams, B. Bennett, O. Jokanola, T. Oldenburg, M. Jones, I. Head, C. Riediger, and M. Fowler, 2006, The controls on the composition of biodegraded oils in the deep subsurface; Part II, Geological controls on subsurface biodegradation fluxes and constraints on reservoir-fluid property prediction, AAPG Bulletin, vol. 90, no. 6, p. 921-938.

Loeber, L., Muller, M. G. J., and O. Sutton, 1998, Bitumen in colloid science: a chemical, structural and rheological approach, Fuel, vol. 77, no. 13, p. 1443-1450.

Lu, X. and U. Isacsson, 2002, Effect of ageing on bitumen chemistry and rheology, Construction and Building Materials, vol. 16, no. 1, p. 15-22.

Luo, P., Machel, H.G. and Shaw, J., 1994, Petrophysical properties of matrix blocks of a heterogeneous dolostone reservoir - the Upper Devonian Grosmont Formation, Alberta, Canada. Bulletin of Canadian Petroleum Geology, v. 42, p. 465-481.

Luo, P. and Machel, H.G., 1995, Pore size and pore-throat types in a heterogeneous Dolostone reservoir, Devonian Grosmont Formation, Western Canada Sedimentary Basin. American Association of Petroleum

Geologists Bulletin, v. 79, p. 1698-1720.

Mackenzie, A. S., G. A. Wolff, and J. R. Maxwell, 1983, Fatty acids in some biodegraded petroleums; possible origins and significance; Advances in organic geochemistry, 1981, Proceedings of the International Meeting on Organic Geochemistry, vol. 10, p. 637-649.

Martinez, J.A., Escobar, E., Forster, L., Ivory, J., Isaacs, E., 2006, Setting the scene: learning from the global experience with carbonate reservoirs, The new horizon---bitumen carbonates workshop, 1-122.

Mastrofini, D. and M. Scarsella, 2000, Application of rheology to the evaluation of bitumen ageing, Fuel, vol. 79, no. 9, p. 1005-1015.

McCaffrey, M. A., H. A. Legarre, and S. J. Johnson, 1996, Using biomarkers to improve heavy oil reservoir management; an example from the Cymric Field, Kern County, California, AAPG Bulletin, vol. 80, no. 6, p. 898-913.

Mezger, T. G., 2006, The Rheology Handbook, Hannover, Vincentz Network, 299 p.

Meyer, F.M., and Attanasi, E.D., 2003, Heavy oil and natural bitumen-strategic petroleum resources: U.S. Geological Survey Fact Sheet 70-03, 1-2.

Michalica, P., I. B. Kazatchkov, J. Stastna, and L. Zanzotto, 2008, Relationship between chemical and rheological properties of two asphalts of different origins, Fuel, vol. 87, no. 15, p. 3247-3253.

Miller, K. A., L. A. Nelson, and R. M. Almond, 2006, Should You Trust Your Heavy Oil Viscosity Measurement? Journal of Canadian Petroleum Technology, vol. 45, no. 4, p. 42-48.

Moldowan, J. M., C. Y. Lee, P. Sundararaman, T. Salvatori, A. Alajbeg, B. Gjukic, G. J. Demaison, N. Slougui, and D. S. Watt, 1992, Source correlation and maturity assessment of select oils and rocks from the

central Adriatic Basin (Italy and Yugoslavia), *in* Moldowan, J. M., P. Albrecht, and R. P. Philp, eds., Biological markers in sediments and petroleum; a tribute to Wolfgang K. Seifert, United States (USA), Prentice Hall, Englewood Cliffs, NJ, United States (USA).

Norris, A.W., 1963. Devonian stratigraphy of northeastern Alberta and northwestern Saskatchewan. Geological Survey of Canada, Memoir 313, 168p.

Peters, K. E., C. C. Walters, and J. M. Moldowan, 2005, The biomarker guide; II, Biomarkers and isotopes in petroleum systems and Earth history, United Kingdom (GBR), Cambridge University Press, Cambridge, United Kingdom (GBR).

Pierre, C., L. Barré, A. Pina, and M. Moan, 2004, Composition and Heavy Oil Rheology Oil & Gas Science and Technology, vol. 59, no. 5, p. 489-501.

Piron, E., 2008, Reservoir characterization of the Grosmont Formation at Saleski, NE AB, a multi-disciplinary data integration exercise in progress: Back to exploration – 2008 CSPG CSEG CWLS Convention abstracts, 224-225.

Schramm, L. L. and Kwak, J. C. T., 1988, Rheological Properties of an Athabasca Bitumen and Some Bituminous Mixtures and Dispersions, ournal of Canadian Petroleum Technology, vol. 27, no. 1, p. 26-35.

Smalley, P. C., N. S. Goodwin, J. F. Dillon, C. R. Bidinger, and R. J. Drozd, 1997, New tools target oil-quality sweetspots in viscous-oil accumulations, SPE Reservoir Engineering (Society of Petroleum Engineers), vol. 12, no. 3, p. 157-161.

Speight, J. G., 2007, The chemistry and technology of petroleum, Boca Raton, CRC Press, 945p.

Stoakes, F.A. and Wendte, J.C., 1987, The Woodbend Group. In: Devonian Lithofacies and Reservoir Styles in Alberta. F.F. Krause and

O.G. Burrowes (eds.), 13th Canadian Society of Petroleum Geologists Core Conference, Guidebook, p. 153-170.

Strausz, O. P. and E. M. Lown, 2003, The chemistry of Alberta oil sands, bitumens and heavy oils, Canada (CAN), Alberta Energy Research Institute, Calgary, AB, Canada (CAN).

Switzer, S.B., Holland, W.G., Christie, D.S., Graf, G.C., Hedinger, A.S., McAuley, R.J., Wierzbicki, R.A., Packard, J.J., 1994, Devonian Woodbend-Winterburn strata of the Western Canada Sedimentary Basin. In: Geologic Atlas of the Western Canada Sedimentary Basin. G.D. Mossop and I. Shetsen (compilers). Calgary, Canadian Society of Petroleum Geologists and Alberta Research Council, p. 165-195.

Theriault, F., 1988. Lithofacies, diagenesis, and related reservoir properties of the Upper Devonian Grosmont Formation, northern Alberta. Bulletin of Canadian Petroleum Geology, v. 36, p. 52-69.

Theriault, F. and Hutcheon, I., 1987. Dolomitization and calcitization of the Devonian Grosmont Formation, northern Alberta. Journal of Sedimentary Petrology, v. 57, p. 955 - 966.

Tia, M. and Ruth, B.E., 1987, Basic Rheology and Rheological Concepts Established by H.E. Schweyer, *in* Briscoe, O. E., ed., Asphalt Rheology: Relationship to Mixture, ASTM STP 941 .

Tissot, B. P. and D. H. Welte, 1984, Petroleum formation and occurrence, Federal Republic of Germany (DEU), Springer-Verlag, Berlin, Federal Republic of Germany (DEU).

Ukwuoma, O. and B. Ademodi, 1999, The effects of temperature and shear rate on the apparent viscosity of Nigerian oil sand bitumen, Fuel Processing Technology, vol. 60, no. 2, p. 95-101.

Vandermeer, J.G. and Presber, T.C., 1980. Heavy oil recovery from the Grosmont carbonates of Alberta. Seminar on Nonconventional Oil Technology, Calgary, Alberta, May 29-30, 1980, 22 pp.

Vigrass, l. W., 1968, Geology of Canadian heavy oil sands; Rocky Mountains-Breaking barrier boundaries, The American Association of Petroleum Geologists Bulletin, vol. 52, no. 10, p. 1984-1999.

Walker, D., 1986, Regional stratigraphy of the Upper Devonian Grosmont Formation, Northern Alberta, Alberta Research Council Open File Report 1986-02.

Ward, S.H. and Clark, K.A., 1950, Determination of the Viscosities and Specific Gravities of the Oils in Samples of Athabaska Bituminous Sand, vol. 57, p. 22.

Wenger, L. M., C. L. Davis, and G. H. Isaksen, 2001, Multiple Controls on Petroleum Biodegradation and Impact on Oil Quality, p. 1095-1108.

Yoon, T., 1986, Bitumen resources of the Upper Devonian Grosmont Formation, Townships 88-98, Northern Alberta. Alberta Research Council Open File Report 1986-01.

APPENDIX 1: SAMPLE LIST

Well ID	Sample	Depth(m)	Well ID	Sample ID	Depth(m)
16-13-89-23W4	N-1	289.3	10-17-84-19W4	UI-20	390.8
	N-2	290.5		UI-21	392.7
	N-3	292.4		UI-22	399.0
	N-4	295.3		UI-23	399.2
	N-5	298.8		UI-24	399.7
	N-6	299.7		UI-25	401.5
	UI-1	324.5		UI-26	402.0
	UI-2	325.8		G3-7	404.0
	UI-3	326.6		G3-8	405.7
	UI-4	328.7		G3-9	407.0
	UI-5	329.6		G3-10	409.0
	UI-6	331.5		G3-11	415.8
	UI-7	332.0		G3-12	416.8
	UI-8	332.7		G3-13	417.0
	UI-9	335.1		G3-14	419.3
	UI-10	336.0		G3-15	419.8
	UI-11	338.8		G3-16	421.2
	G3-1	339.8		G2-1	432.5
	G3-2	341.8		G2-2	436.2
	G3-3	343.1		G2-3	436.7
	G3-4	344.0			
	G3-5	347.2	10-13-93-23W4	G3-17	417.4
	G3-6	348.2		G3-18	418.3
				G3-19	418.6
				G3-20	419.0
6-11-89-25W4	N-7	432.3			
	N-8	432.7	08-01-89-23W4		
	N-9	436.4	Nisku	GRM 125	290.4
	N-10	436.9	Nisku	GRM 128	294.0
	N-11	443.5	Nisku	GRM 124	298.4
	N-12	445.4	Upper Ireton	GRM 127	325.8
	N-13	445.8	Upper Ireton	GRM 130	331.5
			UGM3	GRM 126	336.0
			UGM3	GRM 129	343.7
7-34-90-23W4	N-14	278.0			
	N-15	278.3	11-21-90-23W4	UI-27	300.5
	N-16	280.6		UI-28	301.6
	N-17	281.4		UI-29	302.5
	N-18	281.6		UI-30	302.9
	N-19	282.9		UI-31	303.7
	N-20	287.5		UI-32	305.9
				UI-33	306.5
				UI-34	306.9
11-21-90-23W4	UI-12	300.8		UI-35	308.1
	UI-13	301.4		UI-36	308.1
	UI-14	302.1			
	UI-15	306	7-34-90-23W4	N-21	277.8
	UI-16	306.3		N-22	278.0
	UI-17	307.4		N-23	279.5
	UI-18	307.8		N-25	283.2
	UI-19	309.1		UI-37	287.3
				N-24	280.2

Well ID	Sample	Depth(m)	Well ID	Sample ID	Depth(m)
16-13-89-23W4	N-26	289.9		G3-29	355.3
	N-27	292.6		G3-30	360.1
	N-28	297.5			
	N-29	299.1	7-35-89-24W4	N-40	287.0
	N-30	299.9		N-41	298.5
	UI-38	315.2		UI-61	357.0
	UI-39	331.0		UI-62	361.4
	UI-40	333.4		UI-63	364.7
	UI-41	334.9		UI-64	368.5
	UI-42	336.8			
	G3-21	339.0			
	G3-22	346.2	10-35-88-22W4	G3-31	310.6
				G3-32	331.3
6-11-89-25W4	N-31	432.4			
	N-32	435.0	05-24-88-23W4	N-42	320.5
	N-33	436.6		N-43	321.8
	N-34	443.1		UI-65	333.0
	N-35	445.3		UI-66	339.0
				UI-67	341.1
				UI-68	344.0
11-12-91-24W4	N-36	282.6		UI-69	348.7
	N-37	285.7		UI-70	351.5
	UI-43	295.0		UI-71	355.7
	UI-44	306.4			
	UI-45	310.8			
	UI-46	315.7	16-29-88-23W4	N-44	280.2
	UI-47	319.9		N-45	284.8
	UI-48	320.4		N-46	293.0
	G3-23	329.2		N-47	326.0
	G3-24	354.7		N-48	329.9
				UI-72	359.5
				UI-73	365.5
10-05-90-23W4	N-38	285.5			
	UI-49	302.4			
	UI-50	306.5	10-13-89-24W4	N-49	271.3
	UI-51	310.9		N-50	286.5
	UI-52	318.1		N-51	293.0
	UI-53	320.9		UI-74	354.0
	UI-54	325.8		UI-75	356.4
	G3-25	332.6		UI-76	357.6
	G3-26	336.7		UI-77	357.8
	G3-27	360.4		UI-78	358.0
				UI-79	358.2
				UI-80	362.1
10-23-90-24W4	N-39	264.5			
	UI-55	326.6	10-29-89-23W4	N-52	264.8
	UI-56	326.7		N-53	267.6
	UI-57	327.0		N-54	276.3
	UI-58	327.3		N-55	285.9
	UI-59	327.4		N-56	291.5
	UI-60	330.3		N-57	295.5
	G3-28	332.9		N-57	295.5

Well ID	**Sample**	**Depth(m)**	Well ID	**Sample ID**	**Depth(m)**
	N-58	301.0	10-29-86-19W4	G3-55	280.2
	N-59	305.3		G3-56	282.6
	N-60	306.3		G3-57	284.6
	N-61	307.5		G3-58	284.8
	UI-81	315.5		G3-59	285.3
	UI-82	317.2		G3-60	285.4
	UI-83	321.8		G3-61	304.8
	UI-84	325.0		G3-62	305.0
	UI-85	327.4		G3-63	305.3
	UI-86	327.4			
	UI-87	328.1			
	UI-89	331.6	14-17-87-20W4	G3-64	312.9
	UI-90	334.2		G3-65	314.6
	UI-91	339.0		G3-66	322.8
	G3-33	344.0		G3-67	323.3
	G3-34	346.3			
	G3-35	349.7			
			10-21-92-24W4	UI-92	363.2
11-04-88-21W4	G3-36	323.0		UI-93	364.6
	G3-37	323.6		UI-94	365.9
	G3-38	324.8		UI-95	368.0
	G3-39	339.1		UI-96	371.2
	G3-40	345.0		UI-97	376.9
	G3-41	350.1		UI-98	379.0
11-14-88-21W4	G3-42	304.3	10-12-93-24W4	UI-99	434.0
	G3-43	308.8		UI-100	437.5
	G3-44	318.3		UI-101	440.2
	G3-45	325.0		UI-102	443.5
	G3-46	327.0		G3-68	476.5
14-06-89-21W4	G3-47	253.5	1-21-93-23W4	G3-69	444.1
	G3-48	255.7		G3-70	446.2
				G3-71	451.3
				G3-72	474.1
6-10-87-23W4	N-62	351.5		G3-73	479.3
	N-63	355.3		G3-74	483.3
	N-64	360.5			
			10-27-93-23W4	G3-75	486.3
8-6-90-20W4	G3-49	278.0		G3-76	494.6
	G3-50	290.6		G3-77	501.2
	G3-51	295.7		G3-78	506.9
			06-01-94-23W4	G3-79	500.8
10-16-90-20W4	G3-52	248.3		G3-80	504.1
				G3-81	511.5
				G3-82	514.8
7-31-90-19W4	G3-53	255.0		G3-83	516.9
	G3-54	256.9		G3-85	542.6
				G3-84	534.2

Well ID	**Sample**	**Depth(m)**	Well ID	**Sample ID**	**Depth(m)**
	G3-86	545.0	6-7-95-21W4		
	G3-87	545.6	UGM2?	G3-121	244.0
	G3-88	547.0			
	G3-89	552.0			
			10-14-91-20W4	G3-122	239.3
				G3-123	240.9
10-12-94-22W4				G3-124	242.4
UGM2?	G3-90	379.5		G3-125	242.5
UGM1?	G3-91	398.7		G3-126	243.4
UGM1?	G3-92	407.4		G3-127	244.4
UGM1?	G3-93	409.2			
UGM1?	G3-94	412.0			
UGM1?	G3-95	424.5	10-04-94-23W4		
				G3-128	512.0
			UGM2	G3-129	516.5
11-26-87-20W4	UI-103	263.4	UGM2	G3-130	518.1
	UI-104	264.5	UGM2	G-131	522.8
	UI-105	267.0	UGM2	G3-132	529.6
	UI-106	270.0	UGM2	G3-133	532.2
	G3-96	270.8	UGM2	G3-134	534.8
	G3-97	272.8	UGM2	G3-135	537.0
	G3-98	273.6	UGM1	G3-136	539.0
	G3-99	275.5	UGM1	G3-137	552.0
	G3-100	291.6	UGM1	G3-138	556.9
	G3-101	295.6	UGM1	G3-139	559.9
	G3-102	296.4	UGM1	G3-140	565.5
UGM2?	G3-103	310.1	UGM1	G3-141	566.8
UGM2?	G3-104	311.6			
UGM2?	G3-105	319.4			
UGM2?	G3-106	322.7	10-30-93-22W4		
			UGM2	G3-142	441.2
			UGM2	G3-143	449.7
10-24-94-24W4			UGM2	G3-144	456.3
UGM1	G3-107	576.8	UGM2	G3-145	459.4
UGM1	G3-108	579.5	UGM2	G3-146	464.3
UGM1	G3-109	581.5	UGM1	G3-147	466.4
UGM1	G3-110	585.0	UGM1	G3-148	490.3
			UGM1	G3-149	494.4
			UGM1	G3-150	498.2
6-36-92-22W4	G3-111	320.5			
	G3-112	326.1			
	G3-113	329.3	11-14-90-19W4	G3-151	254.2
				G3-152	259.0
				G3-153	264.0
11-08-92-21W4	G3-114	270.4		G3-154	268.0
	G3-115	272.6			
			2-2-89-19W4	G3-155	242.0
7-14-91-21W4	G3-117	233.0		G3-156	242.3
	G3-118	234.5		G3-157	242.6
	G3-119	236.2		G3-158	242.9
	G3-120	239.4		G3-159	243.2
UGM2	G3-116	286.3			

Well ID	**Sample**	**Depth(m)**	Well ID	**Sample ID**	**Depth(m)**
	G3-160	243.5		UI-111	378.0
	G3-161	243.8			
	G3-162	244.1			
			10-29-89-23W4	N-67	264.8
				N-68	267.5
				N-69	267.8
				G3-187	346.0
6-26-89-20W4	G3-163	262.5		G3-188	349.6
	G3-164	274.0		G3-189	349.8
10-21-88-25W4	UI-107	486.0	10-29-86-19W4	G3-190	304.8
	G3-165	487.0		G3-191	305.1
	G3-166	496.0			
			6-10-87-23W4	N-70	360.6
7-26-91-22W4	G3-167	276.7		N-71	355.1
	G3-168	277.4		N-72	355.1
	G3-169	278.6			
	G3-170a	285.3			
	G3-170b	287.7	06-08-89-23W4	N-73	270.6
	G3-171	289.7		N-74	280.6
	G3-172	294.0		G3-192	322.8
	G3-173	295.0		G3-193	324.2
11-14-93-21W4			07-20-87-19W4		
UGM1	G3-174	293.4	?	G3-194	248.3
UGM1	G3-175	296.2		G3-195	249.5
LG	G3-176	312.6		G3-196	250.8
	G3-177	313.6		G3-197	251.3
				G3-198	273.2
				G3-199	275.4
1-16-92-21W4				G3-200	277.5
UGM2	G3-178	270.3		G3-201	278.5
UGM2	G3-179	274.1		G3-202	279.1
UGM2	G3-180	279.5		G3-203	279.5
UGM2	G3-181	284.5		G3-204	280.2
UGM2	G3-182	285.4			
UGM2	G3-183	285.5			
			07-26-85-19W4	UI-112	328.0
				UI-113	329.5
11-12-91-24W4	N-65	282.6		G3-214	336.4
	N-66	285.1		G3-215	341.1
	UI-108	439.0		G3-216	350.2
	G3-184	444.0		G3-205	350.8
	G3-185	445.0		G3-206	353
	G3-186	446.7		G3-207	355.6
				G3-208	357.1
				G3-209	360.0
10-21-92-24W4	UI-109	376.1		G3-210	364.5
	UI-110	377.0		G3-211	366.8
10-12-93-24W4	UI-107	437.6	?	G3-206	353.0

Well ID	**Sample**	**Depth(m)**	Well ID	**Sample ID**	**Depth(m)**
	G3-212	369.3	8-33-90-23W4	N-77	274.6
	G3-213	369.9		N-78	276.4
				N-79	277.3
				UI-120	283.7
8-1-89-23W4	N-75	267.2		UI-121	284.3
	N-76	307.0		UI-122	285.3
	G3-217	316.0		UI-123	289.7
	G3-218	325.5		UI-124	293.7
	G3-219	327.7		UI-125	295.1
	G3-220	331.3		UI-126	295.4
	G3-221	333.7		UI-127	297.2
	G3-222	335.3		UI 128	301.0
	G3-223	342.5		UI-129	305.6
	G3-224	343.3		UI-130	307.0
			UGM3?	UI-131	308.7
			UGM3?	UI-132	313.1
06-34-92-24W4	UI-114	372.2		G3-240	316.1
	G3-225	373.7		G3-241	318.4
	G3-226	375.6		G3-242	320.3
	G3-227	378.5		G3-243	321.4
	G3-228	378.9		G3-245	339.6
	G3-229	383.3		G3-246	343.8
	G3-230	384.0			
UGM2?	G3-231	388.0			
	G3-232	399.0	9-25-89-23W4	G3-247	307.5
	G3-233	401.3		G3-248	309.2
	G3-234	403.3		G3-249	309.5
	G3-235	408.8		G3-250	311.5
				G3-251	314.5
				G3-252	316.8
11-26-91-24W4	UI-115	316.8		G3-253	241.5
	UI-116	319.0		G3-254	342.6
	UI-117	325.1			
	UI-118	327.8			
	G3-236	330.3			
	G3-237	331.7			
	G3-238	335.3			
	G3-239	336.4			

N-*	Nisku, unless specified
UI-*	Upper Ireton, unless specified
G3-* or UGM3	Upper Grosmont 3, unless specified
G2-* or UGM2	Upper Grosmont 2
UGM1	Upper Grosmont 1
LGM	Lower Grosmont
?	Uncertain

APPENDIX 2: VISCOSITY DATA

Viscosity data from Lab A

Sample	G3-3	**Sample**	G3-4	**Sample**	G3-9	**Sample**	G3-14
% MeCl2	0.07	**% MeCl2**	0.19	**% MeCl2**	0.09	**% MeCl2**	0.30
Viscosity	**Temp**	**Viscosity**	**Temp**	**Viscosity**	**Temp**	**Viscosity**	**Temp**
Poise	°C	Poise	°C	Poise	°C	Poise	°C
6.74E+07	0.3	7.66E+07	1.1	8.71E+07	1	8.59E+07	4.7
6.60E+07	1.1	8.02E+07	2.1	7.21E+07	2.9	5.59E+07	6.5
7.68E+07	2.1	4.74E+07	3	5.08E+07	4.7	8.06E+07	7.3
5.53E+07	3	5.75E+07	3.9	6.19E+07	5.6	4.38E+07	8.2
7.14E+07	4	3.61E+07	4.8	4.52E+07	6.5	2.78E+07	9
4.48E+07	4.8	3.36E+07	5.7	3.42E+07	7.3	2.95E+07	9.8
4.85E+07	5.6	2.49E+07	6.5	2.54E+07	8.2	2.01E+07	10.7
3.51E+07	6.5	1.83E+07	7.3	2.12E+07	9	1.98E+07	11.5
2.99E+07	7.3	1.51E+07	8.2	1.76E+07	9.8	1.44E+07	12.3
2.29E+07	8.2	1.30E+07	9	1.17E+07	10.7	1.12E+07	13.1
1.69E+07	9	9.62E+06	9.8	1.07E+07	11.5	8.79E+06	14
1.36E+07	9.8	6.97E+06	10.7	7.58E+06	12.3	6.74E+06	14.8
1.04E+07	10.7	5.69E+06	11.5	6.45E+06	13.1	5.27E+06	15.7
7.73E+06	11.5	4.77E+06	12.3	4.81E+06	13.9	4.31E+06	16.5
5.74E+06	12.3	3.70E+06	13.1	3.83E+06	14.8	3.41E+06	17.4
4.61E+06	13.1	2.97E+06	13.9	3.05E+06	15.6	2.73E+06	18.2
3.59E+06	14	2.31E+06	14.8	2.42E+06	16.5	2.25E+06	19
2.89E+06	14.8	1.82E+06	15.7	1.89E+06	17.4	1.76E+06	19.9
2.25E+06	15.7	1.46E+06	16.5	1.53E+06	18.2	1.43E+06	20.7
1.81E+06	16.5	1.18E+06	17.4	1.25E+06	19	1.14E+06	21.5
1.44E+06	17.3	9.28E+05	18.2	1.01E+06	19.8	9.12E+05	22.3
1.16E+06	18.2	7.68E+05	19	8.25E+05	20.7	7.47E+05	23.2
9.32E+05	19	6.19E+05	19.9	6.69E+05	21.5	5.96E+05	24
7.59E+05	19.8	5.09E+05	20.7	5.51E+05	22.4	4.94E+05	24.8
6.10E+05	20.7	4.18E+05	21.5	4.50E+05	23.2	4.00E+05	25.7
5.06E+05	21.5	3.41E+05	22.3	3.74E+05	24.1	3.32E+05	26.5
4.20E+05	22.4	2.84E+05	23.2	3.06E+05	24.9	2.69E+05	27.3
3.41E+05	23.2	2.33E+05	24	2.55E+05	25.7	2.26E+05	28.2
2.85E+05	24	1.93E+05	24.9	2.14E+05	26.5	1.90E+05	29
2.32E+05	24.9	1.60E+05	25.7	1.76E+05	27.3	1.56E+05	29.9
1.94E+05	25.7	1.35E+05	26.5	1.46E+05	28.2	1.31E+05	30.7
1.63E+05	26.5	1.13E+05	27.4	1.22E+05	29	1.09E+05	31.5
1.32E+05	27.4	93110	28.2	1.02E+05	29.8	92250	32.4
1.11E+05	28.2	78620	29	85900	30.7	78120	33.2
90890	29	65690	29.8	71090	31.6	65640	34
76000	29.9	55980	30.7	60010	32.4	55710	34.9
62710	30.7	47150	31.5	50140	33.2	46780	35.7
52950	31.6	39370	32.4	42550	34.1	39820	36.5
44660	32.4	34070	33.2	35890	34.9	34010	37.4
37650	33.2	28870	34	30800	35.7	29030	38.2
32660	34	24920	34.9	26380	36.5	24840	39.1
27220	34.9	20990	35.7	22270	37.4	20920	39.9
22810	35.7	17890	36.6	19020	38.2	17890	40.8
19370	36.5	15500	37.3	16200	39.1	15300	41.5

15990	37.4	12990	38.2	13990	39.9	12820	42.4
13550	38.2	11150	39	12130	40.7	11010	43.2
11250	39.1	9417	39.9	10330	41.5	9332	44
9607	39.9	8059	40.7	8806	42.4	7924	44.9
7902	40.7	6913	41.6	7472	43.2	6745	45.7
6581	41.6	5815	42.4	6321	44	5750	46.5
5176	42.4	4966	43.2	5373	44.9	4807	47.4
3491	43.3	4310	44.1	4659	45.7	4216	48.2
2605	44	3821	44.8	4089	46.5	3732	49.1
2000	44.8	3378	45.7	3606	47.4	3241	49.9
1867	45.7	3006	46.6	3192	48.2	2915	50.7
1577	46.5	2667	47.4	2812	49.1	2518	51.5
1456	47.4	2365	48.2	2505	49.9	2294	52.4
1009	48.3	2099	49	2275	50.7	2042	53.2
764.7	49.1	1848	49.9	2027	51.6	1793	54
679.3	49.9	1698	50.7	1847	52.4	1612	54.9
595.2	50.8	1520	51.5	1618	53.2	1405	55.7
474.6	51.6	1374	52.4	1417	54.1	1264	56.6
430.9	52.4	1221	53.1	1294	54.9	1110	57.4
343.2	53.2	1104	54	1178	55.7	979.5	58.2
314.7	54.1	1003	54.9	1066	56.5	893.5	59.1
278.8	54.9	897.9	55.7	971.1	57.4	799.8	59.9
293.7	55.7	845	56.5	885.7	58.2	740.6	60.7
316.8	56.6	758.9	57.4	810.4	59.1	683	61.5
323.1	57.4	705.1	58.2	743.8	59.9	639.8	62.4
284.9	58.2	658.5	59	693	60.7	599.9	63.2
238.3	59	609.2	59.9	654.6	61.6	552.1	64.1
216.9	59.9	587.8	60.8	613.6	62.5	516.2	64.9
209	60.7	551.6	61.6	593.1	63.3	504.7	65.7
210	61.5	520.3	62.4	554	64	465.1	66.6
199.4	62.4	486.3	63.3	517.9	64.9	443.8	67.4
195.3	63.2	443.5	64.1	501.3	65.8	432.2	68.3
204.2	64.1	439.8	64.9	466.9	66.6	409.6	69.1
199.8	64.9	384.8	65.7	434.8	67.4	387.6	69.9
208.2	65.8	378.1	66.6	407.2	68.3	356.1	70.7
202.8	66.5	338.2	67.4	371.7	69.1	332.7	71.6
190.4	67.4	309.9	68.3	355.4	69.9	311	72.4
190.1	68.3	290.3	69.1	326.5	70.7	289.3	73.2
172.9	69.1	276	69.9	302.1	71.6	276	74.1
162.5	69.9	252.5	70.7	290.2	72.4	250.2	74.9
158.3	70.8	246.7	71.6	265.2	73.2	241.4	75.7
140.3	71.5	227	72.4	259	74.1	226.6	76.5
141.8	72.4	213.1	73.2	239.9	74.9	206.2	77.5
126.6	73.2	207.4	74.1	221	75.7	207.5	78.2
120.4	74.1	184.2	74.9	216.8	76.6	185.2	79.1
119.8	74.9	183.6	75.7	197.2	77.4	183.5	79.9
103	75.7	172	76.6	197.3	78.3	173.3	80.7
110.1	76.6	163.3	77.4	183.4	79.1	157.2	81.6
96.13	77.4	160.6	78.2	169.3	79.9	163.3	82.4
93.29	78.2	140.5	79.1	169.6	80.7	142.2	83.3
93.14	79	146.8	79.9	152.2	81.6	147	84.1
76.15	79.9	134.4	80.7	158	82.4	137.6	84.9

Sample	G3-16	**Sample**	N-1	**Sample**	N-5	**Sample**	N-15
% MeCl2	0.55	**% MeCl2**	0.24	**% MeCl2**	0.09	**% MeCl2**	0.01
Viscosity	**Temp**	**Viscosity**	**Temp**	**Viscosity**	**Temp**	**Viscosity**	**Temp**
Poise	°C	Poise	°C	Poise	°C	Poise	°C
5.25E+07	7.3	7.60E+07	4.7	6.70E+07	0.1	6.93E+07	6.5
6.32E+07	9	4.82E+07	6.5	6.04E+07	2	7.75E+07	7.3
8.49E+07	9.8	3.19E+07	7.3	7.42E+07	2.9	6.00E+07	8.2
3.61E+07	10.7	3.35E+07	8.2	4.50E+07	3.8	6.43E+07	9
4.20E+07	11.5	2.36E+07	9	4.41E+07	4.7	5.25E+07	9.8
2.69E+07	12.3	2.24E+07	9.8	3.02E+07	6.5	5.21E+07	10.6
1.65E+07	13.1	1.77E+07	10.7	4.56E+07	7.3	4.72E+07	11.5
1.71E+07	14	1.42E+07	11.5	2.34E+07	8.2	3.18E+07	12.3
1.22E+07	14.8	1.13E+07	12.3	2.76E+07	9	3.92E+07	13.1
1.10E+07	15.7	8.44E+06	13.1	1.74E+07	9.8	2.48E+07	14
7.90E+06	16.5	7.21E+06	14	1.74E+07	10.7	2.49E+07	14.8
6.02E+06	17.4	5.38E+06	14.8	1.58E+07	11.5	1.85E+07	15.6
4.82E+06	18.2	4.52E+06	15.6	1.01E+07	12.3	1.70E+07	16.5
3.80E+06	19	3.50E+06	16.5	9.35E+06	13.1	1.39E+07	17.3
3.08E+06	19.8	2.85E+06	17.4	6.64E+06	13.9	9.86E+06	18.2
2.46E+06	20.7	2.26E+06	18.1	5.46E+06	14.8	8.19E+06	19
1.96E+06	21.5	1.90E+06	19	4.16E+06	15.6	6.32E+06	19.9
1.55E+06	22.3	1.47E+06	19.8	3.33E+06	16.5	5.35E+06	20.7
1.28E+06	23.2	1.21E+06	20.7	2.66E+06	17.3	4.00E+06	21.5
1.02E+06	24	9.71E+05	21.5	2.08E+06	18.1	3.30E+06	22.3
8.47E+05	24.8	7.94E+05	22.3	1.69E+06	19	2.63E+06	23.2
6.84E+05	25.7	6.58E+05	23.2	1.35E+06	19.8	2.08E+06	24
5.70E+05	26.5	5.29E+05	24	1.11E+06	20.6	1.71E+06	24.9
4.71E+05	27.4	4.37E+05	24.9	9.01E+05	21.5	1.35E+06	25.7
3.83E+05	28.2	3.56E+05	25.7	7.33E+05	22.4	1.12E+06	26.5
3.22E+05	29	2.98E+05	26.5	6.02E+05	23.2	9.02E+05	27.4
2.63E+05	29.9	2.43E+05	27.3	4.91E+05	24	7.30E+05	28.2
2.21E+05	30.7	2.03E+05	28.2	4.05E+05	24.8	5.98E+05	29
1.81E+05	31.5	1.70E+05	29.1	3.36E+05	25.7	4.82E+05	29.9
1.53E+05	32.3	1.41E+05	29.8	2.76E+05	26.5	4.02E+05	30.7
1.28E+05	33.2	1.18E+05	30.7	2.29E+05	27.4	3.28E+05	31.6
1.06E+05	34	97030	31.6	1.89E+05	28.2	2.71E+05	32.4
89580	34.9	81300	32.4	1.59E+05	29	2.28E+05	33.2
74700	35.7	69090	33.2	1.31E+05	29.9	1.88E+05	34.1
63220	36.6	57340	34.1	1.10E+05	30.7	1.58E+05	34.9
54120	37.4	48880	34.9	93040	31.6	1.30E+05	35.7
45250	38.2	40910	35.7	77230	32.4	1.10E+05	36.5
38830	39.1	35010	36.6	65250	33.2	91960	37.4
32690	39.9	29650	37.4	53680	34.1	77040	38.2
28230	40.7	25400	38.2	45750	34.8	65050	39.1
23900	41.5	21530	39	38530	35.7	54510	39.9
20300	42.4	17990	39.9	32230	36.5	46090	40.7
17450	43.2	15460	40.7	27390	37.4	38640	41.6
14790	44.1	13030	41.5	23270	38.2	33330	42.3
12850	44.9	11240	42.4	19660	39	28480	43.2
10940	45.7	9433	43.2	16480	39.9	23980	44.1

9393	46.5	7925	44.1	14160	40.7	20550	44.9
8102	47.3	6752	44.9	12090	41.5	17490	45.7
6980	48.2	5625	45.7	10250	42.4	15030	46.6
6108	49	4837	46.6	8815	43.2	12950	47.4
5193	49.9	4125	47.4	7508	44	10790	48.2
4394	50.7	3631	48.2	6398	44.9	9226	49.1
3828	51.6	3171	49.1	5578	45.7	7548	49.9
3380	52.4	2758	49.9	4626	46.6	6422	50.7
2970	53.2	2449	50.7	4060	47.4	5151	51.6
2636	54	2104	51.5	3407	48.2	4101	52.4
2267	54.9	1867	52.4	3049	49	3361	53.2
2078	55.7	1656	53.2	2618	49.9	2833	54.1
1749	56.5	1465	54	2298	50.7	2489	54.9
1564	57.4	1315	54.9	1988	51.6	2146	55.7
1350	58.2	1176	55.7	1744	52.4	1865	56.5
1181	59.1	1058	56.6	1553	53.2	1626	57.4
1069	59.9	958.8	57.4	1347	54.1	1366	58.3
939.7	60.7	858.8	58.2	1178	54.8	1133	59.1
870.9	61.6	804.1	59.1	1052	55.7	978.4	59.9
816.3	62.3	728.5	59.9	931.6	56.6	853.8	60.7
707.5	63.3	658.1	60.7	858.8	57.4	751.5	61.5
654.5	64.1	614.3	61.6	780.8	58.2	667.1	62.4
612.6	64.9	556.2	62.4	712.3	59	591.7	63.3
565.6	65.8	538.1	63.3	655.4	59.9	533.5	64.1
529.4	66.6	493.6	64.1	620.9	60.8	480.4	65
493.1	67.4	461.4	64.9	594.8	61.6	421.2	65.8
464.1	68.2	439.9	65.7	559	62.4	421.5	66.5
440.7	69.1	414.4	66.6	523.7	63.3	454.7	67.4
426.9	69.9	397	67.4	508.7	64.1	443.6	68.3
421.8	70.7	379.6	68.2	484	64.9	418	69.1
415.5	71.6	354.6	69.1	475	65.7	373.4	69.9
411.1	72.4	330.5	69.9	464.8	66.6	372.7	70.7
420.1	73.2	314.1	70.7	441	67.4	356.9	71.6
400.7	74.1	292.2	71.5	423.3	68.3	342.5	72.4
388.8	74.9	280.2	72.4	399.8	69.1	342.9	73.2
366.9	75.7	261	73.3	375.7	69.9	330.6	74.1
339.3	76.6	242.8	74	360.7	70.7	323.7	74.9
332.6	77.4	234.3	74.9	335.5	71.6	318.3	75.7
305.5	78.2	212.6	75.7	319.2	72.4	302.5	76.6
296.1	79.1	208.8	76.5	305.5	73.2	307.8	77.4
281.4	79.9	195.2	77.4	281.7	74.1	296.2	78.2
258.1	80.7	180.6	78.3	277.9	74.9	287.1	79.1
256.3	81.6	178.1	79.1	256.8	75.8	276.4	79.9
233.2	82.4	157.8	79.9	263.3	76.5	251.3	80.7
232.7	83.3	162	80.7	256.9	77.4	249.6	81.6
221	84.1	150.2	81.5	235.3	78.3	228.6	82.4
205.1	84.9	142.1	82.4	237.9	79.1	216.6	83.2
207.3	85.8	139.6	83.3	218.7	79.9	209.9	84.1
184.4	86.6	122.8	84.1	217.1	80.8	186.8	84.9
192.4	87.4	131.9	84.9	209.9	81.5	187.4	85.7

Sample	N-18	**Sample**	GRM	**Sample**	GRM	**Sample**	GRM
% MeCl2	0.67	**% MeCl2**	0.20	**% MeCl2**	0.09	**% MeCl2**	0.01
Viscosity	**Temp**	**Viscosity**	**Temp**	**Viscosity**	**Temp**	**Viscosity**	**Temp**
Poise	°C	Poise	°C	Poise	°C	Poise	°C
7.63E+07	2.9	3.45E+06	0.5	3.08E+06	0.4	3.58E+06	0.5
5.48E+07	4.7	3.00E+06	2	2.67E+06	1.9	3.19E+06	2
3.95E+07	6.5	2.47E+06	3.4	2.21E+06	3.5	2.70E+06	3.5
6.48E+07	7.3	1.97E+06	4.7	1.75E+06	4.9	2.20E+06	5
3.50E+07	8.2	1.53E+06	6.2	1.35E+06	6.3	1.73E+06	6.3
3.80E+07	9	1.17E+06	7.4	1.03E+06	7.7	1.36E+06	7.6
2.64E+07	9.9	8.99E+05	8.8	7.86E+05	9.1	1.05E+06	8.9
2.63E+07	10.7	6.77E+05	10.1	6.03E+05	10.4	8.05E+05	10.3
2.06E+07	11.5	5.08E+05	11.5	4.58E+05	11.8	6.12E+05	11.6
1.76E+07	12.3	3.85E+05	12.9	3.47E+05	13.1	4.69E+05	13
1.67E+07	13.1	2.91E+05	14.3	2.63E+05	14.5	3.63E+05	14.3
1.16E+07	14	2.21E+05	15.7	1.99E+05	15.9	2.81E+05	15.7
1.01E+07	14.8	1.68E+05	17	1.50E+05	17.3	2.16E+05	17
7.26E+06	15.7	1.28E+05	18.4	1.13E+05	18.6	1.64E+05	18.4
6.11E+06	16.5	98210	19.7	86210	20	1.23E+05	19.8
4.62E+06	17.3	76020	21	66280	21.4	91690	21.1
3.83E+06	18.1	59860	22.4	51550	22.8	69460	22.5
3.14E+06	19	46460	23.7	40550	24.1	53330	23.8
2.45E+06	19.9	36180	25.1	31870	25.4	41560	25.2
1.99E+06	20.7	28470	26.5	25080	26.8	32610	26.5
1.57E+06	21.5	22520	27.8	19890	28.2	25830	27.9
1.30E+06	22.3	17940	29.2	15750	29.5	20670	29.2
1.06E+06	23.2	14310	30.5	12550	30.9	16460	30.6
8.58E+05	24	11460	31.9	10030	32.3	13140	31.9
7.02E+05	24.9	9208	33.3	8014	33.6	10560	33.3
5.73E+05	25.7	7486	34.6	6437	35	8507	34.7
4.74E+05	26.6	6069	36	5180	36.3	6880	36
3.86E+05	27.4	4941	37.4	4201	37.7	5613	37.4
3.20E+05	28.2	4052	38.7	3414	39	4593	38.8
2.68E+05	29	3335	40.1	2807	40.3	3746	40.1
2.20E+05	29.8	2748	41.4	2302	41.7	3088	41.5
1.84E+05	30.7	2281	42.8	1900	43.1	2572	42.8
1.52E+05	31.5	1897	44.2	1571	44.4	2124	44.2
1.27E+05	32.4	1588	45.5	1308	45.8	1789	45.6
1.07E+05	33.2	1330	46.9	1097	47.2	1515	46.9
88600	34	1122	48.3	923	48.5	1249	48.3
74750	34.9	945.2	49.6	779.8	49.9	1066	49.6
62770	35.7	802	51	661.7	51.2	898.9	51
53260	36.6	680.5	52.3	562.5	52.6	765	52.4
45050	37.3	580.7	53.7	481.5	53.9	642.8	53.8
38340	38.2	498.2	55.1	411.7	55.3	553.8	55.1
32820	39.1	426.7	56.4	353.4	56.7	472.4	56.4
27930	39.9	375.2	57.8	304.8	58	406.1	57.8
24050	40.7	320.8	59.1	263.1	59.4	351.7	59.1
20420	41.5	280	60.5	228.1	60.8	304.7	60.5
17580	42.4	241.6	61.8	199.2	62.1	264.2	61.9
15260	43.2	213	63.2	174	63.5	231.8	63.3

13070	44.1	187.3	64.6	152.4	64.8	202.6	64.6
11320	44.9	163.8	65.9	133.7	66.2	177.5	66
9811	45.7	144.4	67.3	118	67.5	156.8	67.3
8512	46.5	131.5	68.6	104.5	68.9	138	68.7
7327	47.4	118.1	70	92.75	70.2	122.9	70.1
6396	48.2	105.2	71.4	82.44	71.6	109.8	71.4
5489	49	91.27	72.7	73.5	73	98.15	72.7
4504	49.9	82.51	74.1	65.78	74.4	87.62	74.1
3805	50.7	73.51	75.5	58.96	75.7	80.12	75.5
3125	51.5	65.97	76.8	53.11	77.1	71.86	76.9
2614	52.4	59.48	78.2	48	78.4	64.62	78.2
2257	53.2	53.63	79.5	43.34	79.8	58.09	79.6
2080	54	48.45	80.9	39.32	81.2	52.41	81
1870	54.9	44.09	82.3	35.78	82.5	47.55	82.3
1666	55.7						
1465	56.6						
1342	57.4						
1223	58.2						
1128	59.1						
1008	59.9						
959.7	60.8						
867.2	61.6						
777.8	62.4						
728.3	63.2						
663.6	64.1						
623.3	64.9						
584	65.8						
549.6	66.6						
527.2	67.4						
504.5	68.3						
478.2	69						
466.3	69.9						
439.2	70.7						
426.1	71.6						
406.4	72.4						
384.7	73.2						
358	74.1						
333	74.9						
310.3	75.8						
288.2	76.5						
272	77.4						
256.7	78.3						
242.4	79.1						
228.3	79.9						
212.7	80.8						
204.5	81.6						
196.4	82.4						
187	83.3						
177	84.1						

Sample	GRM	**Sample**	GRM	**Sample**	GRM	**Sample**	GRM
% MeCl2	0.03	**% MeCl2**	0.14	**% MeCl2**	0.09	**% MeCl2**	0.03
Viscosity	**Temp**	**Viscosity**	**Temp**	**Viscosity**	**Temp**	**Viscosity**	**Temp**
Poise	°C	Poise	°C	Poise	°C	Poise	°C
4.32E+06	0.4	1.87E+06	0.6	2.73E+06	0.4	3.27E+06	0.6
4.16E+06	1.9	1.56E+06	2	2.30E+06	2	2.72E+06	2.2
3.97E+06	3.5	1.25E+06	3.6	1.85E+06	3.6	2.15E+06	3.6
3.55E+06	4.8	9.81E+05	5	1.45E+06	5	1.65E+06	5.1
3.04E+06	6.3	7.65E+05	6.4	1.12E+06	6.5	1.25E+06	6.5
2.46E+06	7.6	5.96E+05	7.8	8.68E+05	7.8	9.43E+05	7.9
1.91E+06	8.9	4.64E+05	9.1	6.64E+05	9.2	7.17E+05	9.2
1.50E+06	10.3	3.59E+05	10.5	5.13E+05	10.5	5.45E+05	10.5
1.14E+06	11.6	2.77E+05	11.9	3.93E+05	11.9	4.15E+05	11.9
8.62E+05	13	2.15E+05	13.3	3.02E+05	13.2	3.14E+05	13.2
6.42E+05	14.4	1.68E+05	14.6	2.33E+05	14.6	2.38E+05	14.7
4.86E+05	15.7	1.33E+05	15.9	1.79E+05	16	1.83E+05	16
3.26E+05	17.1	1.07E+05	17.3	1.40E+05	17.4	1.41E+05	17.4
2.85E+05	18.4	84580	18.7	1.10E+05	18.8	1.09E+05	18.7
2.15E+05	19.8	66710	20	86060	20.1	85130	20.1
1.69E+05	21	52050	21.4	68000	21.4	66360	21.5
1.31E+05	22.4	40410	22.6	53230	22.8	51140	22.8
1.01E+05	23.8	32250	24	41440	24.2	39770	24.2
77840	25.1	25670	25.4	32620	25.6	31100	25.5
60290	26.5	20400	26.7	26090	26.9	24580	26.8
48040	27.9	16260	28.1	20750	28.3	19310	28.2
38480	29.2	13020	29.5	16660	29.6	15060	29.6
30260	30.6	10480	30.8	13380	31	11770	30.9
23940	31.9	8480	32.2	10840	32.3	9240	32.3
19020	33.3	6883	33.6	8770	33.7	7270	33.6
15220	34.7	5618	34.9	7181	35.1	5772	35
12230	36	4596	36.3	5874	36.4	4632	36.4
9880	37.3	3795	37.6	4846	37.8	3734	37.7
8088	38.6	3127	39	3998	39.2	3030	39.1
6587	40	2581	40.3	3312	40.5	2473	40.4
5382	41.4	2137	41.7	2760	41.9	2027	41.8
4415	42.7	1770	43.1	2313	43.2	1666	43.2
3673	44	1475	44.4	1945	44.6	1376	44.6
3045	45.4	1236	45.8	1629	45.9	1146	45.9
2535	46.8	1033	47.1	1370	47.3	959.3	47.3
2107	48.1	866.8	48.5	1155	48.7	807.2	48.6
1759	49.5	731.5	49.9	983.8	49.9	687.1	50
1471	50.8	619.4	51.2	839.6	51.3	590.1	51.3
1239	52.2	527	52.6	719.7	52.7	505.8	52.7
1044	53.5	447.6	54	613.7	54.1	437.9	54.1
888.1	54.9	382.3	55.3	526.1	55.4	378.2	55.4
758.4	56.2	328.4	56.7	451.5	56.8	330.2	56.8
643.4	57.5	283	58	390.5	58.2	288	58.1
550.2	58.9	244.2	59.4	338.7	59.5	252.2	59.5
471	60.2	211.6	60.8	294.5	60.9	221	60.8
404.5	61.6	184.4	62.1	257.2	62.2	194.8	62.2

349.3	63	160.4	63.5	224.3	63.6	171.1	63.6
302	64.4	140.4	64.9	197	65	150.4	64.9
262	65.7	123.4	66.2	172.7	66.3	132.4	66.3
229.1	67.1	108.9	67.5	153	67.7	116.8	67.7
200	68.4	95.86	68.9	135.1	69	103.5	69.1
175.6	69.8	84.9	70.3	120.5	70.4	91.86	70.4
154.8	71.2	75.35	71.6	107	71.7	82.02	71.7
136.6	72.5	67.12	73	95.23	73.1	73.04	73.1
121.1	73.9	60.09	74.3	85.68	74.5	65.37	74.4
107.5	75.2	53.74	75.8	77.87	75.8	58.63	75.8
95.98	76.6	48.25	77.1	70.09	77.2	52.58	77.2
85.59	78	43.58	78.4	63.24	78.5	47.46	78.6
76.74	79.4	39.35	79.8	57.21	79.9	43.01	79.9
68.87	80.7	35.62	81.2	51.58	81.3	38.97	81.3
61.8	82	32.31	82.6	46.8	82.6	35.47	82.6

Viscosities from Lab B

	Well ID	Sample ID	Depth (m)	Formation	Temp (ºC)	Viscosity (cP)
Legacy	11-12-91-24W4	N1	282.5-285.7	Nisku	20	159,000,000
	10-21-92-24W4	UI1	363-366	UIreton	20	405,000,000
		UI2	377-379	UIreton	30	2,800,000
	10-12-93-24W4	G1	444-446.7	UGM3	30	27,500,000
	10-29-89-23W4	N2	265-267	Nisku	30	8,900,000
		N3	305.3-307.45	Nisku	30	48,300,000
		UI3	327.35-328.1	UIreton	30	17,300,000
		G2	346-349	UGM3	30	10,000,000
	6-10-87-23W4	N4	349.4-358.2	Nisku	30	3,000,000
	11-26-87-20W4	UI4	263.4-267	UIreton	30	2,800,000
	10-29-86-19W4	G3	283-283.3	UGM3	30	36,400,000
		G4	303-303.6	UGM3	30	15,000,000
Fresh	11-26-91-24W4	UI5	316.8-319	UIreton	20	1,270,393
		G5	335.25-336.4	UGM3	20	5,255,580
	06-08-89-23W4	N5	270.6-280.6	Nisku	20	2,907,186
		G6	322.8-324.2	UGM3	20	16,421,718
	07-26-85-19W4	UI6	325-326.2	UIreton	20	17,321,273
		G7	350.2-350.8	UGM3	20	58,862,816

Viscosity from Lab C

Batch # Well ID	Sample ID	Solvent	Viscosity (cP) @ Temperature (°C)						
			11°C	20°C	30°C	40°C	60°C	80°C	40°C Re
Batch 1									
16-13-89-23W4	N-1	DCM	—	2.02E+7	—	6.35E+5	4.92E+4	7.26E+3	6.24E+5
	G3-4	DCM	—	1.97E+7	—	6.35E+5	4.94E+4	7.40E+3	6.57E+5
08-01-89-23W4	GRM 127	DCM	—	2.74E+6	—	1.33E+5	1.49E+4	2.85E+3	1.52E+5
	GRM 129	DCM	—	2.27E+6	—	1.20E+5	1.34E+4	2.61E+3	1.27E+5
Batch 2									
10-04-94-23W4	G3-130	Toluene	—	3.31E+7	—	7.66E+5	5.05E+4	6.50E+3	8.01E+5
	G3-140	Toluene	—	1.90E+7	—	5.46E+5	4.10E+4	6.00E+3	6.04E+5
10-29-89-23W4	N-52	Toluene	—	2.41E+7	—	6.80E+5	5.18E+4	7.55E+3	7.12E+5
	N-57	Toluene	—	6.51E+7	—	1.35E+6	8.36E+4	1.09E+4	1.46E+6
	UI-81	Toluene	—	3.44E+7	—	1.10E+6	6.62E+4	1.00E+4	1.25E+6
	G3-35	Toluene	—	1.55E+7	—	5.08E+5	3.94E+4	6.10E+3	5.41E+5
10-29-86-19W4	G3-63	Toluene	—	2.63E+7	—	7.11E+5	5.20E+4	7.61E+3	8.00E+5
Batch 3									
10-29-89-23W4	N2	Toluene	—	8.57E+7	1.33E+77	1.95E+6	1.21E+5	1.44E+4	2.10E+6
	N2	DCM	—	3.00E+7	4.45E+6	9.22E+5	7.15E+4	9.85E+3	1.01E+6
	N3	Toluene	—	6.24E+7	9.15E+6	1.51E+6	9.16E+4	1.19E+4	1.64E+6
	UI3	Toluene	—	1.23E+7	2.05E+6	4.34E+5	3.66E+4	5.72E+3	4.77E+5
	G2	Toluene	—	1.32E+7	2.02E+6	4.41E+5	3.98E+4	6.45E+3	5.46E+5
	G2	DCM	—	1.68E+7	2.67E+6	5.63E+5	4.43E+4	6.66E+3	5.62E+5
06-08-89-23W4	N5	Toluene	—	5.86E+6	—	2.49E+5	2.36E+5	4.19E+3	2.54E+5

	N5	DCM	—	3.45E+6	6.70E+5	1.64E+5	1.80E+4	3.26E+4	—
	G6	Toluene	—	1.32E+7	—	4.44E+5	3.71E+4	5.75E+3	4.69E+5
	G6	DCM	—	3.53E+7	—	9.68E+5	6.88E+4	9.37E+3	9.62E+5
07-26-85-19W4	G7	DCM	—	3.14E+6	6.09E+5	1.48E+5	1.66E+4	3.09E+3	1.77E+5
Batch 4									
10-29-89-23W4	UI-90	DCM	—	4.97E+07	—	1.30E+06	8.54E+04	1.12E+04	1.42E+06
	G3-33	DCM	—	9.74E+06	—	3.83E+05	3.40E+04	5.67E+03	4.00E+05
8-33-90-23W4	N-77	DCM	—	2.07E+06	—	1.06E+05	1.22E+04	2.47E+03	1.18E+05
	N-79	DCM	2.80E+07	4.81E+06	—	2.09E+05	2.08E+04	3.68E+03	2.00E+05
	UI-122	DCM	1.66E+07	2.87E+06	—	1.27E+05	1.38E+04	2.60E+03	1.41E+05
	UI-125	DCM	9.80E+06	1.87E+06	—	9.34E+04	1.06E+04	2.12E+03	9.23E+04
	UI-129	DCM	7.49E+06	1.47E+06	—	7.61E+04	8.76E+03	1.85E+03	7.83E+04
	G3-240	DCM	1.74E+07	3.11E+06	—	1.43E+05	1.50E+04	2.85E+03	1.47E+05
	G3-243	DCM	1.58E+07	2.72E+06	—	1.32E+05	1.45E+04	2.76E+03	1.40E+05
	G3-245	DCM	1.61E+07	2.82E+06	—	1.25E+05	1.33E+04	2.46E+03	1.29E+05
	G3-246	DCM	1.04E+07	2.00E+06	—	1.01E+05	1.16E+04	2.34E+03	1.05E+05

APPENDEIX 3: GC-MS DATA

GC-MS Method

1. 6890 GC Method

1.1 Oven

Initial temp: 40 'C (On)
Initial time: 5.00 min
Ramps:

#	Rate	Final temp	Final time
1	4.00	300	20.00
2	0.0(Off)		

Post temp: 0 'C
Post time: 0.00 min
Run time: 90.00 min

Maximum temp: 325 'C
Equilibration time: 0.50 min

1.2 Front inlet (split/splitless)

Mode: Pulsed Splitless
Initial temp: 280 'C (On)
Pressure: 52.5 kPa (On)
Pulse pressure: 150 kPa
Pulse time: 1.00 min
Purge flow: 5.0 mL/min
Purge time: 0.00 min
Total flow: 9.0 mL/min
Gas saver: On
Saver flow: 20.0 mL/min
Saver time: 2.00 min
Gas type: Helium

Back inlet (unknown)

1.3 Column 1

Capillary Column
Model Number: Agilent 19091S-433
HP-5MS 5% Phenyl Methyl Siloxane
Max temperature: 325 'C
Nominal length: 30.0 m
Nominal diameter: 250.00 um
Nominal film thickness: 0.25 um
Mode: constant flow
Initial flow: 1.1 mL/min

Column 2

(not installed)

Nominal init pressure: 52.6 kPa
Average velocity: 37 cm/sec
Inlet: Front Inlet
Outlet: MSD
Outlet pressure: vacuum

1.4 Front detector (NO DET)
SIGNAL 1
Data rate: 20 Hz
Type: test plot
Save Data: Off
Zero: 0.0 (Off)
Range: 0
Fast Peaks: Off
Attenuation: 0

Back detector (NO DET)
SIGNAL 2
Data rate: 20 Hz
Type: test plot
Save Data: Off
Zero: 0.0 (Off)
Range: 0
Fast Peaks: Off
Attenuation: 0

1.5 Thermal AUX 2
Use: MSD Transfer Line Heater
Description:
Initial temp: 230 'C (On)
Initial time: 0.00 min

1.6 GC injector
Front Injector:

Sample Washes	0
Sample Pumps	2
Injection Volume	1.00 microliters
Syringe Size	10.0 microliters
PreInj Solvent A Washes	1
PreInj Solvent B Washes	1
PostInj Solvent A Washes	5
PostInj Solvent B Washes	5
Viscosity Delay	5 seconds
Plunger Speed	Fast
PreInjection Dwell	0.00 minutes
PostInjection Dwell	0.00 minutes

Back Injector:
No parameters specified

2. MS Acquisition Parameters

2.1 General Information

Tune File : atune.u

Acquistion Mode : SIM

2.2 MS Information

Solvent Delay : 5.00 min

2.3 EM Absolute : False

EM Offset : 0

Resulting EM Voltage : 1494.1

2.4 Sim Parameters

GROUP 1

Group ID : 1

Resolution : Low

Plot 1 Ion : 85.10

Ions/Dwell In Group	(Mass, Dwell)	(Mass, Dwell)	(Mass, Dwell)
	(85.10, 35)	(91.10, 35)	(97.10, 35)
	(98.10, 35)	(105.10, 35)	(119.10, 35)
	(123.10, 35)	(128.10, 35)	(133.10, 35)
	(135.10, 35)	(136.10, 35)	(142.10, 35)
	(149.10, 35)	(152.10, 35)	(154.10, 35)
	(156.10, 35)	(162.10, 35)	(163.10, 35)
	(166.10, 35)	(168.10, 35)	(170.10, 35)
	(176.10, 35)	(177.20, 35)	(178.20, 35)
	(180.20, 35)	(182.20, 35)	(183.20, 35)
	(184.20, 35)	(187.20, 35)	(188.20, 35)
	(191.20, 35)	(192.20, 35)	(193.20, 35)
	(194.20, 35)	(197.20, 35)	(198.20, 35)
	(201.20, 35)	(202.20, 35)	(205.20, 35)
	(206.20, 35)	(212.20, 35)	(216.20, 35)
	(217.20, 35)	(218.20, 35)	(220.20, 35)
	(221.20, 35)	(226.20, 35)	(228.20, 35)
	(231.20, 35)	(234.20, 35)	(239.20, 35)
	(240.20, 35)	(242.20, 35)	(245.20, 35)
	(248.20, 35)	(252.20, 35)	(253.20, 35)
	(259.20, 35)	(266.30, 35)	(365.30, 35)

MS Quad :150 C maximum 200 C

MS Source : 230 C maximum 250 C

3. Tune Parameters for SN: US62733867

EMISSION	:	34.610
ENERGY	:	69.922
REPELLER	:	29.955
IONFOCUS	:	90.157
ENTRANCE_LE	:	22.000
EMVOLTS	:	1494.118
AMUGAIN	:	1562.000
AMUOFFSET	:	121.813
FILAMENT	:	1.000
DCPOLARITY	:	0.000
ENTLENSOFFS	:	19.075
MASSGAIN	:	-765.000
MASSOFFSET	:	-39.000

m/z 191 and m/z 177 Fragmentograms

N1

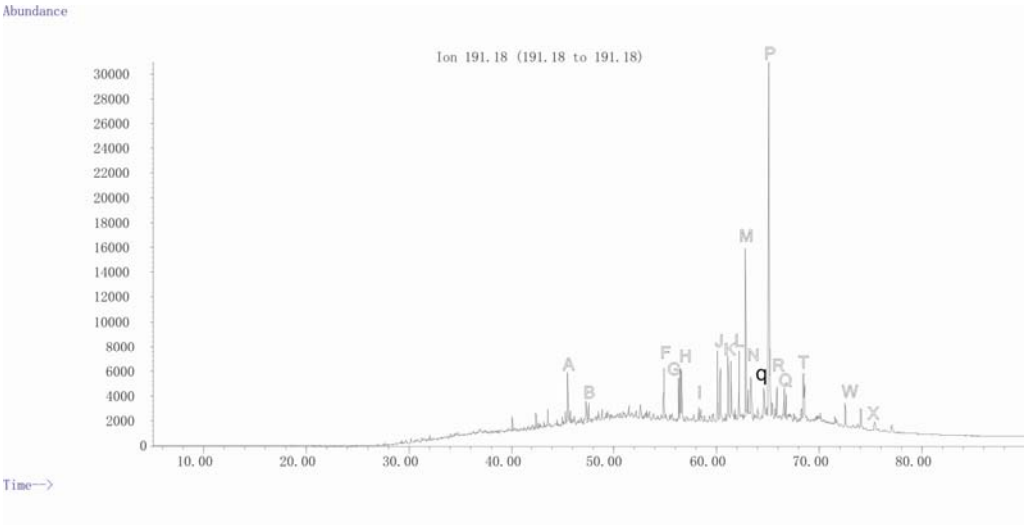

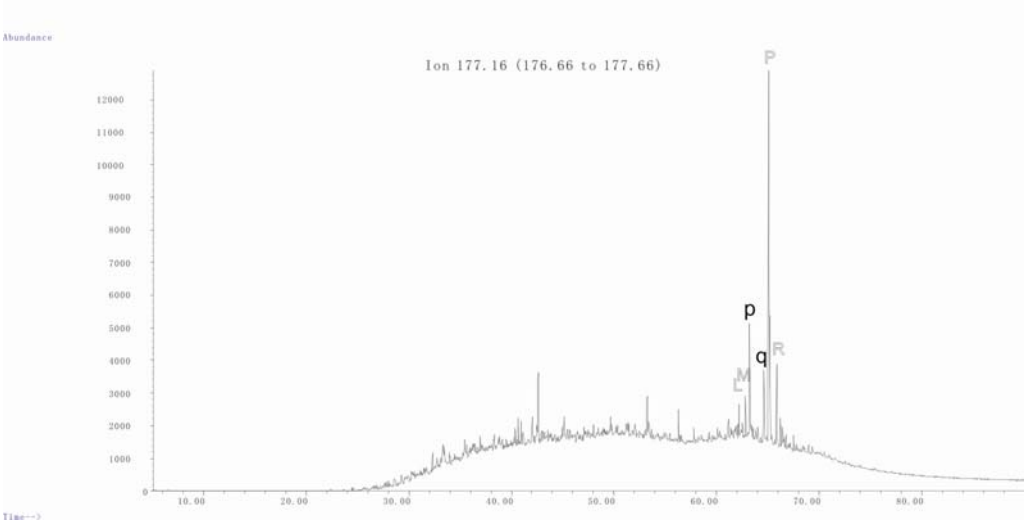

N2

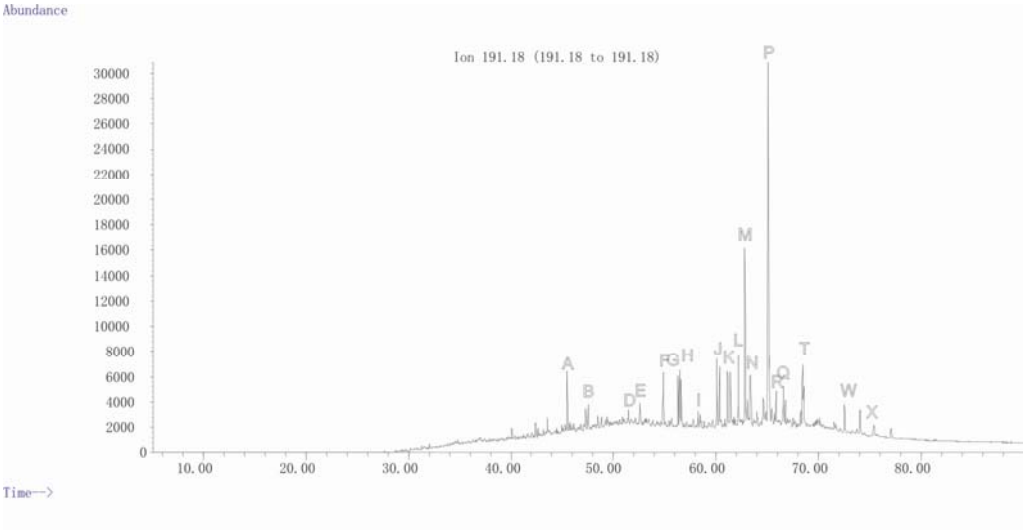
Abundance
Ion 191.18 (191.18 to 191.18)
30000
28000
26000
24000
22000
20000
18000
16000
14000
12000
10000
8000
6000
4000
2000
0
A
B
D
E
F
G
H
I
J
K
L
M
N
P
Q
R
T
W
X
10.00
20.00
30.00
40.00
50.00
60.00
70.00
80.00
Time-->

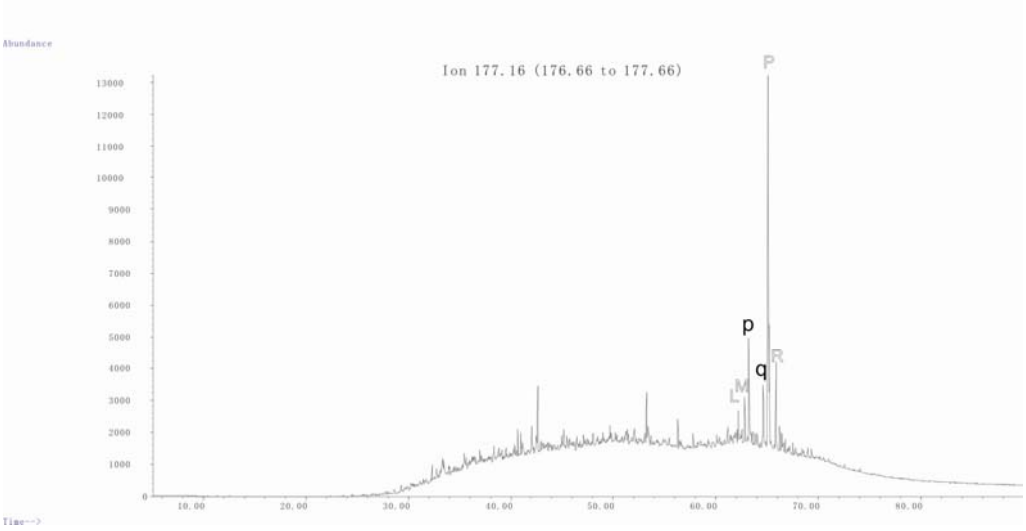
Abundance
Ion 177.16 (176.66 to 177.66)
13000
12000
11000
10000
9000
8000
7000
6000
5000
4000
3000
2000
1000
0
P
p
q
R
M
L
10.00
20.00
30.00
40.00
50.00
60.00
70.00
80.00
Time-->

N3

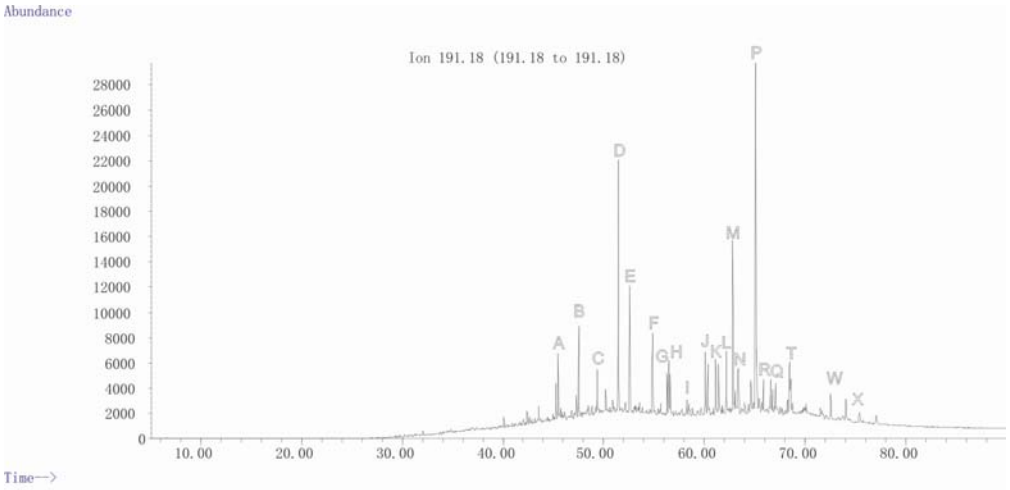
Abundance
Ion 191.18 (191.18 to 191.18)
28000
26000
24000
22000
20000
18000
16000
14000
12000
10000
8000
6000
4000
2000
0
A
B
C
D
E
F
G
H
I
J
K
L
M
N
P
Q
R
T
W
X
10.00
20.00
30.00
40.00
50.00
60.00
70.00
80.00
Time-->

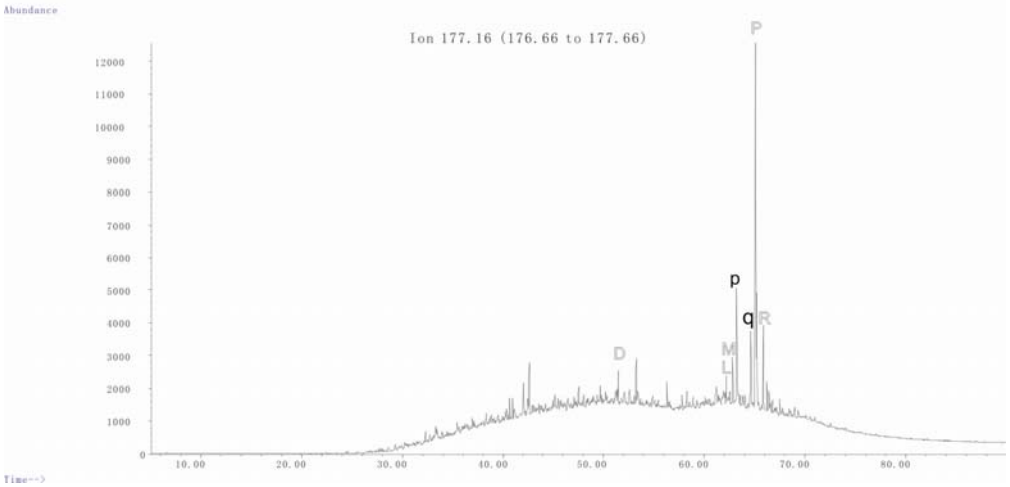
Abundance
Ion 177.16 (176.66 to 177.66)
12000
11000
10000
9000
8000
7000
6000
5000
4000
3000
2000
1000
0
D
L
M
p
q
P
R
10.00
20.00
30.00
40.00
50.00
60.00
70.00
80.00
Time-->

N4

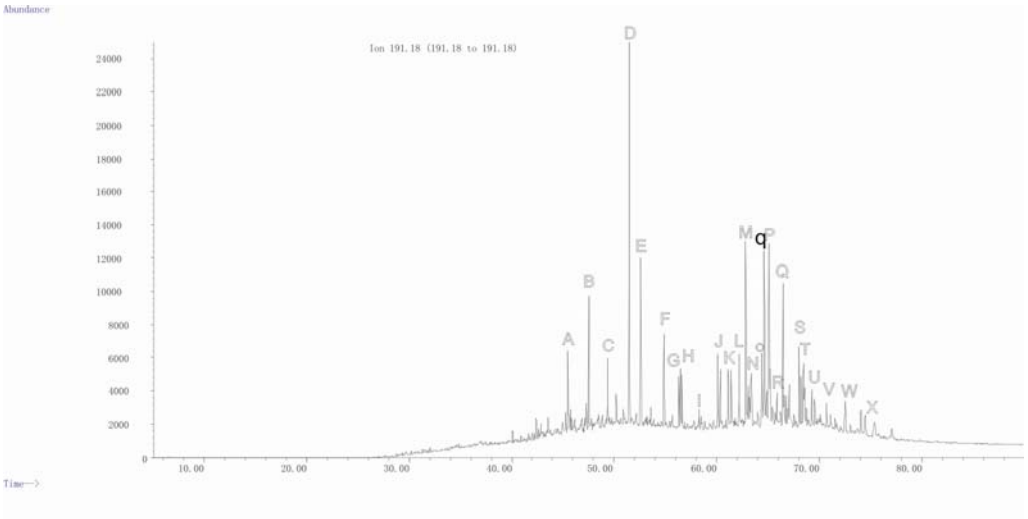
Abundance
Ion 191.18 (191.18 to 191.18)
24000
22000
20000
18000
16000
14000
12000
10000
8000
6000
4000
2000
0
A
B
C
D
E
F
G
H
I
J
K
L
M
N
O
P
q
R
S
T
U
V
W
X
10.00
20.00
30.00
40.00
50.00
60.00
70.00
80.00
Time-->

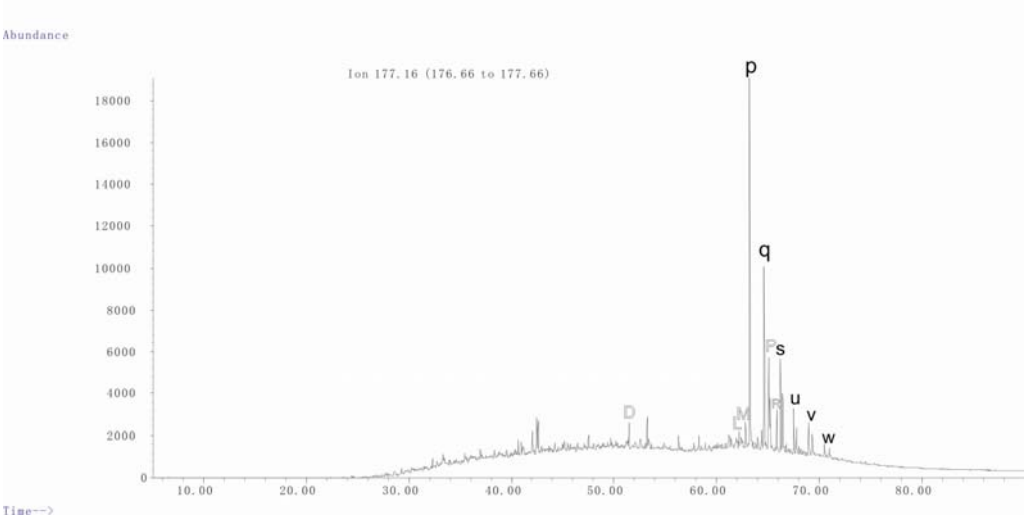
Abundance
Ion 177.16 (176.66 to 177.66)
18000
16000
14000
12000
10000
8000
6000
4000
2000
0
D
L
M
R
p
q
s
u
v
w
10.00
20.00
30.00
40.00
50.00
60.00
70.00
80.00
Time-->

N5

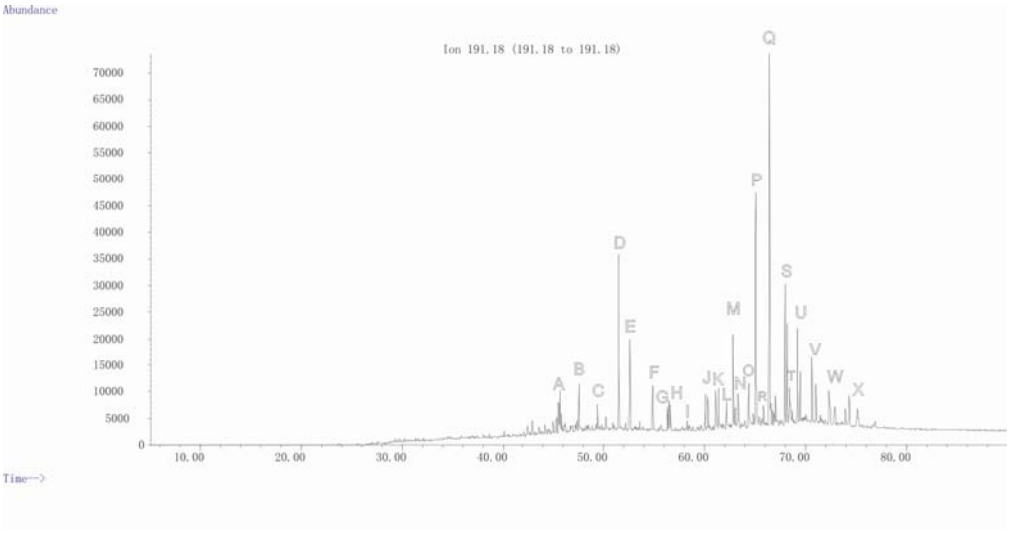
Abundance
Ion 191.18 (191.18 to 191.18)
70000
65000
60000
55000
50000
45000
40000
35000
30000
25000
20000
15000
10000
5000
0
A
B
C
D
E
F
G
H
I
J
K
L
M
N
O
P
Q
R
S
T
U
V
W
X
10.00
20.00
30.00
40.00
50.00
60.00
70.00
80.00
Time-->

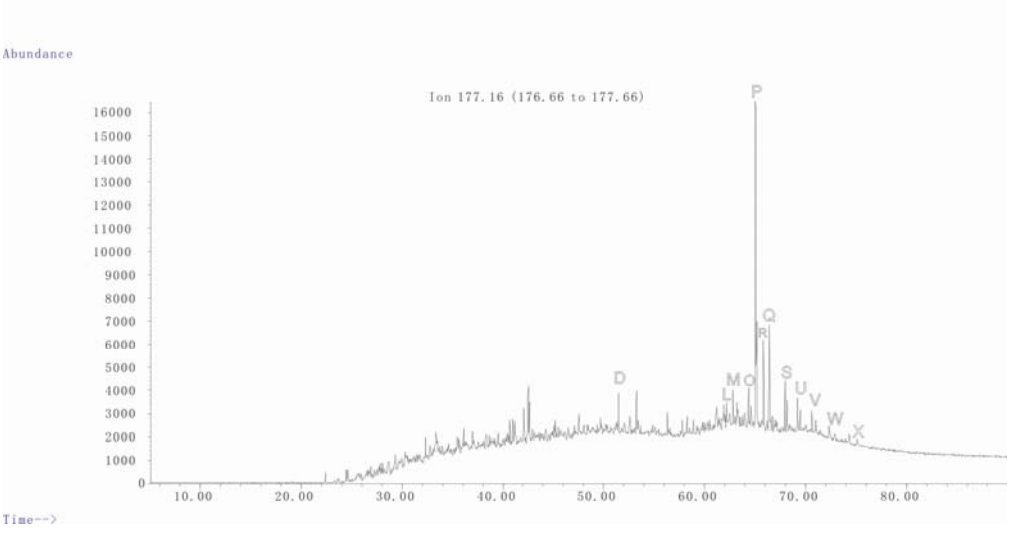
Abundance
Ion 177.16 (176.66 to 177.66)
16000
15000
14000
13000
12000
11000
10000
9000
8000
7000
6000
5000
4000
3000
2000
1000
0
D
L
M
O
P
Q
R
S
U
V
W
X
10.00
20.00
30.00
40.00
50.00
60.00
70.00
80.00
Time-->

UI1

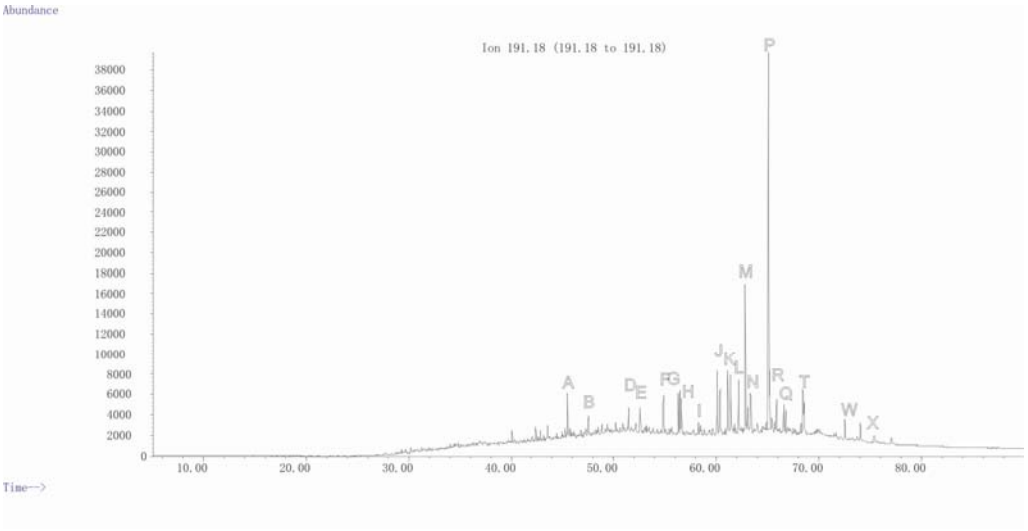
Abundance
Ion 191.18 (191.18 to 191.18)
38000
36000
34000
32000
30000
28000
26000
24000
22000
20000
18000
16000
14000
12000
10000
8000
6000
4000
2000
0
A
B
D
E
F
G
H
I
J
K
L
M
N
P
Q
R
T
W
X
10.00
20.00
30.00
40.00
50.00
60.00
70.00
80.00
Time-->

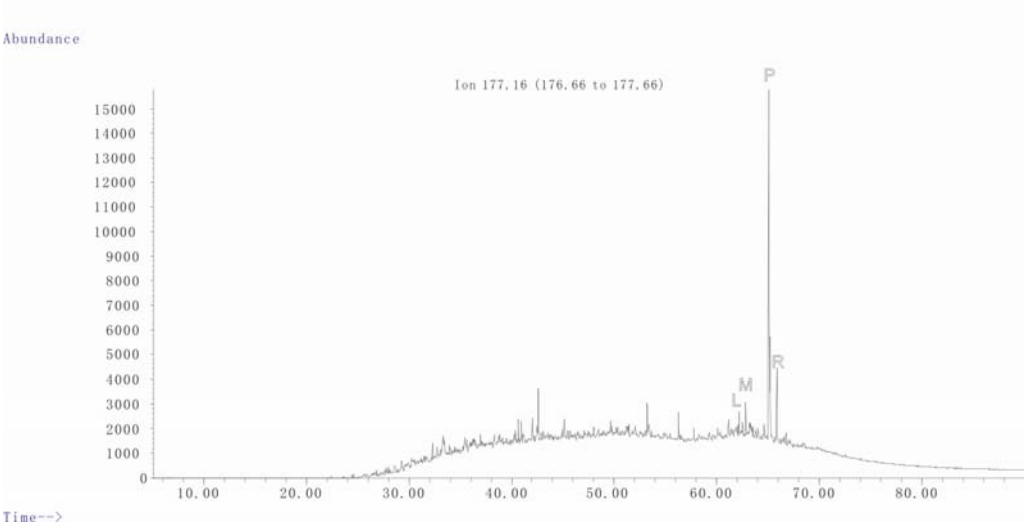
Abundance
Ion 177.16 (176.66 to 177.66)
15000
14000
13000
12000
11000
10000
9000
8000
7000
6000
5000
4000
3000
2000
1000
0
L
M
P
R
10.00
20.00
30.00
40.00
50.00
60.00
70.00
80.00
Time-->

UI2

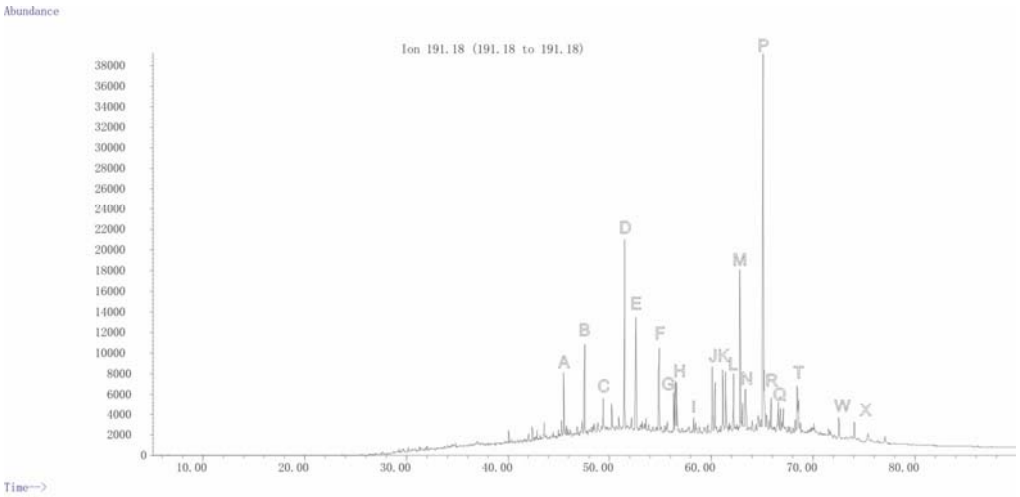
Abundance
Ion 191.18 (191.18 to 191.18)
38000
36000
34000
32000
30000
28000
26000
24000
22000
20000
18000
16000
14000
12000
10000
8000
6000
4000
2000
0
A
B
C
D
E
F
G
H
I
JK
L
M
N
P
R
Q
T
W
X
10.00
20.00
30.00
40.00
50.00
60.00
70.00
80.00
Time-->

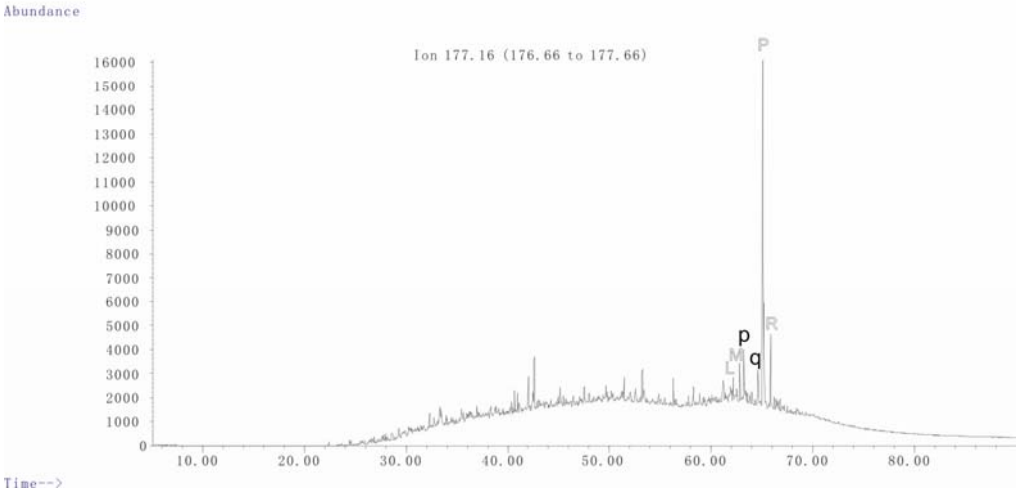
Abundance
Ion 177.16 (176.66 to 177.66)
16000
15000
14000
13000
12000
11000
10000
9000
8000
7000
6000
5000
4000
3000
2000
1000
0
P
R
p
q
M
L
10.00
20.00
30.00
40.00
50.00
60.00
70.00
80.00
Time-->

UI3

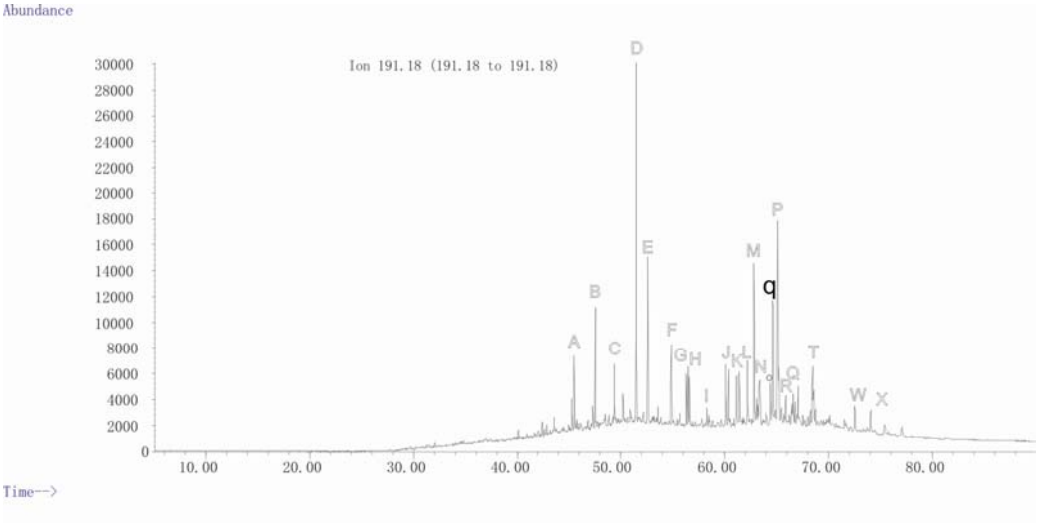
Abundance
Ion 191.18 (191.18 to 191.18)
30000
28000
26000
24000
22000
20000
18000
16000
14000
12000
10000
8000
6000
4000
2000
0
A
B
C
D
E
F
G
H
I
J
K
L
M
N
O
P
Q
R
T
W
X
q
10.00
20.00
30.00
40.00
50.00
60.00
70.00
80.00
Time-->

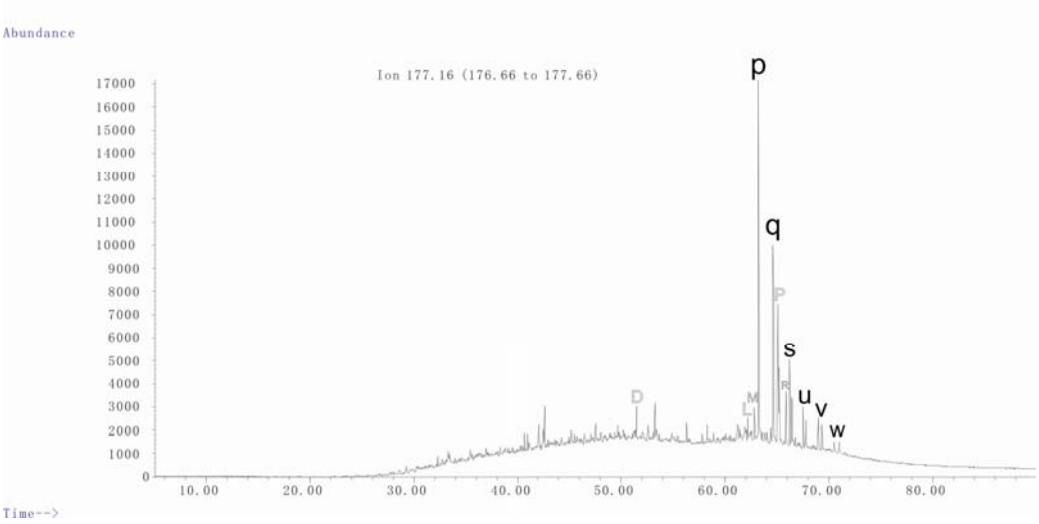
Abundance
Ion 177.16 (176.66 to 177.66)
17000
16000
15000
14000
13000
12000
11000
10000
9000
8000
7000
6000
5000
4000
3000
2000
1000
0
p
q
P
s
R
u
v
w
D
M
10.00
20.00
30.00
40.00
50.00
60.00
70.00
80.00
Time-->

UI4

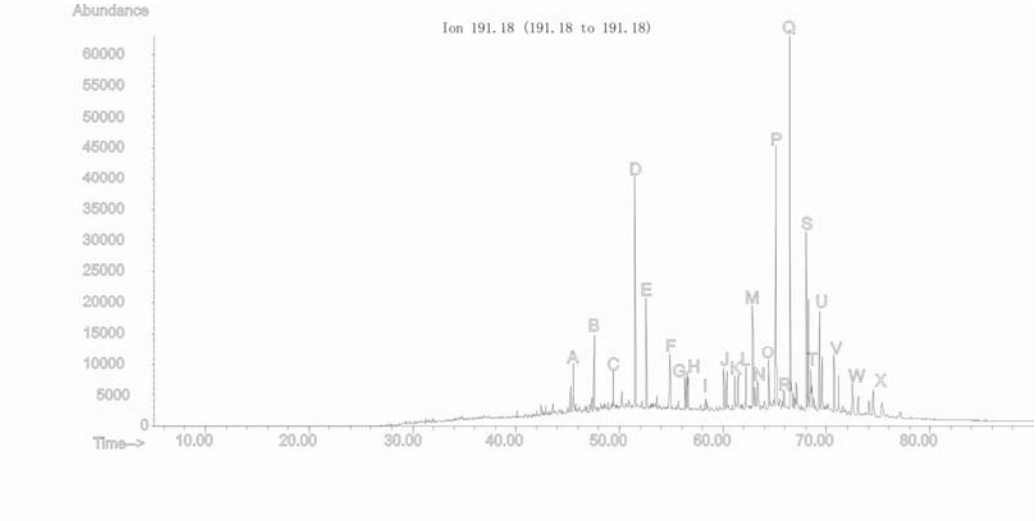
Abundance
Ion 191.18 (191.18 to 191.18)
60000
55000
50000
45000
40000
35000
30000
25000
20000
15000
10000
5000
0
Time-->
10.00
20.00
30.00
40.00
50.00
60.00
70.00
80.00
A
B
C
D
E
F
G
H
I
J
K
L
M
N
O
P
Q
R
S
T
U
V
W
X

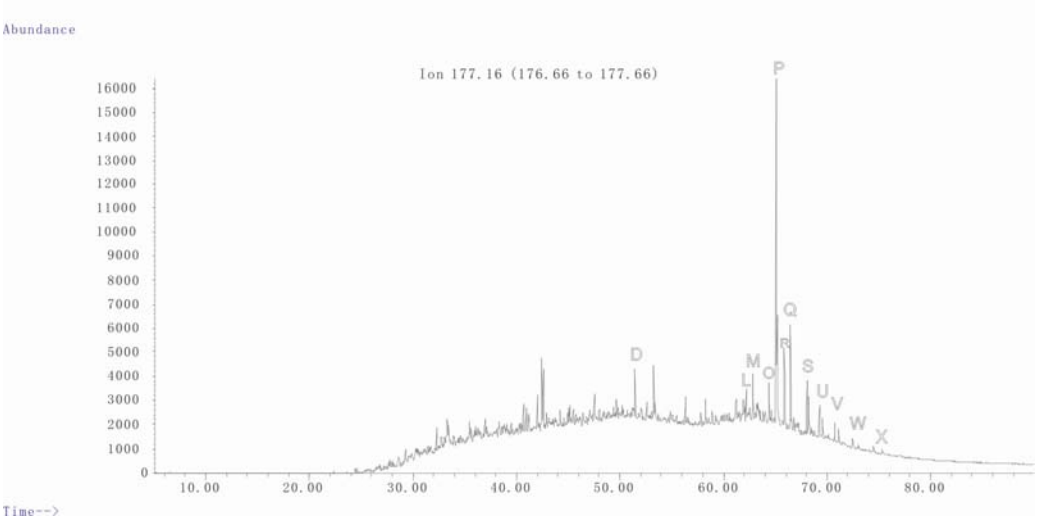
Abundance
Ion 177.16 (176.66 to 177.66)
16000
15000
14000
13000
12000
11000
10000
9000
8000
7000
6000
5000
4000
3000
2000
1000
0
Time-->
10.00
20.00
30.00
40.00
50.00
60.00
70.00
80.00
D
L
M
O
P
Q
R
S
U
V
W
X

UI5

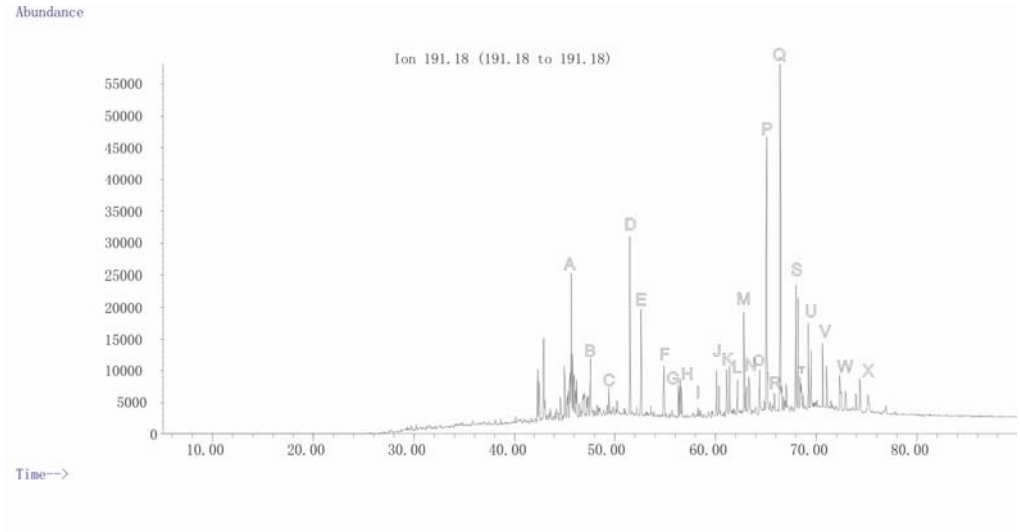
Abundance
Ion 191.18 (191.18 to 191.18)
55000
50000
45000
40000
35000
30000
25000
20000
15000
10000
5000
0
A
B
C
D
E
F
G
H
I
J
K
L
M
N
O
P
Q
R
S
T
U
V
W
X
10.00
20.00
30.00
40.00
50.00
60.00
70.00
80.00
Time-->

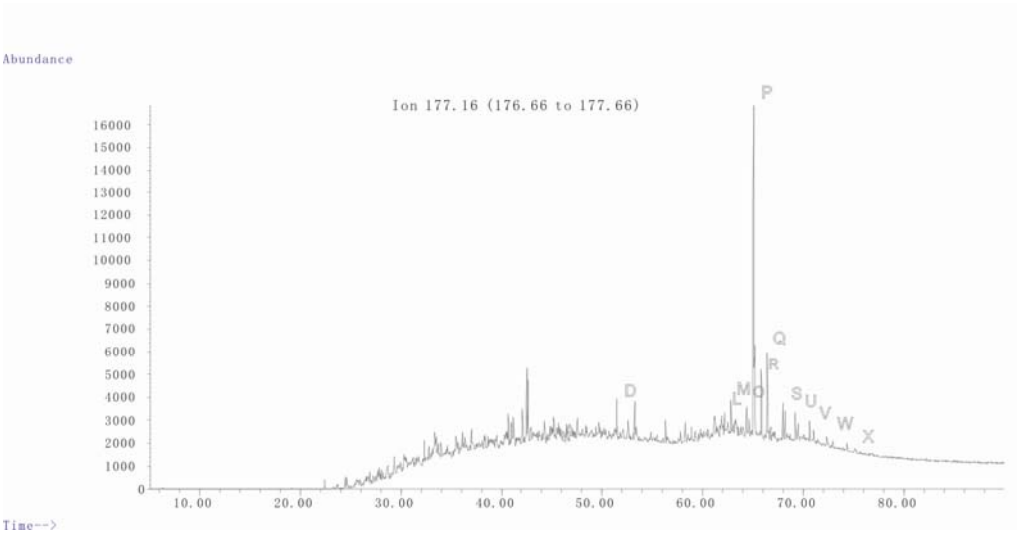
Abundance
Ion 177.16 (176.66 to 177.66)
16000
15000
14000
13000
12000
11000
10000
9000
8000
7000
6000
5000
4000
3000
2000
1000
0
D
L
M
N
O
P
Q
R
S
U
V
W
X
10.00
20.00
30.00
40.00
50.00
60.00
70.00
80.00
Time-->

UI6

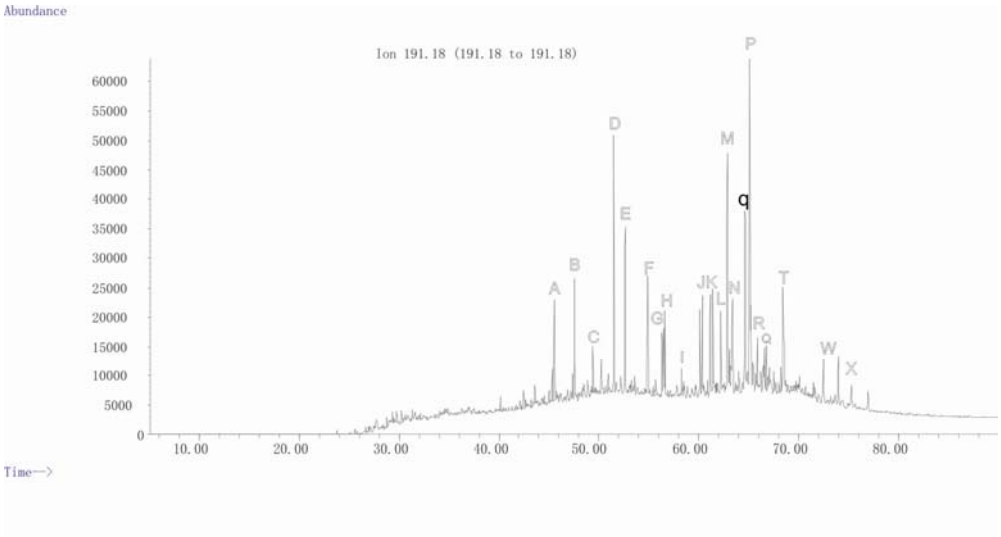
Abundance
Ion 191.18 (191.18 to 191.18)
60000
55000
50000
45000
40000
35000
30000
25000
20000
15000
10000
5000
0
A
B
C
D
E
F
G
H
I
JK
L
M
N
P
q
R
S
T
W
X
10.00
20.00
30.00
40.00
50.00
60.00
70.00
80.00
Time-->

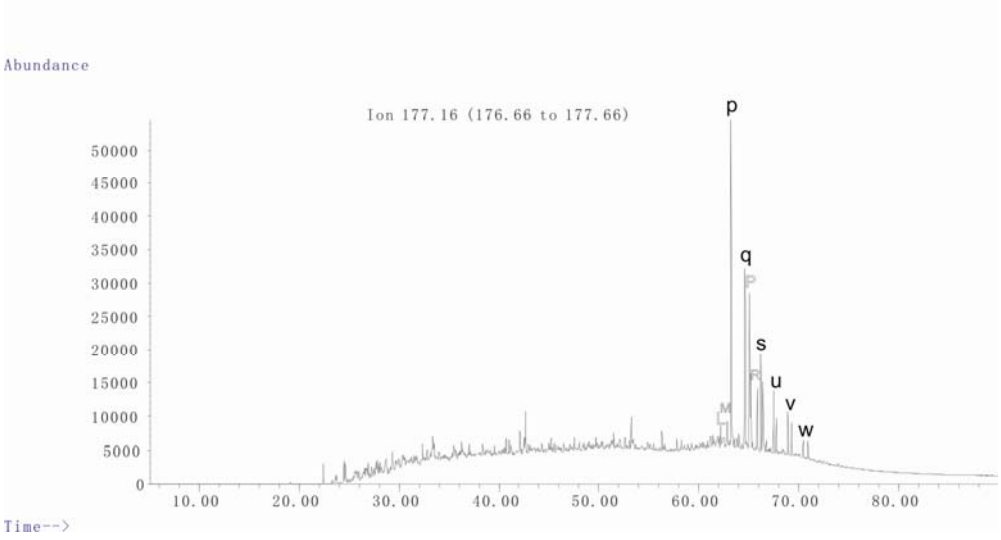
Abundance
Ion 177.16 (176.66 to 177.66)
50000
45000
40000
35000
30000
25000
20000
15000
10000
5000
0
p
q
P
s
u
v
w
10.00
20.00
30.00
40.00
50.00
60.00
70.00
80.00
Time-->

G1

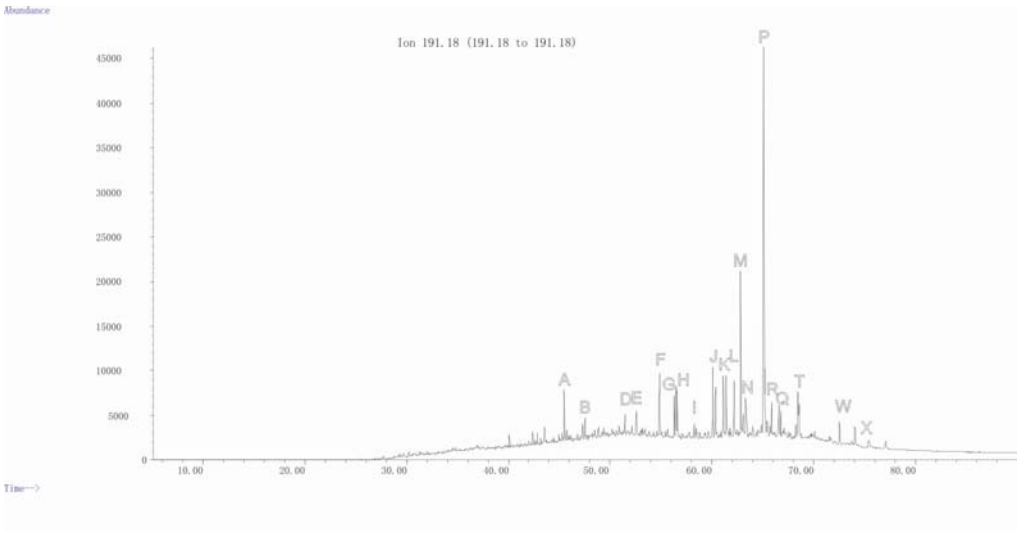
Abundance
Ion 191.18 (191.18 to 191.18)
45000
40000
35000
30000
25000
20000
15000
10000
5000
0
A
B
DE
F
G
H
I
J
K
L
M
N
P
R
Q
T
W
X
10.00
20.00
30.00
40.00
50.00
60.00
70.00
80.00
Time-->

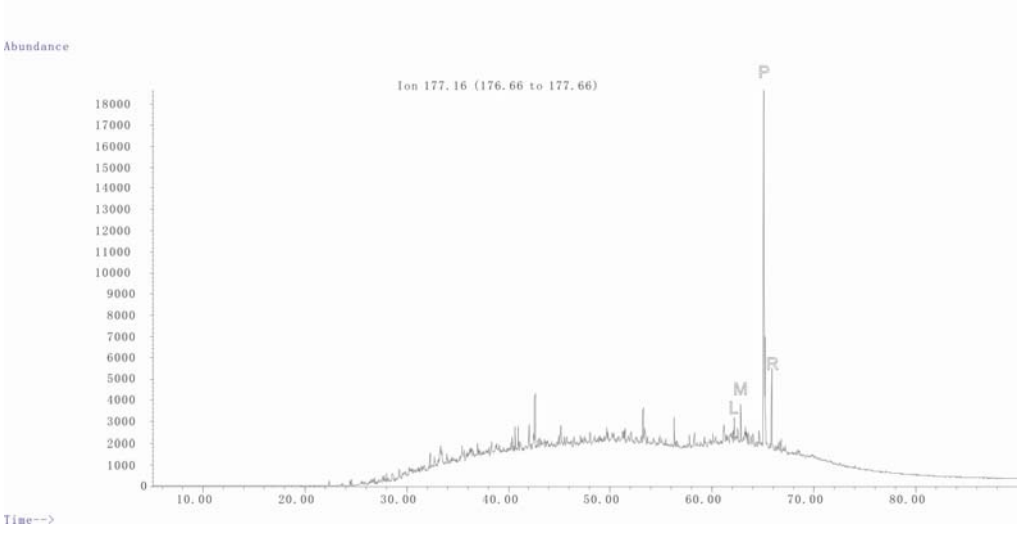
Abundance
Ion 177.16 (176.66 to 177.66)
18000
17000
16000
15000
14000
13000
12000
11000
10000
9000
8000
7000
6000
5000
4000
3000
2000
1000
0
P
R
M
L
10.00
20.00
30.00
40.00
50.00
60.00
70.00
80.00
Time-->

G2

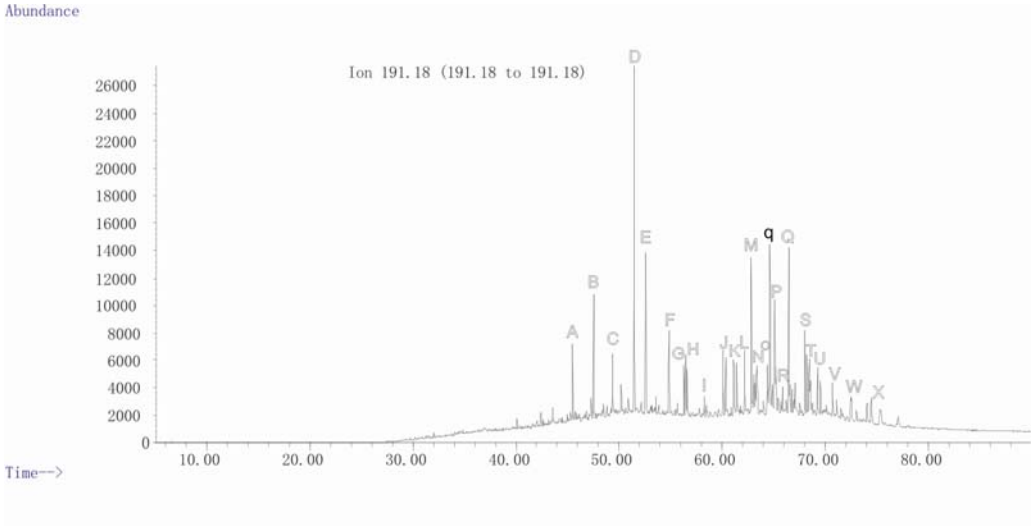
Abundance
Ion 191.18 (191.18 to 191.18)
26000
24000
22000
20000
18000
16000
14000
12000
10000
8000
6000
4000
2000
0
A
B
C
D
E
F
G
H
I
J
K
L
M
N
O
P
q
Q
R
S
T
U
V
W
X
10.00
20.00
30.00
40.00
50.00
60.00
70.00
80.00
Time-->

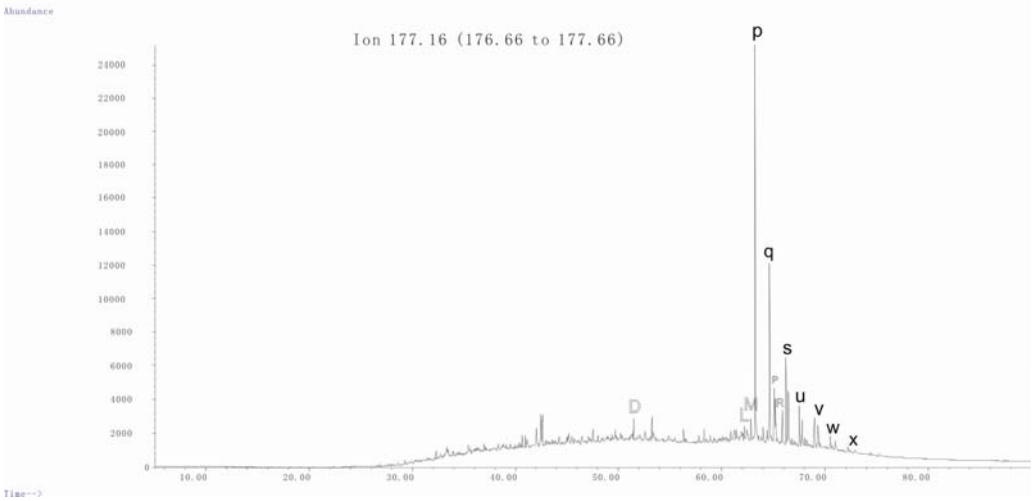
Abundance
Ion 177.16 (176.66 to 177.66)
24000
22000
20000
18000
16000
14000
12000
10000
8000
6000
4000
2000
0
p
q
s
u
v
w
x
D
M
P
10.00
20.00
30.00
40.00
50.00
60.00
70.00
80.00
Time-->

G3

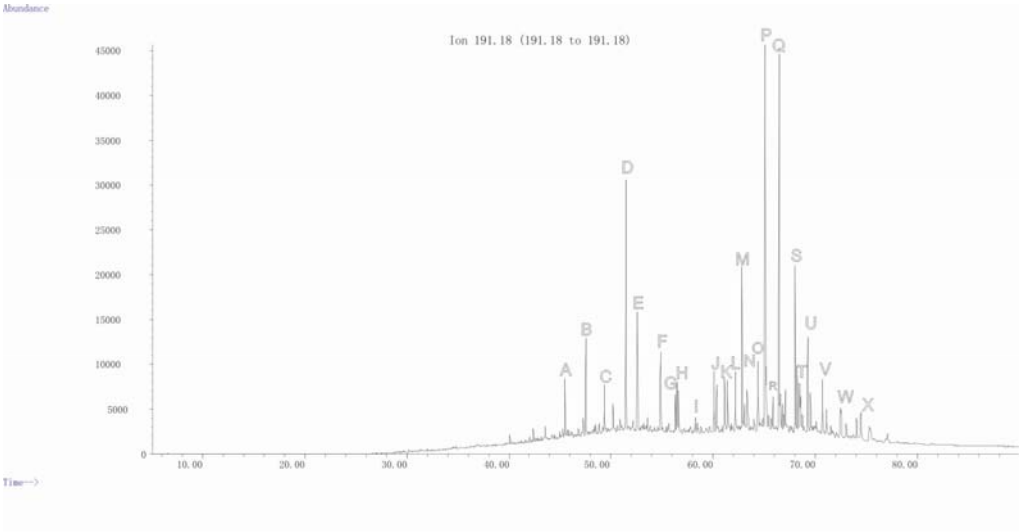
Abundance
Ion 191.18 (191.18 to 191.18)
45000
40000
35000
30000
25000
20000
15000
10000
5000
0
A
B
C
D
E
F
G
H
I
J
K
L
M
N
O
P
Q
R
S
T
U
V
W
X
10.00
20.00
30.00
40.00
50.00
60.00
70.00
80.00
Time-->

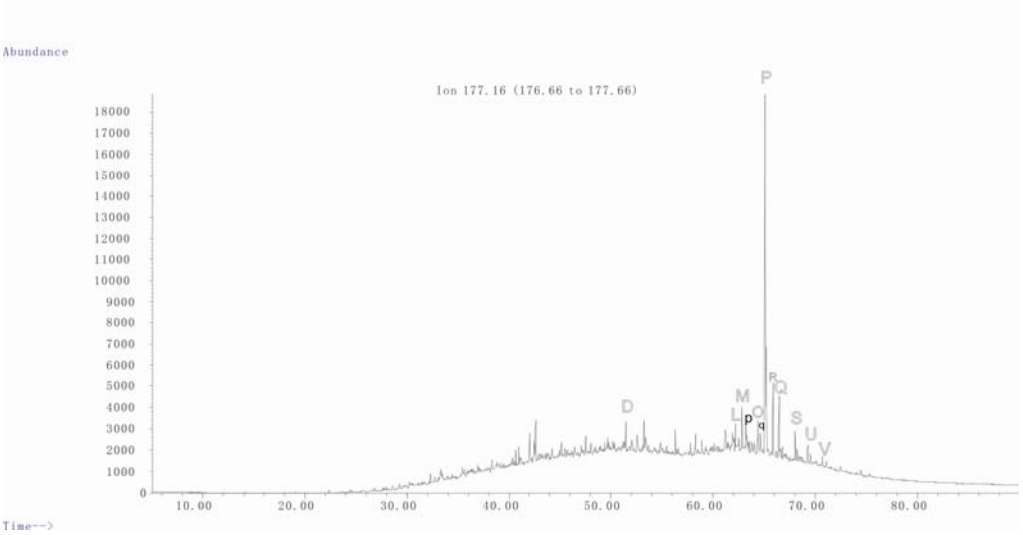
Abundance
Ion 177.16 (176.66 to 177.66)
18000
17000
16000
15000
14000
13000
12000
11000
10000
9000
8000
7000
6000
5000
4000
3000
2000
1000
0
D
L
M
P
Q
R
S
U
V
10.00
20.00
30.00
40.00
50.00
60.00
70.00
80.00
Time-->

G4

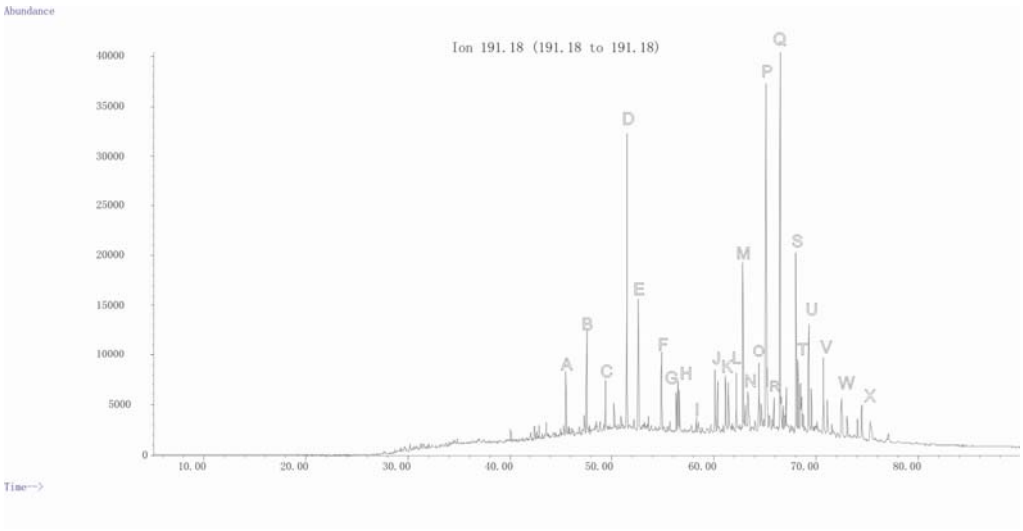
Abundance
Ion 191.18 (191.18 to 191.18)
40000
35000
30000
25000
20000
15000
10000
5000
0
A
B
C
D
E
F
G
H
J
K
L
M
N
O
P
Q
R
S
T
U
V
W
X
10.00
20.00
30.00
40.00
50.00
60.00
70.00
80.00
Time-->

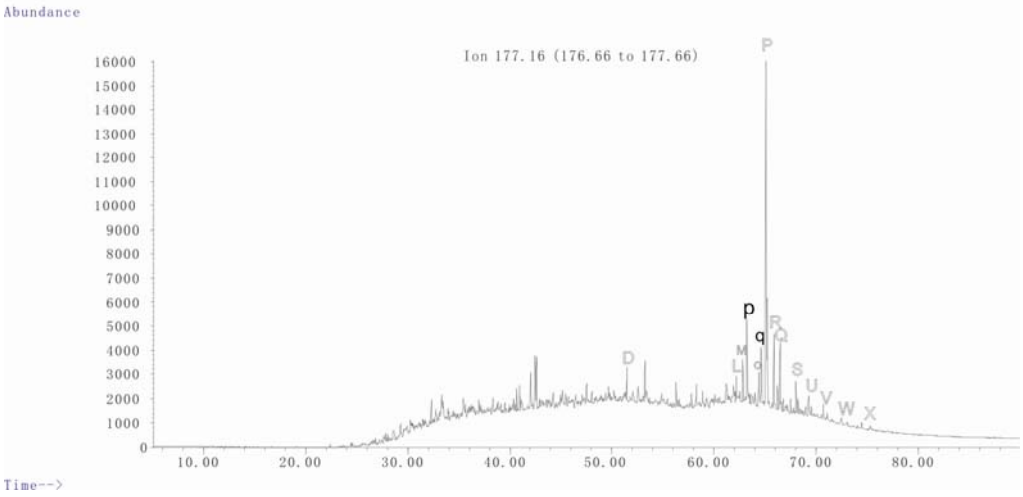
Abundance
Ion 177.16 (176.66 to 177.66)
16000
15000
14000
13000
12000
11000
10000
9000
8000
7000
6000
5000
4000
3000
2000
1000
0
P
p
q
R
Q
M
L
D
S
U
V
W
X
10.00
20.00
30.00
40.00
50.00
60.00
70.00
80.00
Time-->

G5

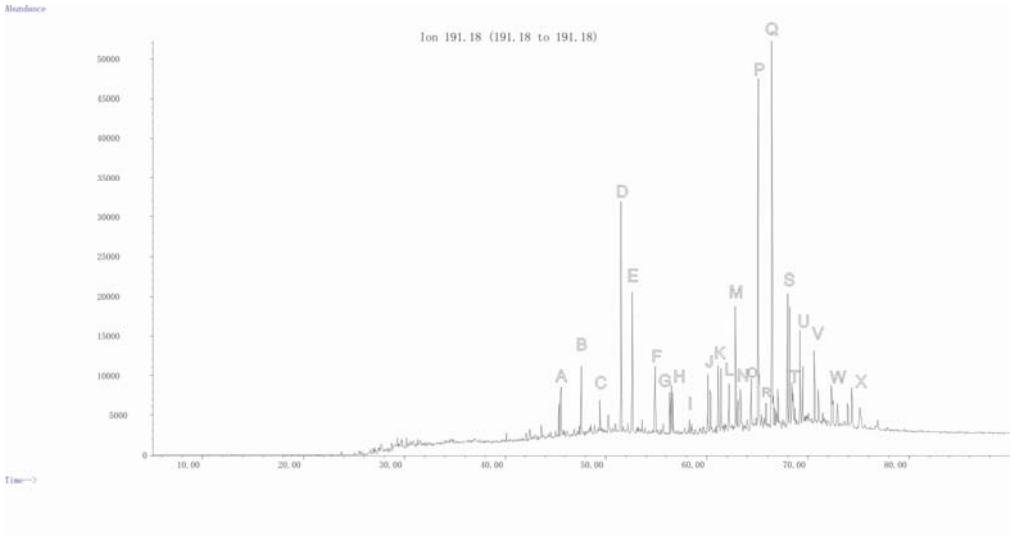
Abundance
Ion 191.18 (191.18 to 191.18)
Time-->

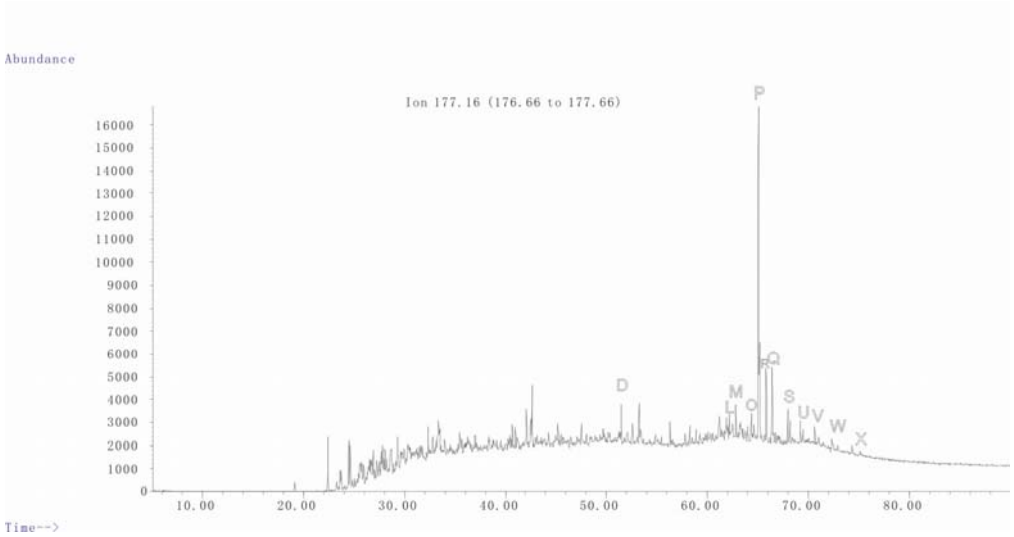
Abundance
Ion 177.16 (176.66 to 177.66)
Time-->

G6

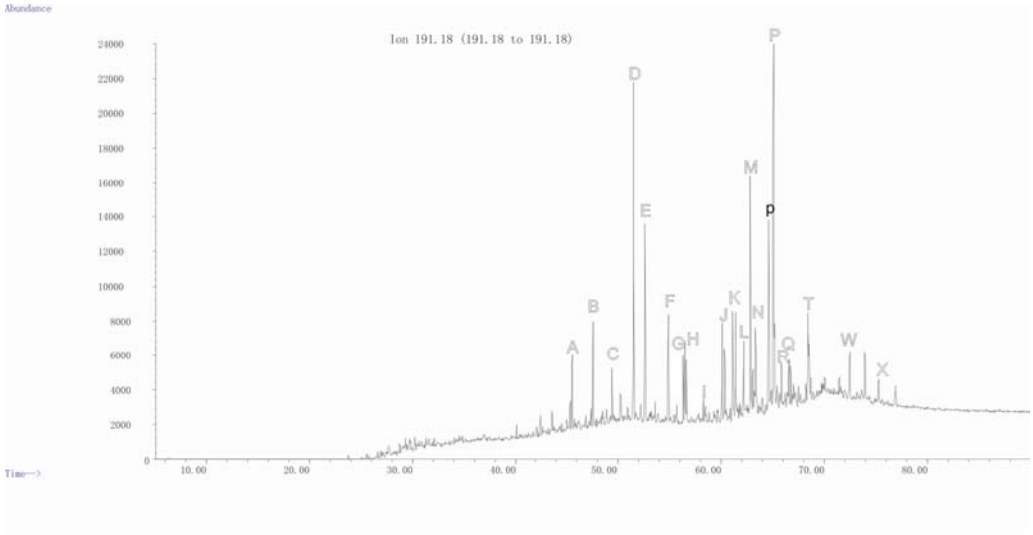
Abundance
Ion 191.18 (191.18 to 191.18)
Time-->
A
B
C
D
E
F
G
H
J
K
L
M
N
P
p
Q
R
T
W
X

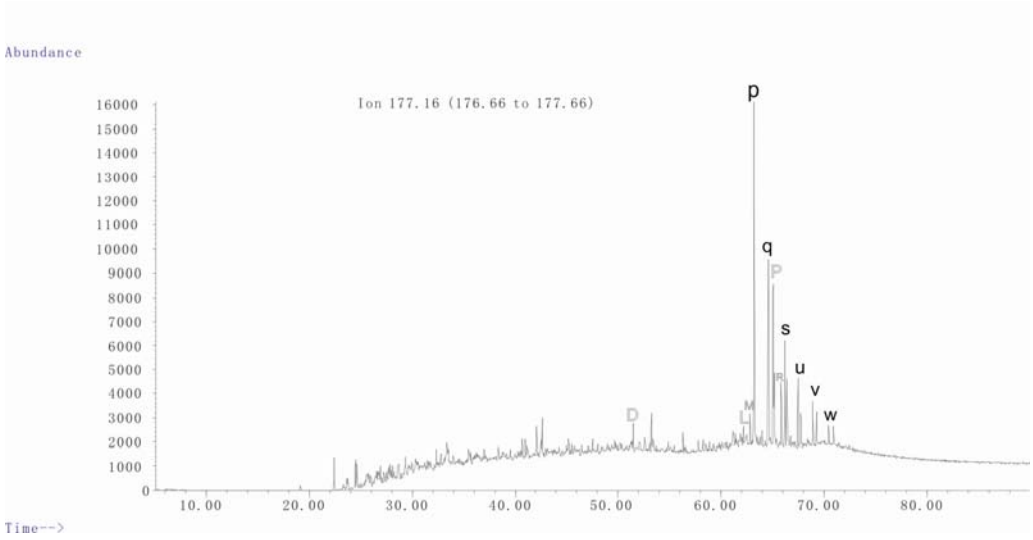
Abundance
Ion 177.16 (176.66 to 177.66)
Time-->
D
L
M
N
P
p
q
s
u
v
w

G7

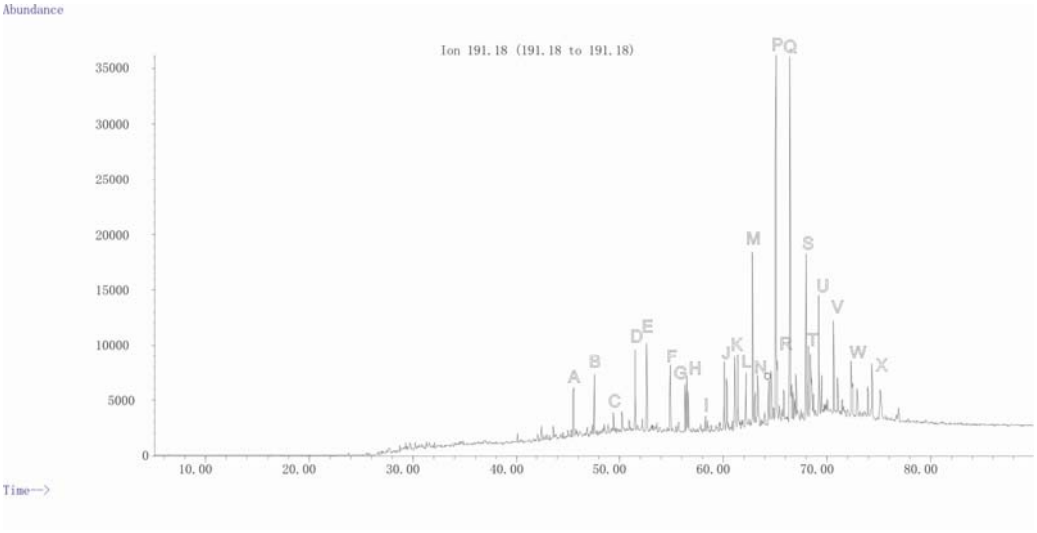
Abundance
Ion 191.18 (191.18 to 191.18)
35000
30000
25000
20000
15000
10000
5000
0
A
B
C
D
E
F
G
H
I
J
K
L
M
N
O
PQ
R
T
S
U
V
W
X
10.00
20.00
30.00
40.00
50.00
60.00
70.00
80.00
Time-->

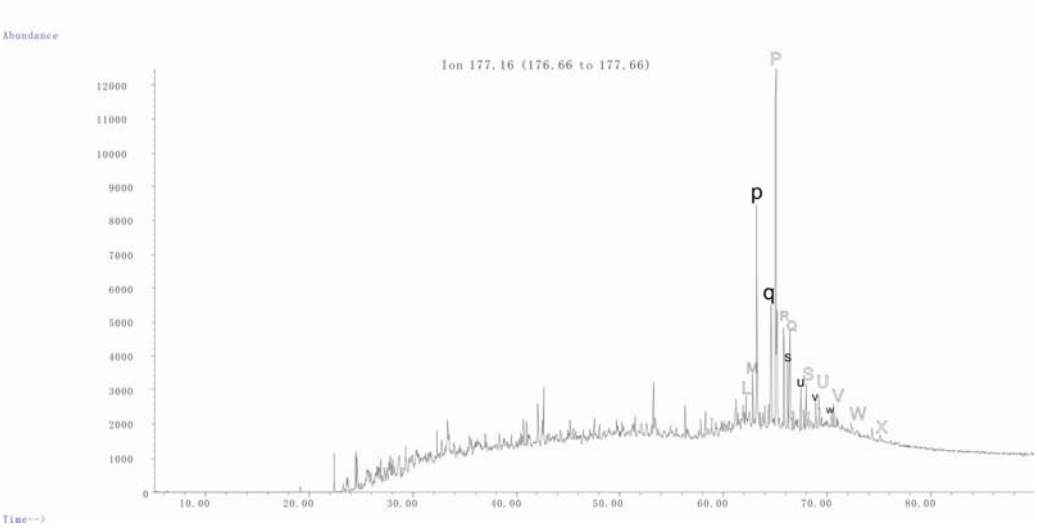
Abundance
Ion 177.16 (176.66 to 177.66)
12000
11000
10000
9000
8000
7000
6000
5000
4000
3000
2000
1000
0
P
p
q
R
o
s
M
L
S
u
U
V
Y
w
W
X
10.00
20.00
30.00
40.00
50.00
60.00
70.00
80.00
Time-->

Compounds identified in the m/z 191and m/z 177 fragmentograms	
Peak	**Compound**
A	C20 tricyclic terpane
B	C21 tricyclic terpane
C	C22 tricyclic terpane
D	C23 tricyclic terpane
E	C24 tricyclic terpane
F	C25 tricyclic terpane
G	C24 tetracyclic terpane
H	C26 tricyclic terpane isomers
I	C27 tricyclic terpane isomers
J	C28 tricyclic terpane isomers
K	C29 tricyclic terpane isomers
L	18a(H)-trisnorhopane(Ts)
M	17a(H)-trisnorhopane(Tm)
N	C30 tricyclic terpane isomers
O	28,30-bisnorhopanes
P	17α(H),21β(H}-norhopane
Q	17α(H) 21β(H)-hopane
R	17β(H), 21α(H)-normoretane
S	(20S) and 20(R) 17α(H), 21β(H)-homohopanes
T	gammacerane
U	(20S) and 20(R) 17α(H), 21β(H)-bishomohopanes
V	(20S) and 20(R) 17α(H), 21β(H)-C33 hopanes
W	(20S) and 20(R) 17α(H), 21β(H)-C34 hopanes
X	(20S) and 20(R) 17α(H), 21β(H)-C35 hopanes
p	17α(H)-25,30 bisnorhopane
q	17α(H)-25 norhopane
s	(20S) and 20(R) 17α(H)-25 norhomohopanes
u	(20S) and 20(R) 17α(H)-25 norbishomohopanes
v	(20S) and 20(R) 17α(H)-25 nor C32 hopanes
w	(20S) and 20(R) 17α(H)-25 nor C33 hopanes